ORNL/Sub/85-28611/2

OAK RIDGE NATIONAL LABORATORY

MARTIN MARIETTA

IMPACT OF STEEP-FRONT SHORT-DURATION IMPULSE ON ELECTRIC POWER SYSTEM INSULATION

PHASE II: LABORATORY EVALUATION OF SELECTED POWER SYSTEM COMPONENTS

L. M. Burrage
E. F. Veverka
J. H. Shaw
B. W. McConnell (ORNL)

Published April 1991

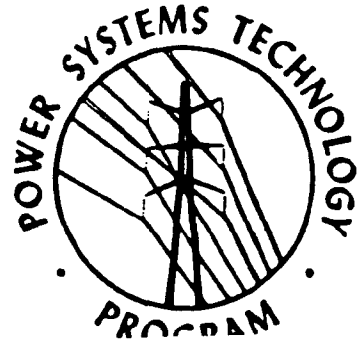

MANAGED BY
MARTIN MARIETTA ENERGY SYSTEMS, INC.
FOR THE UNITED STATES
DEPARTMENT OF ENERGY

ORNL/Sub/85-28611/2

IMPACT OF STEEP-FRONT SHORT-DURATION IMPULSE ON ELECTRIC POWER SYSTEM INSULATION

PHASE II: LABORATORY EVALUATION OF SELECTED POWER SYSTEM COMPONENTS

L. M. Burrage
E. F. Veverka
J. H. Shaw
B. W. McConnell (ORNL)

Manuscript completed November 1990
Published April 1991

Prepared for the U.S. Department of Energy,
Assistant Secretary for Conservation and Renewable Energy,
Office of Energy Storage and Distribution,
Electric Energy Systems Program

Prepared by

McGraw-Edison Technical Center
Cooper Power Systems
Cooper Industries, Inc.
11131 Adams Rd.
Franksville, WI 53126
under
Subcontracts 11X-28611C and 17X-SB374V

for the

Power Systems Technology Program
Energy Division
OAK RIDGE NATIONAL LABORATORY
Oak Ridge, TN 37831-6285
operated by
MARTIN MARIETTA ENERGY SYSTEMS, INC.
for the
U.S. DEPARTMENT OF ENERGY

CONTENTS

LIST OF FIGURES

LIST OF TABLES

LIST OF ABBREVIATIONS AND ACRONYMS

ANSI	=	American National Standards Institute
BIL	=	basic insulation level
CIFO	=	critical impulse flashover
CISO	=	critical impulse sparkover
cm	=	centimeter
DNA	=	Defense Nuclear Agency
EI	=	electrical insulation
EMP	=	electromagnetic pulse
FFT	=	fast Fourier transform
FO	=	flashover
FOW	=	front-of-wave
ft	=	foot
HEMP	=	high-altitude electromagnetic pulse
Hz	=	hertz
IEEE	=	Institute of Electrical and Electronic Engineers
in.	=	inch
IX	=	circuit reactance
kA	=	kiloampere
kHz	=	kilohertz
kV	=	kilovolt
kVA	=	kilovolt-ampere
kg	=	kilogram
lb	=	pound
m	=	meter
MOV	=	metal-oxide varistor
MVA	=	megavolt ampere
μH	=	microhenry
μs	=	microsecond
NEMP	=	nuclear electromagnetic pulse
ns	=	nanosecond
pF	=	picofarad
RLC	=	resistance/inductance/capacitance
rms	=	root-mean-squared
SFSD	=	steep-front short-duration
SiC	=	silicon carbide

ACKNOWLEDGMENTS

The authors would like to express their gratitude to P. R. Barnes and Dr. S. J. Dale of Martin Marietta Energy Systems, Inc., at the Oak Ridge National Laboratory; to R. H. McKnight, formerly at the National Bureau of Standards and presently at the Department of Energy; and to A. Ramrus and E. Strickland at Maxwell Laboratories, Inc., for their highly valued input and interaction during this project.

We would also like to acknowledge the extra effort under trying conditions provided by all the laboratory personnel at Maxwell Laboratories and especially by Dan Wirtz and Don Gingras at the McGraw-Edison Technical Center, Cooper Power Systems.

We wish to recognize D. R. Volzka of the Wisconsin Electric Power Company and O.R. Compton of the Virginia Electric Power Company for their technical contributions and assistance. In addition, the support provided by Wisconsin Electric and Virginia Electric in providing a multitude of test specimens is greatly appreciated.

It would have been impossible to carry out this program without the help of all the aforementioned individuals, their coworkers, and their companies.

EXECUTIVE SUMMARY

This final report documents all the experimental work performed by Cooper Power Systems, Cooper Industries, Inc., for the Oak Ridge National Laboratory under the subcontracts 11X28611C and 17X-SB-374V.

This research effort required the performance evaluation of three specific insulation systems in common usage by electric power transmission and distribution utilities under stresses imposed by

- three characteristic impulse waveforms [two waves representative of steep-front short duration (SFSD) impulses and one representative of lightning],
- the cumulative effect of multiple "shots" of each pulse,
- 60 Hz voltage, and, where appropriate,
- mechanical load.

The insulation systems evaluated are the cellulose-paper/oil combination typical of power transformer and condenser bushing usage, the cellulose-paper/enamel/oil combination used in distribution transformer construction, and the porcelain/air combination representing transmission and distribution line structural insulation.

The impulse waveshapes used in this evaluation are defined in the final report of the first phase of this project. These waveshapes are

- a lightning wave having a 1.2-μs rise time and 50 μs to half crest on the tail,
- a fast-front wave of 100-ns rise time typical of slower electromagnetic-pulse- (EMP-) coupled impulses and system transients and having a nominal 500-ns time to half crest, and
- an SFSD wave of 10- to 20-ns rise time typical of the faster EMP-coupled impulse, with very fast switching transients and with half-crest times in the range of 100–300 ns. All effort reported herein used conducted impulses.

The major results of this investigation are:

1. Electric power apparatus having basic insulation levels (BILs) greater than 550 kV are less likely to be damaged by large-magnitude SFSD impulses than are apparatus having basic insulation levels (BILs) less than 550 kV.
2. The likelihood of damage increases as the BIL is reduced to less than 550 kV. Severe damage can be expected for apparatus in the 95- to 200-kV BIL range.
3. The insulation system of unprotected and poorly protected distribution transformers can be damaged to failure by SFSD impulses in both the energized and unenergized conditions. Poorly

protected distribution transformers are those with arresters mounted some distance from the transformer bushing.

4. Line insulation, usually porcelain suspension insulators, has also failed when subjected to SFSD impulses in both the energized and unenergized conditions.

5. The cellulose/oil insulation system used in power-apparatus bushings failed when subjected to SFSD impulses.

6. The dielectric degradation of the insulation system of an insulator or a transformer experiencing an SFSD impulse may or may not result in an immediate catastrophic event. Cumulative damage is the norm, leading to failure at an indefinite future time.

7. Conventional silicon-carbide and metal-oxide varistor lightning arresters are capable of mitigating the impact of the SFSD conducted impulses on transformers.

8. The best application of lightning arresters—viz., the very close juxtaposition of arrester and transformer input bushing, with a direct connection between them—has prevented failure of the transformer in all cases.

PREFACE

The Office of Energy Storage and Distribution of the United States Department of Energy has formulated a program for the research and development of technologies and systems for the assessment, operation, and control of electric power systems exposed to electromagnetic pulses (EMPs). Because high-altitude EMPs can induce kiloampere currents having nanosecond rise times that can potentially damage insulation systems, a section of the program is identified as Insulation Damage Studies. The work being discussed was performed as a major part of this section and addresses the impact of steep-front short-duration (SFSD) impulses on power system insulation.

Examination of dielectric behavior under steep front (ns rise time), short duration (to 1 μs) pulses is just beginning. Interest in this area has been enhanced by the increased use of solid hydrocarbon insulation, some observed insulation breakdown under certain conditions of pre-stress,[1] and the postulated failure of transformers under fast surges.[2] While it is difficult to predict the response of a specific insulating material or insulation system under SFSD pulses, breakdown would seem to be possible for pulses of adequate duration and intensity. Experimental data is needed to further quantify this behavior.

Clayton and others have postulated that the delayed or anomalous failure of transformers may also be initiated by the SFSD pulse.[2] Consider a mixture of liquid and solid insulation, as found in transformers, and assume that an SFSD pulse of adequate duration breaks down the liquid but only "damages" the solid in some unspecified manner. The implication that such a damaged system might later fail under less-than-design operating conditions is the basis for postulating that SFSD impulses cause delayed or anomalous failures.

What are the sources of such SFSD pulses? Multiple-stroke lightning is perhaps the most likely source. However, the back-flashover of lightning to tower or shield wire is also capable of producing such effects.[2] Because the currents induced by the nuclear electromagnetic pulse (NEMP) have rise times of tens of nanoseconds and are capable of generating kiloamp currents of several microseconds duration,[3,4,5] a better understanding is required of the potential impact of SFSD impulses on the insulation systems used in power apparatus.

The above effects have been discussed as potential problem areas for many years; however, the techniques and experimental apparatus necessary for examining these issues in detail were not readily available to the electric power industry. This work will attempt to solve some of these problems.

Phase I of this effort resulted in an extensive literature search to determine what was known about how SFSD impulses interact with electric power insulation systems.[6] Included in that report was identification of perceived dielectric problem areas for power systems and apparatus, followed by the characterization of the problem of insulation response and identification of models and proposed experiments to explain the perceived response.

One method of attacking the experimental problem has been to test several insulation types starting with a known standard waveform, such as the 1.2- by 50-μs impulse used for lightning simulation, and perform a series of tests using steeper rise times and shorter-duration impulses.

The insulation system models ranged from the elementary to the complex, simulating use in power system apparatus. However, the extrapolation of this data to the performance of power system apparatus has not been very successful. Therefore, this project used the staged approach to test production apparatus insulation systems rather than individual insulation materials.

The sources of SFSD impulses and their characteristics as developed in the Phase I effort and since updated are summarized in the table below.

Characteristics of SFSD impulse sources

CHARACTERISTIC		SFSD IMPULSE TYPE		
		LIGHTNING	EMP PLANE WAVEFORM (TYPICAL WAVEFORM)	SYSTEM-GENERATED
FIELD STRENGTH (FREE SPACE)	Electric (E)	40 kV/m	50 kV/m	10 kV/m
	Magnetic(M)	300 A/m	1000 A/m	300 A/m
IMPULSE SHAPE	Rise time	20-500 ns	10 ns	10 ns
	Time to half value	5-20 μs	10-200 μs	1-5 μs
PEAK CURRENT		200 kA	10 kA*	---
PEAK VOLTAGE		---	2000 kV*	2-3X system voltage
PULSE DURATION		10-1000 μs	1 μs	1-10 μs

*Peak induced values.

From most vulnerable to least vulnerable, the perceived susceptibility of various electric-power-system apparatus to damage by the SFSD impulse is ranked as follows (updated from the Phase I report):

1. electronic controls,

2. cables, cable potheads,

3. distribution transformers,

4. line insulation, porcelain support structures,

5. power transformers, and

6. heavily protected generators.

REFERENCES

1. I. Kitani and K. Arii, "Impulse Breakdown of Prestressed Polyethylene Films in the ns Range," *IEEE Trans.*, EI-17, 571-76 (1982).

2. R. Clayton et al., "Surge Arrester Protection and Very Fast Surges," *IEEE Trans.*, PAS-102, 2400-2412 (1983).

3. K. S. H. Lee, F. C. Yang, and N. Encheta, "Interaction of High-Altitude Electromagnetic Pulse (EMP) with Transmission and Distribution Lines: An Early-Time Consideration," Air Force Weapons Laboratory Interaction Note IN435, 1983.

4. P. R. Barnes, "The Axial Current Induced on an Infinitely Long, Perfectly Conducting, Circular Cylinder in Free Space by a Transient Electromagnetic Pulse Wave," Air Force Weapons Laboratory Interaction Note IN64, 1971.

5. E. F. Vance, *Electromagnetic Pulse Handbook for Electric Power Systems,* DNA-3466F, Stanford Research Institute, Menlo Park, Calif., 1975.

6. L. M. Burrage et al., *Assess the Impact of the Steep Front, Short Duration Impulse on Electric Power System Insulation - Phase I Final Report,* ORNL/Sub/85-28611/1, Oak Ridge Natl. Lab., Martin Marietta Energy Systems, Inc., February 1987.

1. PROJECT GOALS

1.1 INTRODUCTION

Examination of the response characteristics of materials subjected to pulses with different rise times and durations has led to the definition of three specific pulses, namely 10 by 150 ns, 100 by 500 ns, and 1.2 by 50 μs. These pulses, which reflect different physical response regions, were defined in Phase I of this effort.[1] Based upon insulation structure and exposure, work in Phase I indicated that conductor structural insulation, cables, electronic controls, and both power and distribution-class transformers are the components that appear to have the greatest susceptibility to damage when exposed to steep-front surge voltages. Liquid and gaseous dielectrics are generally self-restoring following breakdown, but solid insulation (such as paper, polymers, ceramics, glass, or rubber) and combinations of solid and liquid or gases are not self-restoring. Hence, solids and combinations involving solids are most vulnerable to permanent damage.

This research seeks to provide models for the dielectric response of key apparatus installed in electric power systems that may be susceptible to damage from steep-front short-duration (SFSD) voltage impulses and to confirm the validity of these models and the apparatus' susceptibility to damage through testing. These models can be elaborate mathematical models or relatively simple stochastic failure models. The intent is to assess the response of power systems insulation to impulses of equal or greater amplitude, shorter duration, and faster rise times than those presently used for insulation evaluation, and then use the results to recommend methods of predicting this response.

Transformers and generators are the most costly discrete components and require the longest time to replace should dielectric failure occur. In addition, the possibility of multiple failures of the structural insulation of overhead transmission and distribution lines must be considered. While unit costs of such components are relatively low, the failure of a significant number of units within a relatively short time requires that time for replacement be considered in assessing the components' vulnerability, particularly for insulation failure induced by nuclear electromagnetic pulse (NEMP).

This investigation examines closely the modeling and testing of critical portions of transformers and their accompanying overvoltage protective devices, and, where appropriate, the modeling and testing of bushings and structural insulation for transmission/distribution lines. The insulation systems involved are paper/oil for power transformers, enamel/paper/oil for distribution transformers, and porcelain/air for structural insulation systems. The paper/oil system is similar to that used in power-apparatus bushings and in some cables. Both enamel/paper/oil and paper/oil systems are also used in instrument transformers as well as in regulating transformers. The porcelain/air system, which is the predominant structural insulation system installed on existing electric power transmission and distribution lines, is also closely examined. Several different designs of line structural insulation are covered, such as porcelain pin, post, cap-and-pin, and suspension insulators. The basic objective is to determine the responses of these insulation systems to fast-rising voltage impulses.

Limited evaluation of other insulation systems is considered. Although electronic controls containing solid state devices may be vulnerable to SFSD impulses, evaluation of the insulation systems and of the performance of the assembled devices is not a part of this project.

Both unenergized and energized models/specimens are evaluated using conducted SFSD impulses. Radiated SFSD impulse evaluations are not included in this effort.

1.2 STATEMENT OF GOALS

The primary objective of this research was to examine the physical and engineering structure of the insulation systems most frequently subjected to overstress by SFSD voltage impulses and to determine how these insulation systems respond. Unenergized and energized systems were used as appropriate. To achieve this objective, the following tasks were completed:

- Select a representative set of components for extensive testing and modeling. Obtain an extensive amount of quality experimental data on each selected type for both 1.2- by 50-μs and SFSD impulses.

- Perform controlled laboratory experiments with smaller models and insulation test cells to identify failure mechanisms and their dependency on temperature, time before breakdown, volume, thickness, history, age, etc., for unenergized specimens.

- Use low-voltage, fast-front impulses conductively coupled to the terminals of selected experimental models to measure the voltage distribution to determine the location(s) of the most severe dielectric stresses within the selected model. Measure the effect of the transformer bushing where applicable. Use unenergized specimens.

- Using existing computer models to predict the response of the components, determine the location of the highest dielectric stress area, based upon wave propagation theory, winding parameters, transmission line theory, and appropriate computer calculational techniques.

- Perform controlled laboratory experiments on full-size models as appropriate and verify forecasted failure (highest stress) locations. Perform these experiments on both unenergized and energized models.

- Correlate laboratory experimental results and field experience relative to anomalous apparatus failures.

- Recommend improved protection practices for electric power apparatus.

2. LOW-VOLTAGE IMPULSE DISTRIBUTION: EXPERIMENTS AND MODELS

These studies were performed on transformer windings and a condenser bushing core that were carefully penetrated to permit the attachment of leads at each desired measuring point. These penetrations were performed with the least possible disturbance to the specimen. After attachment of the leads, the specimens were retanked (in the case of the transformers) or mounted in a manner simulating installation (in the case of the bushing). Typically, a low-voltage (50-V or less) impulse of the desired waveshape was applied to the specified terminals. The response at each of the discrete attachment points was recorded simultaneously with the impulse application. From this data a normalized distribution of the impulse voltages was prepared.

2.1 WAVESHAPES

Based upon prior studies, three waveshapes were selected. These are:

- the 1.2- by 50-μs lightning impulse, for comparison with known/published data;
- the 100- by 500-ns fast-impulse wave, typical of some power system transients and slower EMP waves; and
- the 10- by 165-ns SFSD impulse wave, typical of the high-altitude electromagnetic pulse (HEMP), some lightning phenomena, and certain switching transients in substations.

Whenever these waveforms could not be produced, the priority was to obtain a wavefront as close as possible to that desired. The time to half-crest on the tail (i.e., pulse duration) was allowed to increase.

2.2 FACILITIES

This section discusses the instrumentation and low-voltage pulse source used.

2.2.1 Instrumentation

The primary instrumentation consisted of a two-channel state-of-the-art LeCroy Transient Waveform Digital Recording package. This package includes a Model 6880 Transient Recorder; a TR8828C Transient Waveform Digital Recorder with expanded memory MM8104A; a Model 6010 MAGIC Controller; and a Model 6103 Dual Amplifier, Attenuator, and Trigger Generator. The system is housed in a Model 8013 Housing and Power Supply connected to a Compaq™ Portable Computer and Printer via an IEEE 488 bus. The LeCroy CATALYST Software System is used. This package had greater than 0–300 MHz bandwidth on one channel and greater than 0–200 MHz bandwidth on the second channel. The equipment is transportable, and after certain modifications by the manufacturer to the faster digitizer, the TR6880, it functioned without problems at each of the widely scattered laboratories used in these tests. Voltage measurements were made either by direct connection to the transient recorder inputs or through voltage dividers and attenuators. Current measurements were made through use of modified, miniature, high-frequency current transformers

supplied by Pearson. It was mandatory to maintain 50-Ω impedance matching for all voltage, current, and transient recording connections. See Fig. 2.1 for a full description of this package.

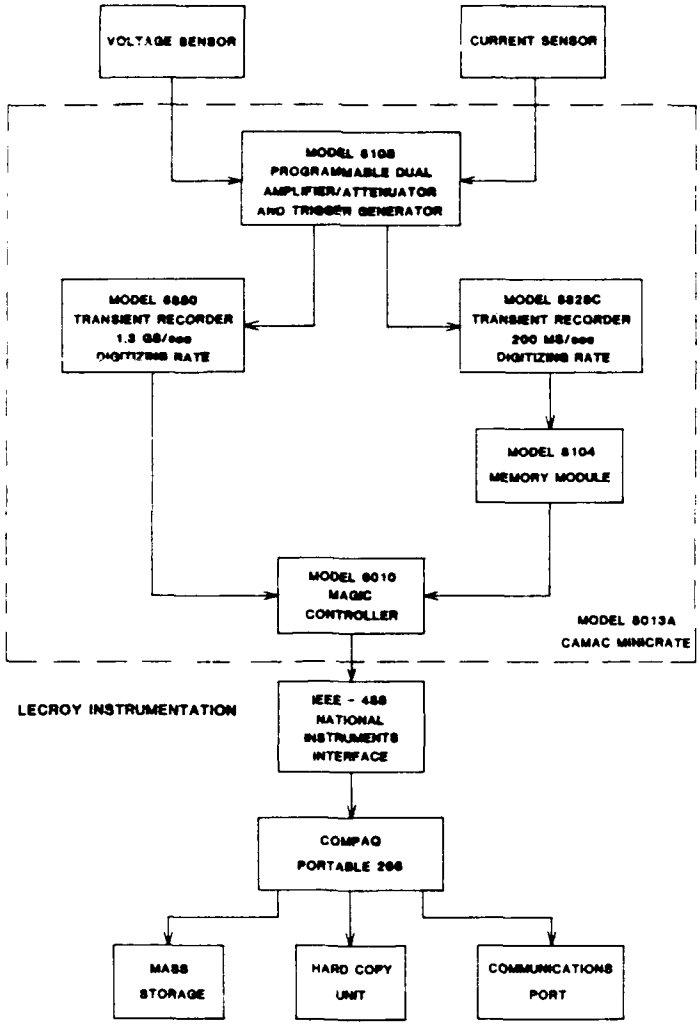

Fig. 2.1. Transportable high-speed data acquisition system used throughout the program based on LeCroy Transient Recorders, IEEE 488 BUS, and a portable personal computer.

Where necessary this equipment was supplemented by additional instrumentation specific to the variable being detected. Figure 2.2 shows one example of additional instrumentation used.

2.2.2 Low-Voltage Pulse Source

All of the low-voltage impulse studies were performed with pulse magnitudes of 50 V or less. The pulses were repetitive, providing stable and repeatable measurements. Several wave-form generators were used, their outputs being modified to produce the desired waveforms. This assembled equipment was also readily transportable and performed without error at the several locations involved in this program. Figure 2.3 provides a schematic and the details of a typical experimental setup.

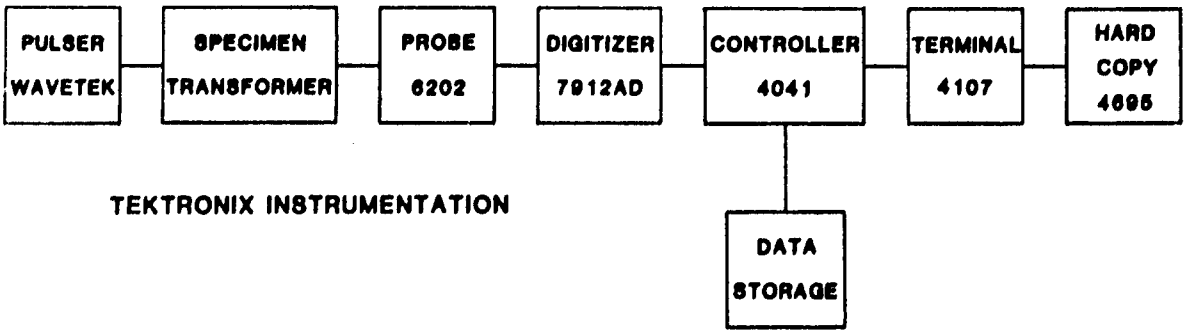

Fig. 2.2. Supplemental high-speed data acquisition system based on the Tektronix 7912AD Digitizer.

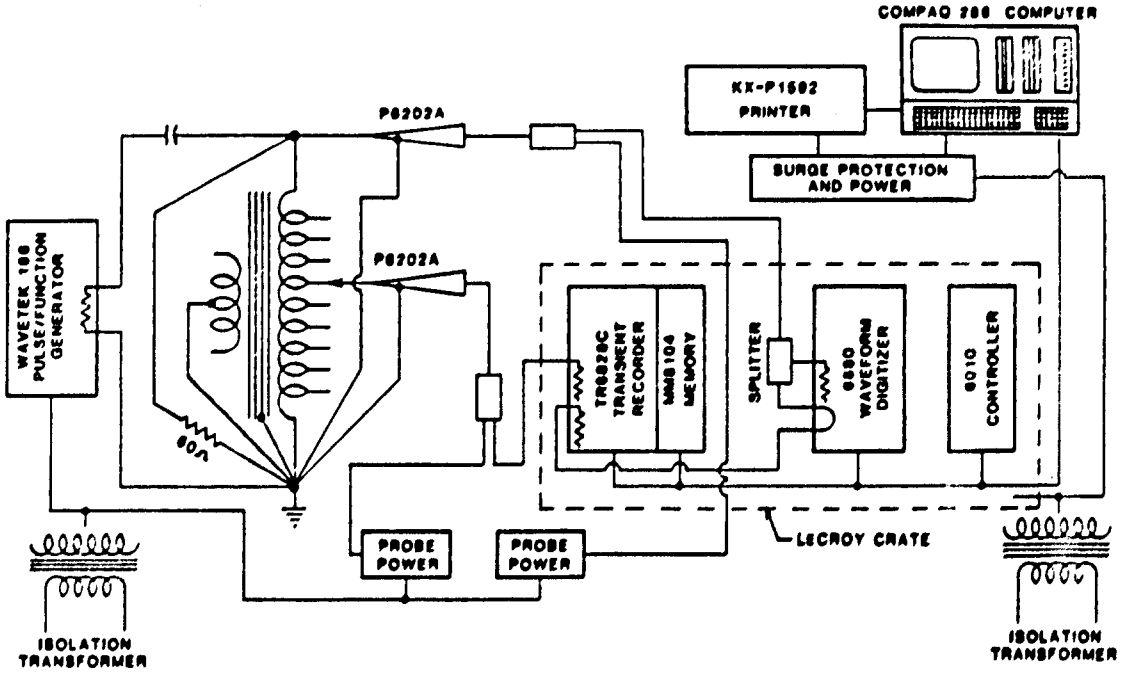

Fig. 2.3. Schematic for low-voltage SFSD impulse tests on distribution transformers. The grounded transformer tank is not shown.

2.3 MODELS

Low-voltage impulse distribution studies were performed on a shell-form distribution transformer, a core-form distribution transformer, a core-form power transformer, and a power-apparatus bushing core. The shell- and core-form distribution transformers are representative of the available transformer types. The core-form power transformer was used because of availability, and the power transformer bushing was tested to determine the bushing's response as a separate component. A

description of each insulation system is presented at the beginning of the section describing the particular system. Test results follow each system description.

2.3.1 Shell-Form Distribution Transformer Model

The shell-form distribution transformer that was tested had the following characteristics: 75 kVA, pole mount, 14.4 kV→120/240 V, 125-kV BIL, 2 bushings, oil insulated, and no taps.

This transformer was one of a group of identical units being subjected to high-voltage SFSD impulses. The low-voltage impulse distribution analyses identified the high-stress regions for each of the three impulse waves. Subsequently, other units from this same group were intentionally made to fail by high-voltage impulse testing only, one unit being made to fail with each of the three impulse waves. The low-voltage studies were used to advantage during subsequent analysis of the failed transformers.

The coil assembly of this transformer uses a split secondary, with one half on either side of the primary for conventional LO-HI-LO construction. The primary winding used enameled, flattened copper wire. The secondary winding was of sheet construction.

The insulation systems used in this design rely upon oil and paper/oil for the major insulation between primary and secondary windings and between windings and ground. Primary layer insulation is also paper/oil. Primary turn insulation is enamel/oil. Secondary turn insulation is paper/oil.

Probes were attached to the primary high-side and low-side terminals and to the outer turn of each primary winding layer at the common connection between adjacent layers. These probes divided the primary winding into 17 segments to detect the impulse voltage as it distributed itself throughout the winding. This provided a well-defined overall picture of the impulse distribution. The outermost primary coil layer was approximately one-half the height of the coil, the terminal connection being made at the approximate mid-point of the coil. Because additional detail was desired in the region of the first few turns of the high end of the primary, a window was cut through the outer insulation, through the center section of the outermost secondary winding, and through the LO-HI barrier insulation, thereby exposing the first few turns of the primary. Short lengths of wire were carefully soldered to each of these turns in an echelon pattern. Probes were subsequently clipped to these leads and restrained in place. After it was verified that all leads and probes were correctly located, the core/coil and probe assembly was retanked. This transformer was subsequently reimpregnated using repeated vacuum cycles at room temperature.

Figure 2.4 schematically displays the connection of the probes to the primary winding of this shell-form distribution transformer. Figure 2.5 shows the interchangeable probe tips in place on this winding. Figure 2.6 shows the completed core/coil/probe assembly ready for retanking and impregnating.

2.3.2 Core-Form Distribution Transformer Model

The insulation system used in the core-form distribution transformer is very similar to that used in the shell-form transformer, being a combination of paper, enamel, and oil. There are generally only small differences between the papers, enamels, and oils of the core and shell designs. However, there was expected to be a difference between their impulse voltage distributions based on the significant difference between the coil positions in the designs. Accordingly, a 50-kVA, 14.4/24.9-kV→120/240-V,

75 kVA 14.4/24.9 Y kV

120/240 Y

1.8% Z 125 kV BIL

AL HIV AND LOV 860 lb

TOTAL: 16 LAYERS

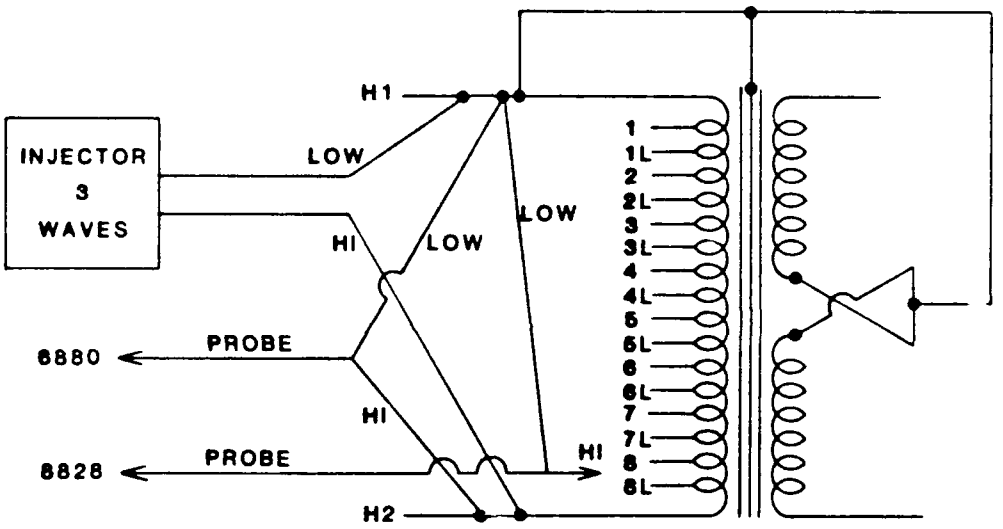

TAP	FILE	WAVE
H1	SHELLDIS	10 X 150 ns
1 to 8	SHDIS1 to SHDIS8	10 X 150 ns
H1	SHELLD12	100 X 500 ns
1 to 8	SHDIS11 to SHDIS18	100 X 500 ns
H1	SHELLD13	1.2 X 50 μs
1 to 8	SHDIS21 to SHDIS28	1.2 X 50 μs
8L to 1L	SHDI208L to SHDI201L	1.2 X 50 μs
1L to 8L	SHDI101L to SHDI108L	100 X 500 ns
8L to 1L	SHDI008L to SHDI001L	10 X 150 ns

Fig. 2.4. Schematic of probe connections to the shell-form distribution transformer.

Fig. 2.5. Interchangeable probe tips in place on the shell-form distribution transformer's primary winding.

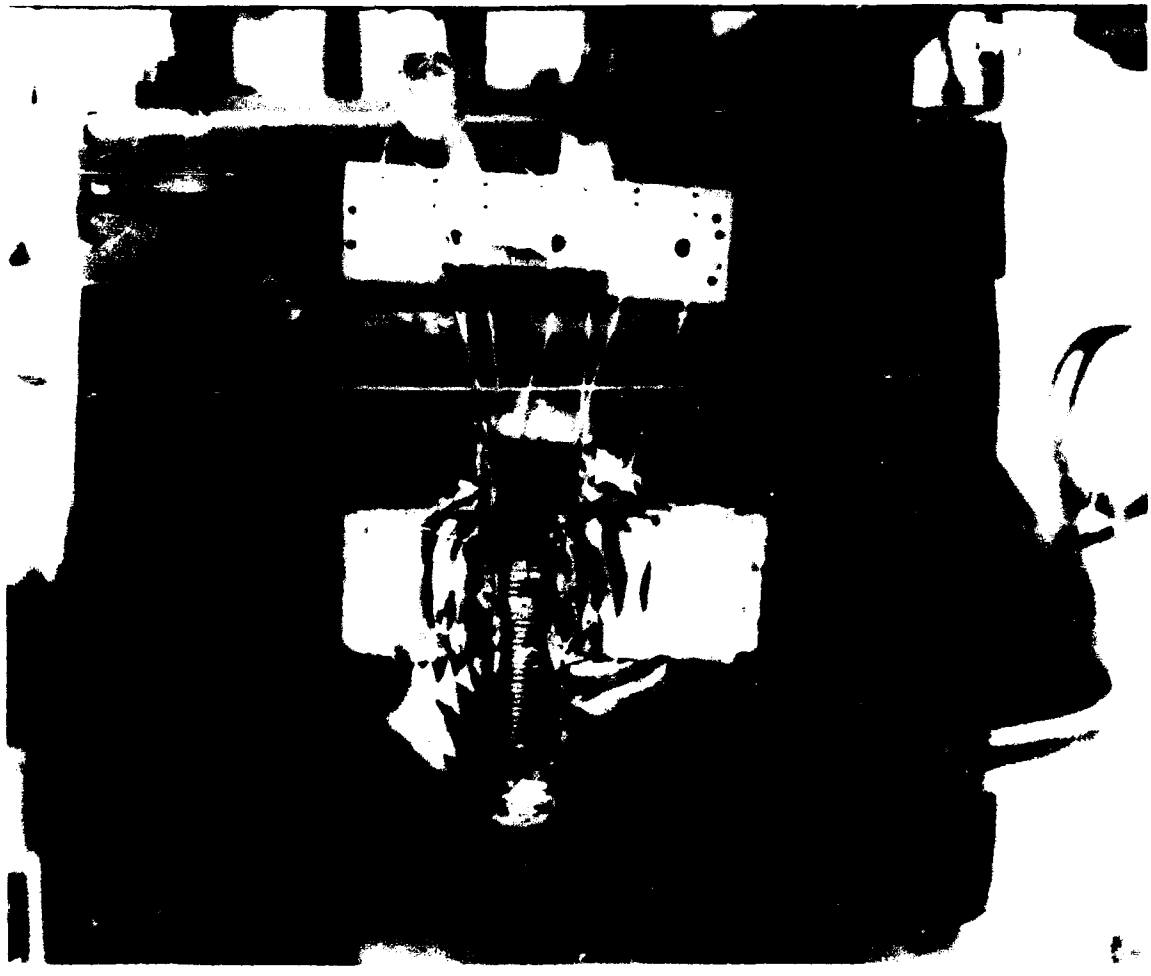

Fig. 2.6. **Leads attached to individual turns through an access window cut in the outer secondary winding and LO-HI barrier insulation, and winding/core probe assembly ready for retanking.** Insufficient space existed between the outer perimeter of the secondary and the tank wall to allow placement of the probe tips immediately adjacent to the windowed area.

125-kV BIL, single-phase, 2-bushing, tapped-primary, oil-insulated, c .e-form, pole-mount unit was selected. The core/coil assembly of this transformer consisted of LO-HI coils on each of the core legs.

As in the shell-form core, probes were attached to the primary high-side and low-side terminals and to the outer turn of each primary-winding layer at the common connection between adjacent layers. The additional detail required at the high-side entrance to the primary was readily obtained by removing part of the outer insulating wrap, exposing the primary winding. In this core, no secondary coils had to be penetrated. As before, short leads were soldered to the first few turns of the high-side end of the primary coils, and probes were attached to these leads. Following verification that all leads/probes were properly located and restrained, the core/coil/probe assembly was tanked and reimpregnated.

Figure 2.7 shows schematically the probe connections to the core-form primary windings. Figure 2.8 shows the core-form core/coil/probe assembly ready for retanking.

2.3.3 Core-Form Power Transformer Model

The typical core-form power transformer uses oil as the major insulation between the energized coil assembly and tank, paper/oil as turn insulation, and oil/paper/press-board spacers as insulation between layers (pancakes or disks). Other materials such as fiberglass-reinforced resin tubes may be used as coil forms and in primary/secondary barrier insulation. The insulation system of interest is the turn insulation, typically multiple layers of kraft paper spirally wrapped around the conductors. These insulated conductors have been formed into pancake coils that are separated by press-board (kraft) strips. The entire assembly is typically vacuum-impregnated with hot, dry oil.

The model selected for low-voltage impulse distribution analysis of power-transformer coil insulation was one phase of a 3-phase, 16.4/21.9/27.3-MVA, 230-kV, grounded-Y, 750-kV BIL primary to 13.8-kV W, 110-kV BIL secondary core-form power transformer.

Figure 2.9 displays one outboard phase of the untanked core/coil assembly of this transformer. This particular specimen was well-suited to the physical modeling requirements. The center-start balanced primary winding was of the continuous disk type, consisting of a single, multilayered-paper insulated, rectangular cross-section conductor. Sensing leads could be conveniently fastened to the outer peripheral transitions between disks. Segments of the primary windings from this phase and the other outboard phase were also available for other test purposes.

Figure 2.10 shows the sensing leads attached and fastened in place. All sensing leads were of identical length from the attachment point to a temporary terminal board located above the primary winding but below the oil level (see Fig. 2.11). Following verification that all leads were satisfactorily installed, the complete core/coil assembly was retanked and impregnated using a hot-oil/vacuum process. Figure 2.12 shows schematically the locations of the sensing leads on the primary winding.

The procedure followed in gathering data from this specimen was similar to that used for the distribution transformers. The desired waveshape was injected into the high side of the primary winding, and the response was measured simultaneously at a tap. All measurements were referenced to the transformer core/tank. A positive connection between the core and tank was made at the core ground point located between B and C phases. All of these measurements were made with the tap switch position selected to insert the full primary winding, tap A. The transformer cover and the three

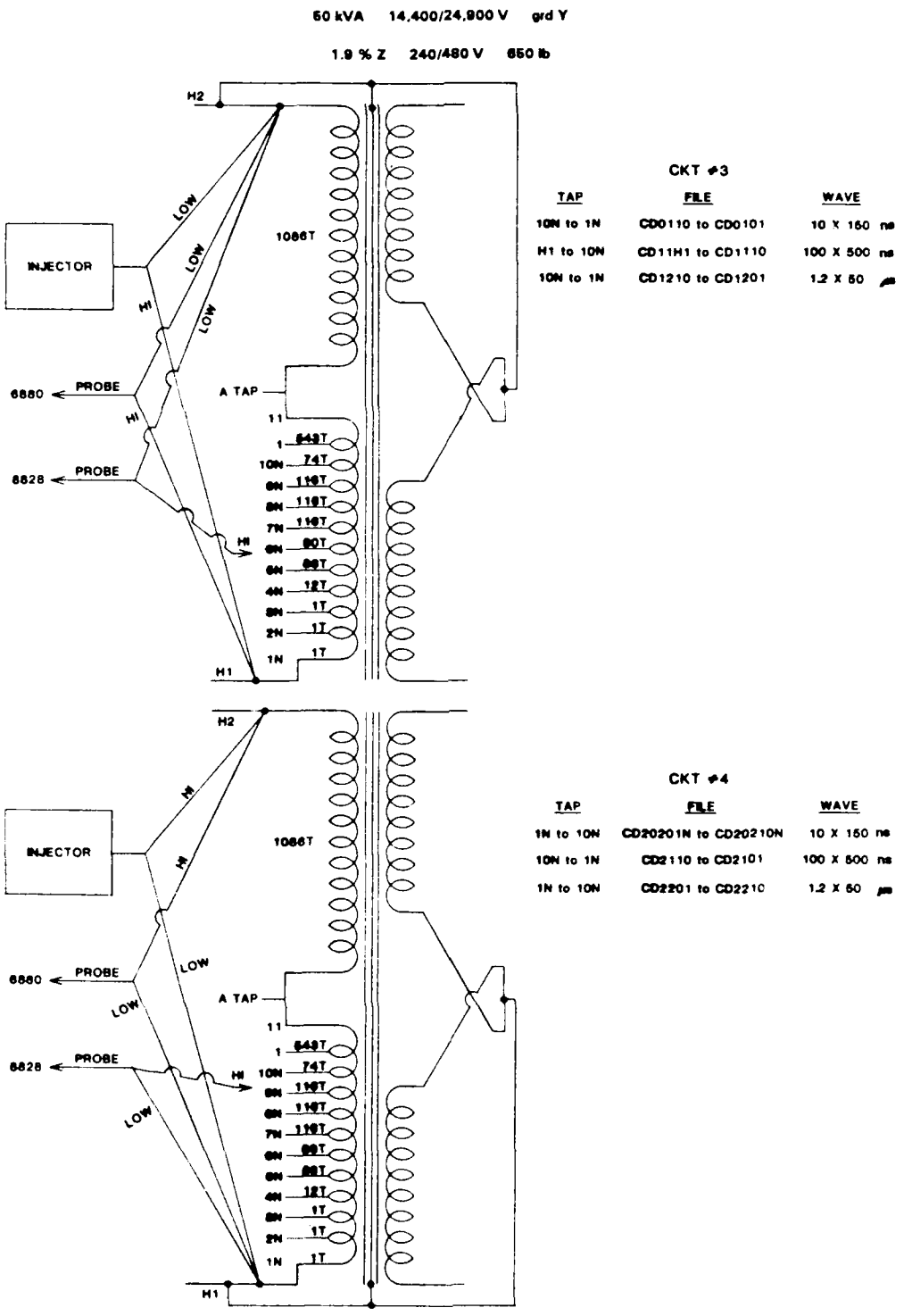

Fig. 2.7. Schematic showing sensing-lead attachment points on the primary winding of a 50-kVA core-form distribution transformer.

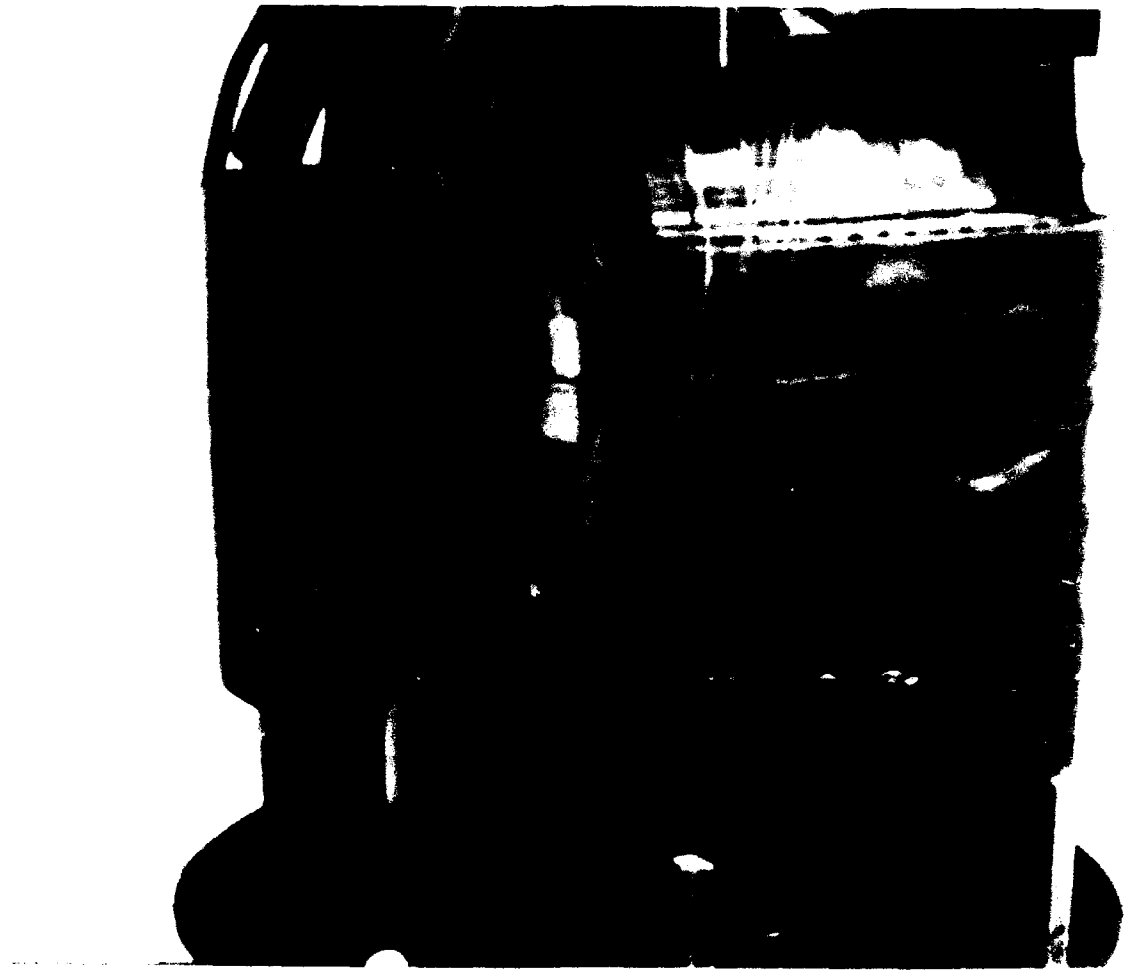

Fig. 2.8. Core-form distribution transformer's core/coil/sensing-lead/probe assembly ready for retanking.

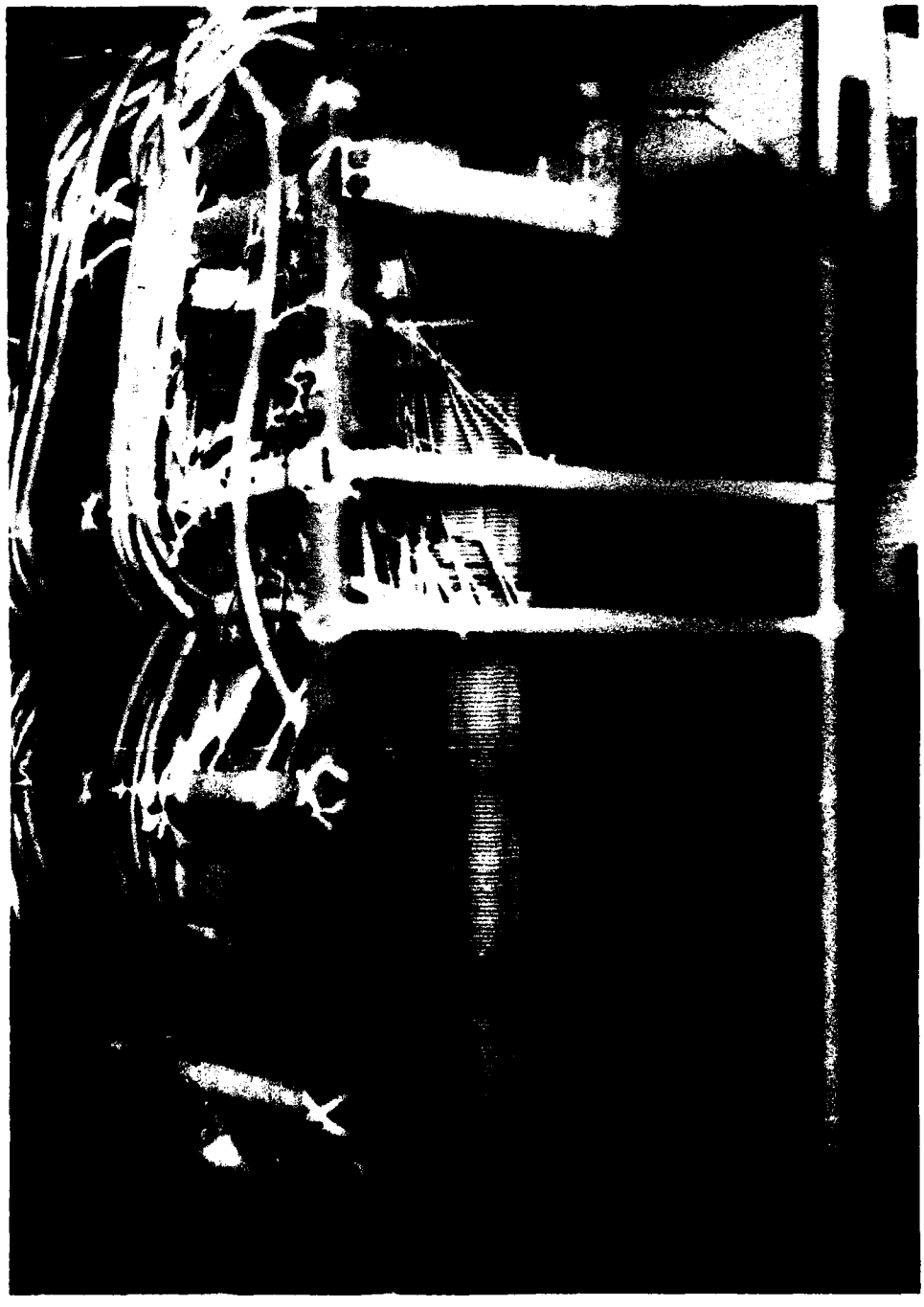

Fig. 2.9. Outboard phase of the 16.4-MVA core-form power transformer with sensing leads and temporary terminal board in place, ready for retanking.

Fig. 2.10. Details of sensing-lead attachment to the disk transition points, core-form power transformer.

Fig. 2.11. Temporary terminal board installed under oil above the primary winding; sensing leads are numbered.

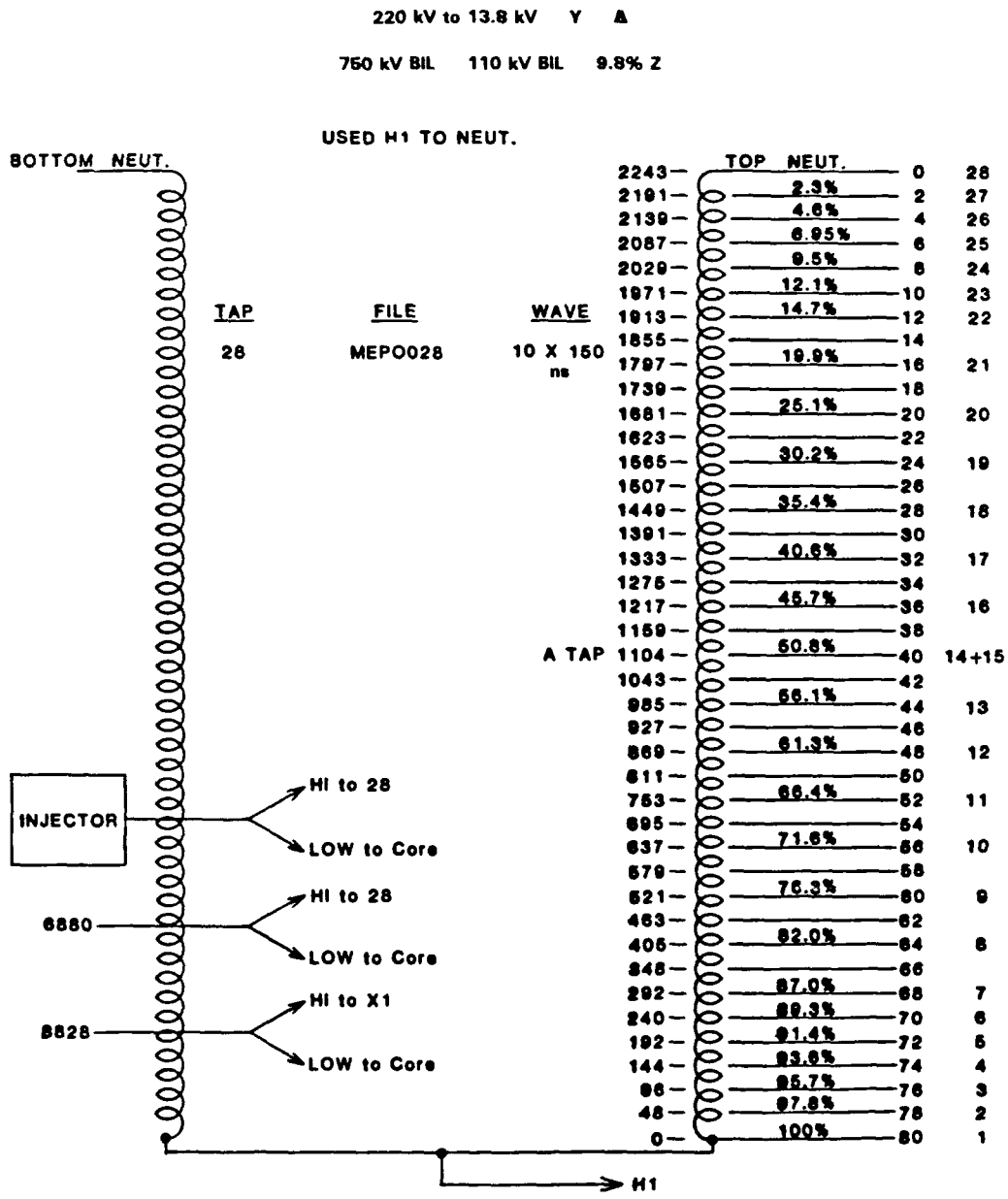

Fig. 2.12. Schematic showing sensing-lead attachment points to one side of the core-form power transformer's primary winding.

primary bushings were not installed. The delta-connected secondary was not grounded. Subsequently, impulse voltage measurements were made with a primary bushing suspended approximately at its as-installed position. The test impulse was then injected on the entrance terminal of this bushing, and the voltage division among the bushing, primary winding, and secondary winding was determined.

2.3.4 Power-Apparatus Bushing Model

Power-apparatus bushings used with oil-filled equipment also use a paper/oil insulation system. A typical example is a condenser-type bushing using a graded core wound on a central conductor having metallic foils between one or more layers of paper. This core assembly is installed in an oil-filled porcelain housing. The paper sheet stock used in these bushings is typically thicker than the paper strip used for conductor insulation for the power transformer and thinner than that used for layer insulation in the distribution transformer. Multiple layers of paper are used between adjacent layers of foil. The resulting thickness is substantially greater than the total thickness of paper used for the power transformer's turn insulation or the distribution transformer's layer insulation. This added thickness of insulation significantly alters the capacitance of the system being tested, hence the transient response.

When the power-apparatus bushing is subjected to lightning-type impulses having an amplitude greater than the BIL, the typical response is external flashover (FO). In the absence of dielectric degradation, the bushings are self-protecting.

Several aspects of bushing performance are to be determined in this program:

- Does the self-protecting mode (external FO) hold true for each of the two faster waves specified?
- If so, what is the front-of-wave flashover (FOWFO) level for each of the waves, and what is the resulting ratio of the steeper-wave FO to the lightning FO?
- Are the bushings damaged by the application of 800–1100-kV steep-front impulses?
- If so, is the damage cumulative or catastrophic?
- Can the potential tap normally used for bushing diagnostics be used reliably for monitoring transient responses of the bushing?

Based upon prior experimental testing with conducted SFSD and lightning-wave impulses and the evaluation of station-class lightning-arrester performance under similar conditions, power-apparatus bushings having a 550-kV BIL, 800-A rating were selected as the desired devices for modeling. An alternative rating of 650-kV BIL, 800 A could also be used. These bushings were interchangeable, able to be installed in either power transformers or oil circuit breakers as desired.

A 650-kV-BIL bushing core assembly was selected for the low-voltage impulse distribution study. This core assembly was prepared by removing a narrow strip of all the paper insulation from both the upper and lower tapered sections of the core, extending from the maximum diameter at the mounting flange area down to the central conductor (see Fig. 2.13). This procedure resulted in a narrow trench exposing the edge of each of the foils embedded in the core (see Fig. 2.14). Sensing leads could then

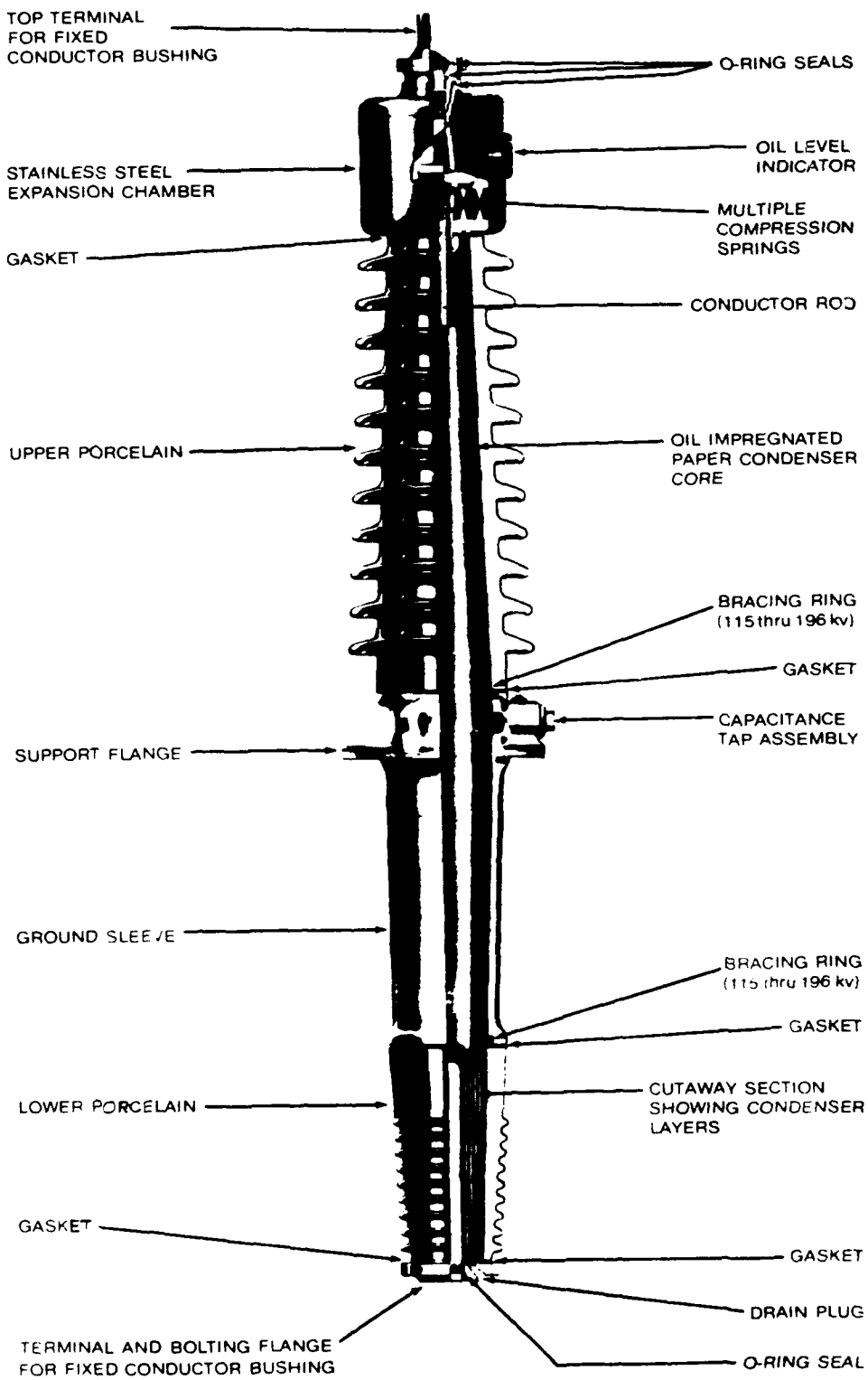

Fig. 2.13. Power-apparatus bushing cutaway identifying principal components.

Fig. 2.14. **Prepared tapered section of a 138-kV, 550-kV-BIL power apparatus bushing core.** The exposed edges of the foils are visible in the bottom of the trench.

be clipped to the foil edges to permit the impulse-voltage distribution to be determined. The bushing ground sleeve, Fig. 2.13, was simulated by using aluminum foil in the appropriate region on the core. This bushing core was held vertically in a nonconducting stand (see Fig. 2.15).

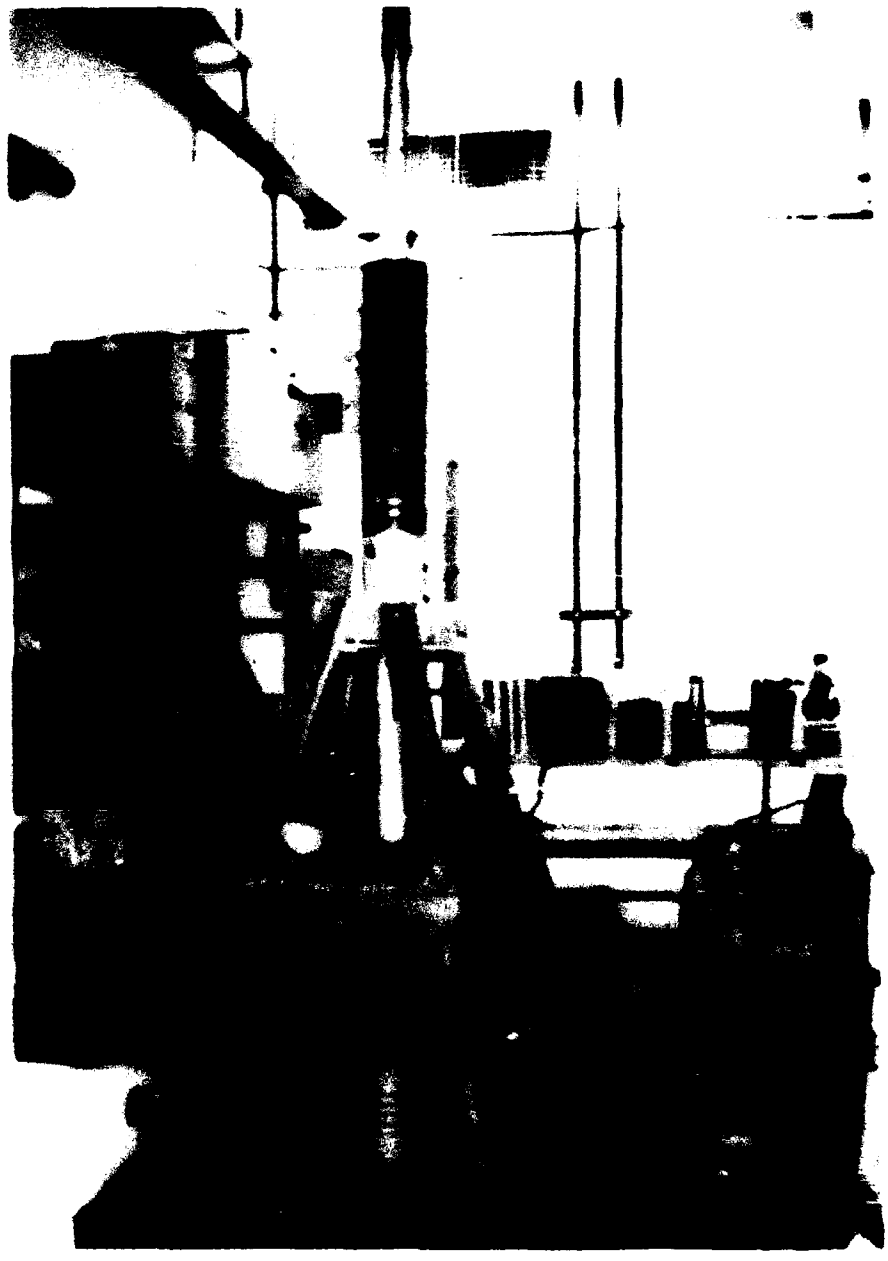

Fig. 2.15. Prepared bushing core in place in a nonconducting stand. The bushing ground sleeve has been simulated by wrapping aluminum foil around the core within the desired region.

2.4 RESULTS OF LOW-VOLTAGE IMPULSE DISTRIBUTION ANALYSIS

This section gives results of low-voltage impulse distribution analysis for shell-form and core-form distribution transformers, core-form power transformers, and 138-kV condenser power-apparatus bushing cores.

2.4.1 Results of Low-Voltage Impulse Distribution Analysis of the Shell-Form Distribution Transformer

Figure 2.16 displays the impulse-voltage distribution for each of the three waves, yielding the maximum voltage appearing at the sensing taps independent of the time of occurrence. For the 1.2- by 50-μs and 100- by 500-ns waves, the voltage difference between any given sensing tap and the second tap point on either side provides a measure of the layer-to-layer voltage stress. The voltage difference between adjacent taps, when divided by the number of turns per layer, will yield a measure of the average turn-to-turn voltage stress because the voltage stress was expected to vary more rapidly. In the case of the 10- by 150-ns wave, the sensing-tap spacing along the winding is not uniform, i.e., near the high-side end of the winding, the taps were spaced as closely as one turn, yielding turn-to-turn stresses. Selected tap points will yield the layer-to-layer stress.

Interpretation of Fig. 2.16 yields:

(a) The highest stress for the 1.2- by 50-μs wave occurs across the turn insulation on the first layer at the high terminal connection between 100% and the first data point. This stress is less than the stress in the same area for either of the other two waves.

(b) The highest stress for the 100- by 500-ns wave also occurs across the turn insulation of the first layer of the primary winding. This stress is about four times that which occurred in the case of the 1.2- by 50-μs wave. The highest layer-to-layer stress occurs between the first and second layers and the second and third layers. This stress is about two times the highest stress determined for the 1.2- by 50-μs wave.

(c) The maximum turn-insulation stress for the 10- by 150-ns wave occurs among the first few turns and among the last few turns of the primary winding. Although not directly obtainable from Fig. 2.16, these stresses are 25 to 50 times those measured for the 1.2- by 50-μs wave. The maximum layer-insulation stress appears between the first and second layers. This stress is about four times that of the 1.2- by 50-μs wave and approximately twice that of the 100- by 500-ns wave.

Those regions identified as having the highest stresses for each of the waves are the regions in which failures are expected when transformers of this design are tested at high impulse voltages.

Caution must be used when interpreting Fig. 2.16. Because of the traveling waves, reflections, and related propagational phenomena, the transformer responds differently to each wave. As the wave penetrates, the winding voltage peaks will occur at different times and at different positions. Hence, voltage measurement at the sensing taps allows a comparison between adjacent and second adjacent tap points only.

The low-voltage impulse distribution measurements did not involve the primary-to-secondary winding voltage division. The winding-to-tank portion of the impulse distribution also was not involved.

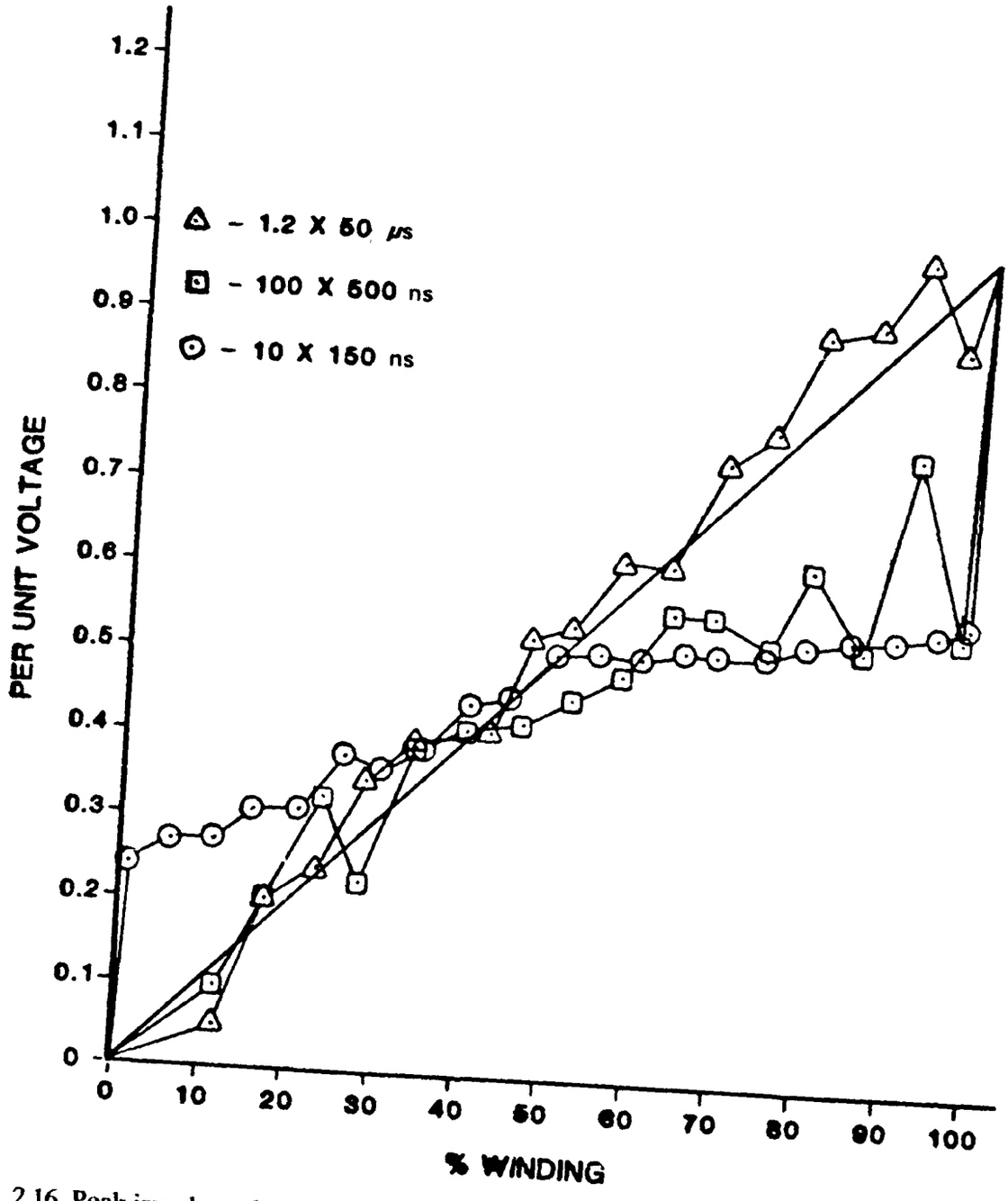

Fig. 2.16. Peak impulse-voltage distribution for the three waves across the shell-form distribution transformer's primary. The straight diagonal line represents uniform voltage distribution.

The low-voltage impulse measurements were used as input to a mathematical model of the shell-form distribution transformer, as discussed in Appendix A.

2.4.2 Results of Low-Voltage Impulse Distribution Analysis of the Core-Form Distribution Transformer

Figure 2.17 displays the low-voltage impulse distribution for each of the three waves, yielding the maximum voltage appearing at the sensing taps, independent of the time of occurrence of that peak.

The core-form distribution transformer had LO-HI winding construction (Fig. 2.17) on each of the two core legs, with cross-over connections between the two halves of the primary. These crossovers occurred at the 25%, 50%, and 75% winding points. A coarse interpretation of the information displayed in Fig. 2.17 can be made as was done for Fig. 2.16, except at the 25%, 50%, and 75% points. The maximum turn-to-turn stresses and the maximum layer-to-layer stresses are very similar to those stresses determined for the shell-form transformer.

Because there was no major difference between the shell-form and the core-form stress levels, and because the primary interest of the project is the insulation-system behavior, no high-voltage testing to failure was performed on the core-form distribution transformer.

2.4.3 Results of Low-Voltage Impulse Distribution Analysis of the Core-Form Power Transformer

Figures 2.18 and 2.19 display the low-voltage impulse distribution for each of the three waves, yielding the maximum voltage appearing at the sensing taps, independent of the time of occurrence of the peak voltage. These voltages appear across a pair of disks, each disk consisting of approximately 24 turns. It was virtually impossible to insert taps or probes either into a disk or at the inner peripheral disk transition points without severely disrupting the dielectric system. The center-start design also prevented any turn-to-turn connections from being made to the first disk without completely destroying the insulation system and severely disrupting the physical placement of the disk. The 27 sensing tap points therefore provide a good measure of the impulse voltage as distributed among the disk pairs only. These measurements were also used for the mathematical modeling of this transformer. The figures displaying the performance of this transformer (Figs. 2.18-2.25) are intended to indicate trends only.

Sections of the first pair of disks were interleaved in manufacturing to assist in making the impulse-voltage distribution more uniform. This technique was also used in the second and third pairs of disks. The first 10 disks were more heavily insulated than were the remainder of the disks. These are common practices in the design and construction of such transformers.

Figures 2.18 and 2.19 show the general distribution of the impulse voltages independent of time. Figures 2.20, 2.22, and 2.24 display the voltages measured on the first fourteen sensing taps as a function of time.

Figure 2.21(a) shows the response at the first sensing tap. A fast Fourier transform (FFT) of the signal detected at the first tap is shown in Fig. 2.21(b). Tabulated values of the frequencies and associated amplitudes are also listed in Fig. 2.21. A major resonance is indicated at 2.5 MHz.

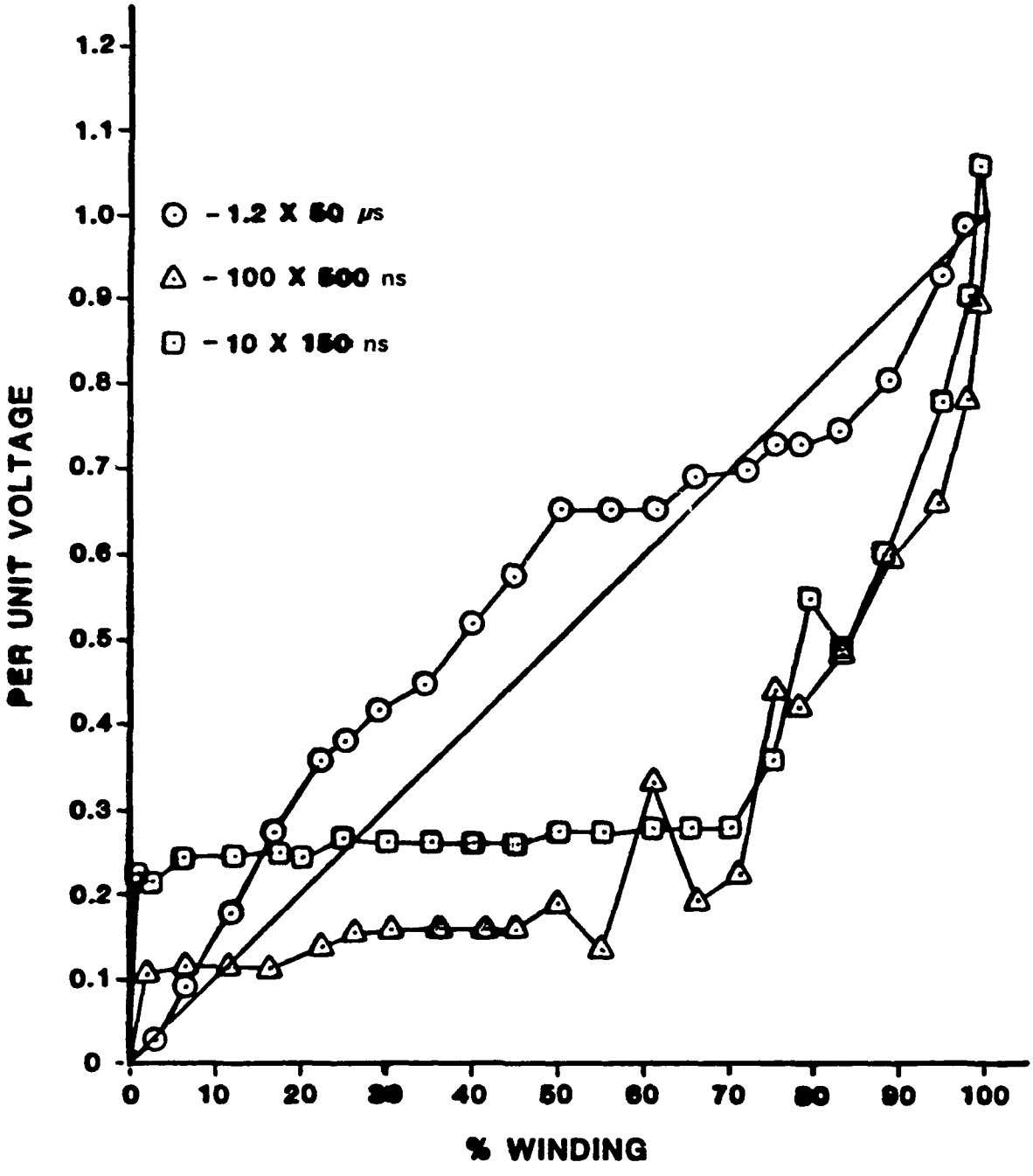

Fig. 2.17. Peak impulse-voltage distribution for the three waves across the core-form distribution transformer primary. The straight diagonal line represents uniform voltage distribution.

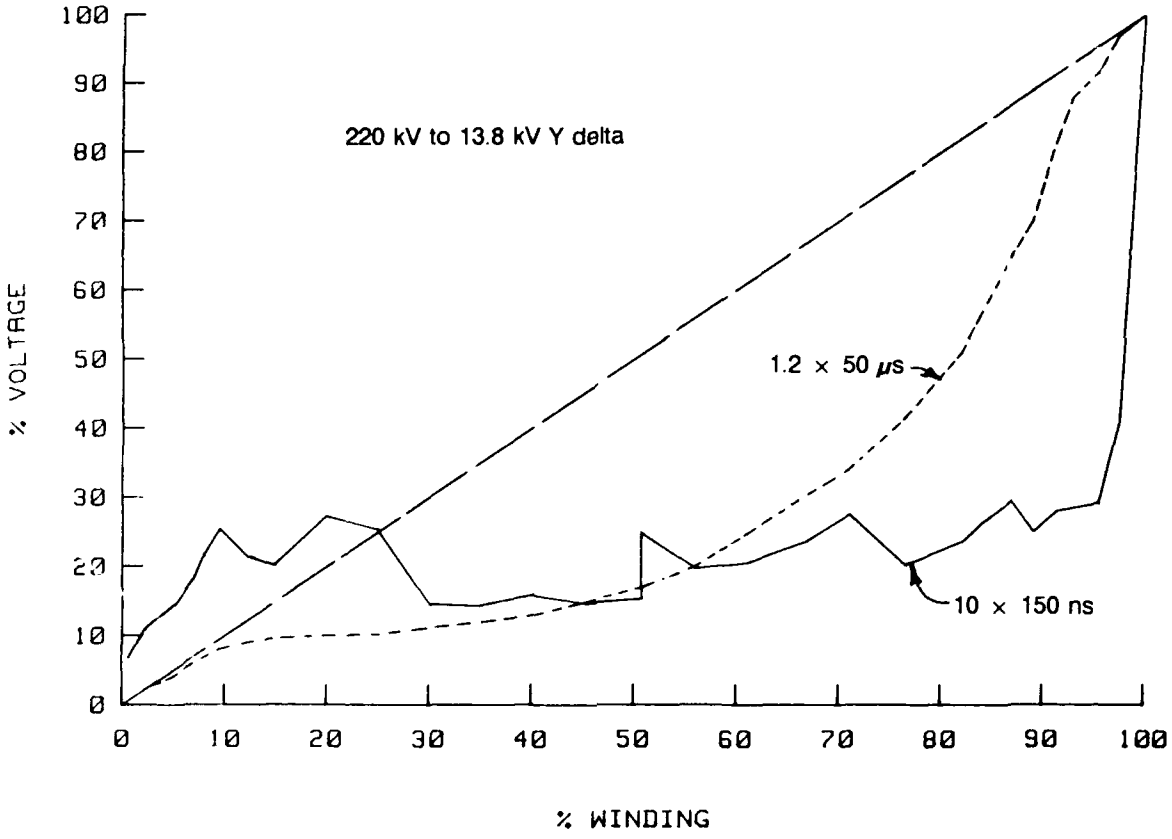

Fig. 2.18. Low-voltage impulse distribution for the primary winding of the core-form power transformer for the 1.2- by 50 μs and 10- by 150-ns waves. The straight diagonal line represents uniform voltage distribution.

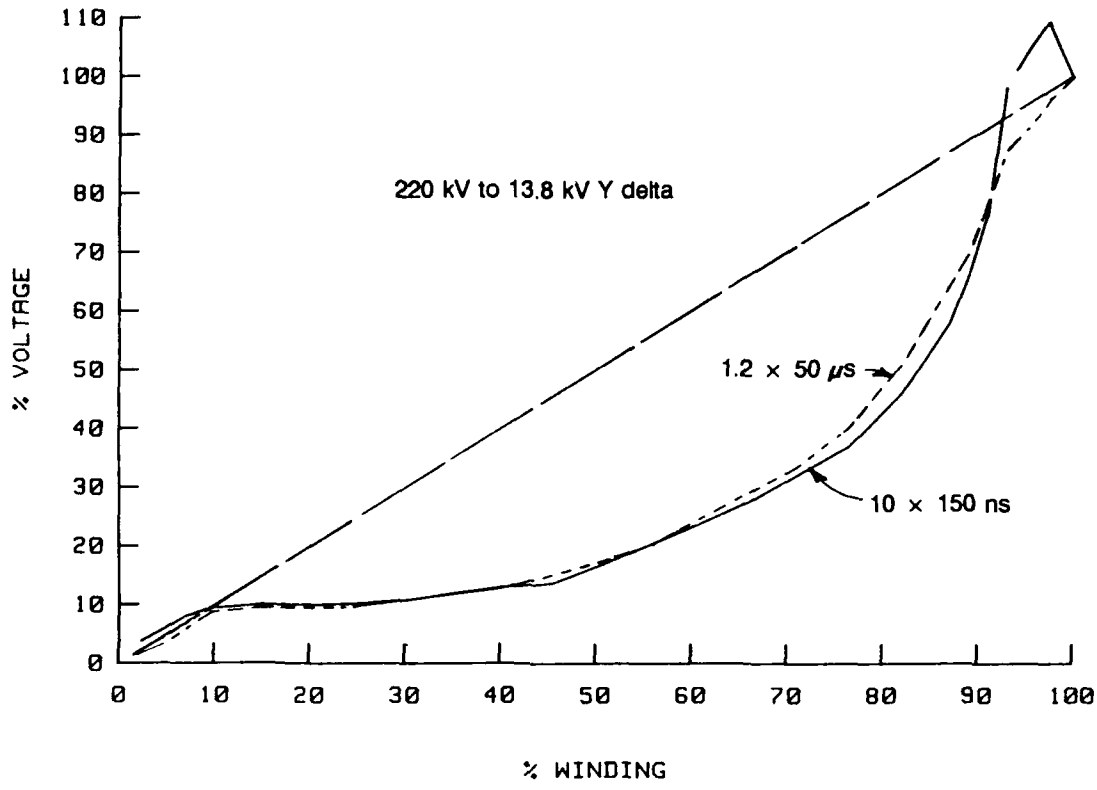

Fig. 2.19. Low-voltage impulse distribution for the primary winding of the core-form power transformer for the 100- by 500-ns wave. The straight line represents uniform voltage distribution.

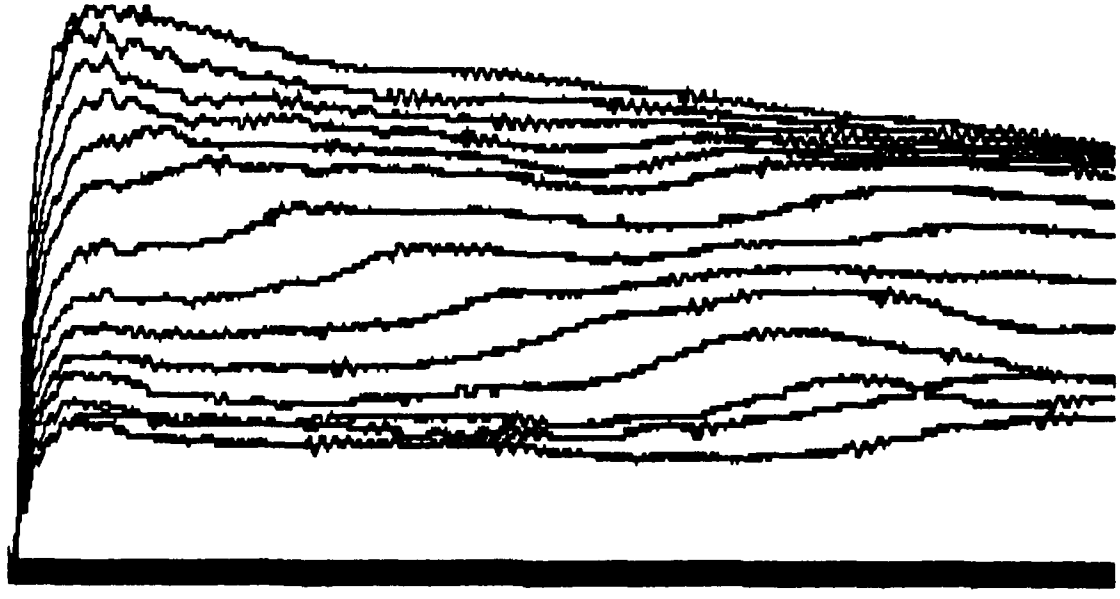

Fig. 2.20. Superimposed 1.2- by 50-μs response traces of the first 14 sensing taps for the primary winding of the core-form power transformer.

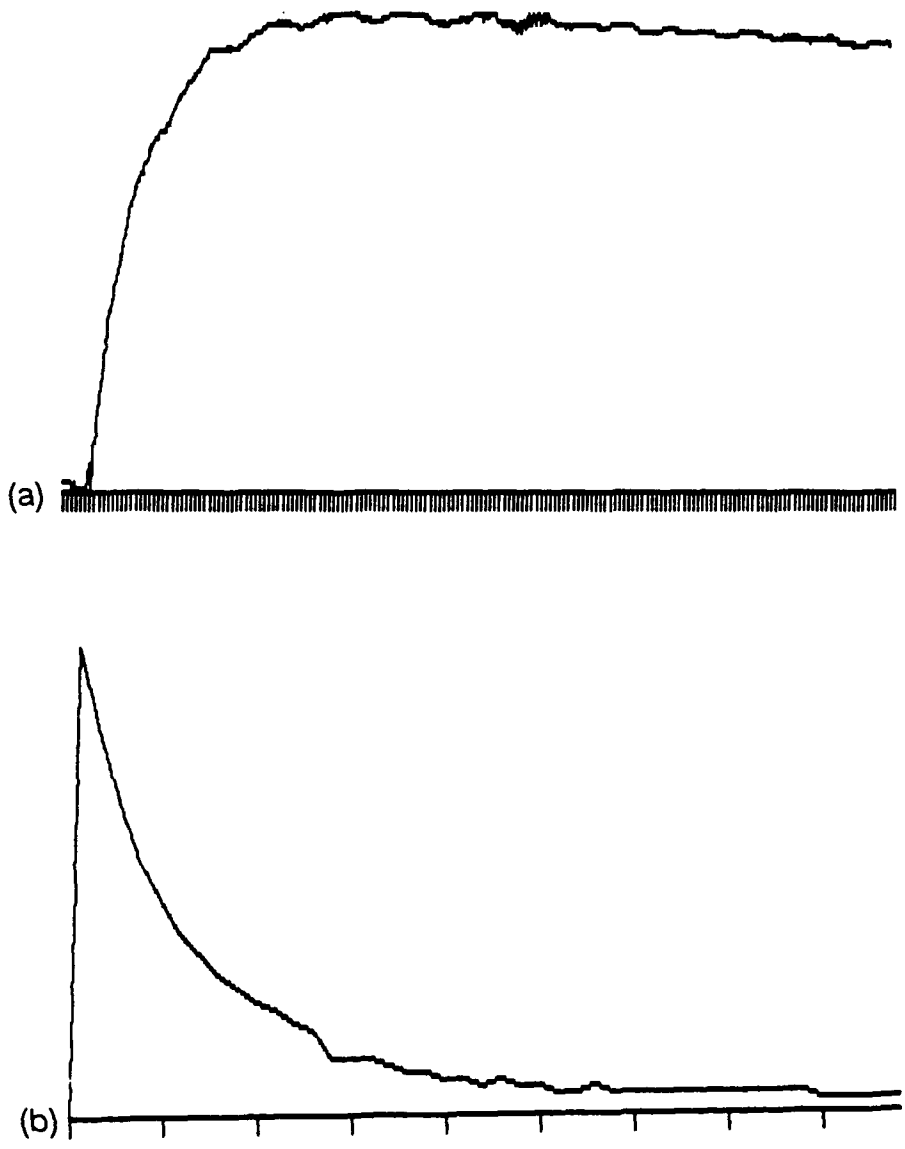

FREQUENCY	AMPL.
1.95E+05	66
3.91E+05	54
5.86E+05	44
7.81E+05	36
9.77E+05	31
1.17E+06	26
1.37E+06	23
1.56E+06	20
1.76E+06	18
1.95E+06	16
2.15E+06	15
2.34E+06	13
2.54E+06	12
2.73E+06	8
2.93E+06	8
3.13E+06	8
3.32E+06	7
3.52E+06	6
3.71E+06	6
3.91E+06	5
4.10E+06	5
4.30E+06	4
4.49E+06	5
4.69E+06	4
4.88E+06	4
5.08E+06	3
5.27E+06	3
5.47E+06	4
5.66E+06	3
5.86E+06	3
6.05E+06	3
6.25E+06	3
6.45E+06	3
6.64E+06	3
6.84E+06	3
7.03E+06	3
7.23E+06	3
7.42E+06	3
7.62E+06	3
7.81E+06	2
8.01E+06	2

Scale factors for (a): amplitude is linear, time scale is 1 μs per major division.
Scale factors for (b): amplitude is linear, frequency scale is 1 MHz/division.

Fig. 2.21. (a) First sensing-tap response, 1.2- by 50-μs wave. (b) Fast Fourier transform of this response and tabulated frequency and amplitude values.

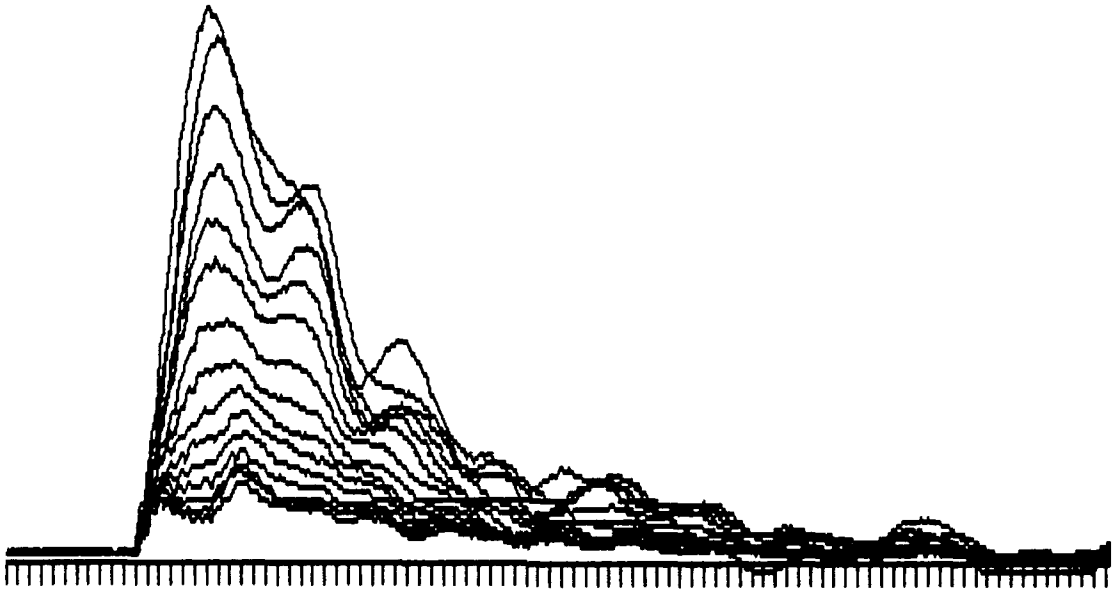

Fig. 2.22. Superimposed 100- by 500-ns traces of the first 15 sensing taps for the core-form power transformer's primary winding.

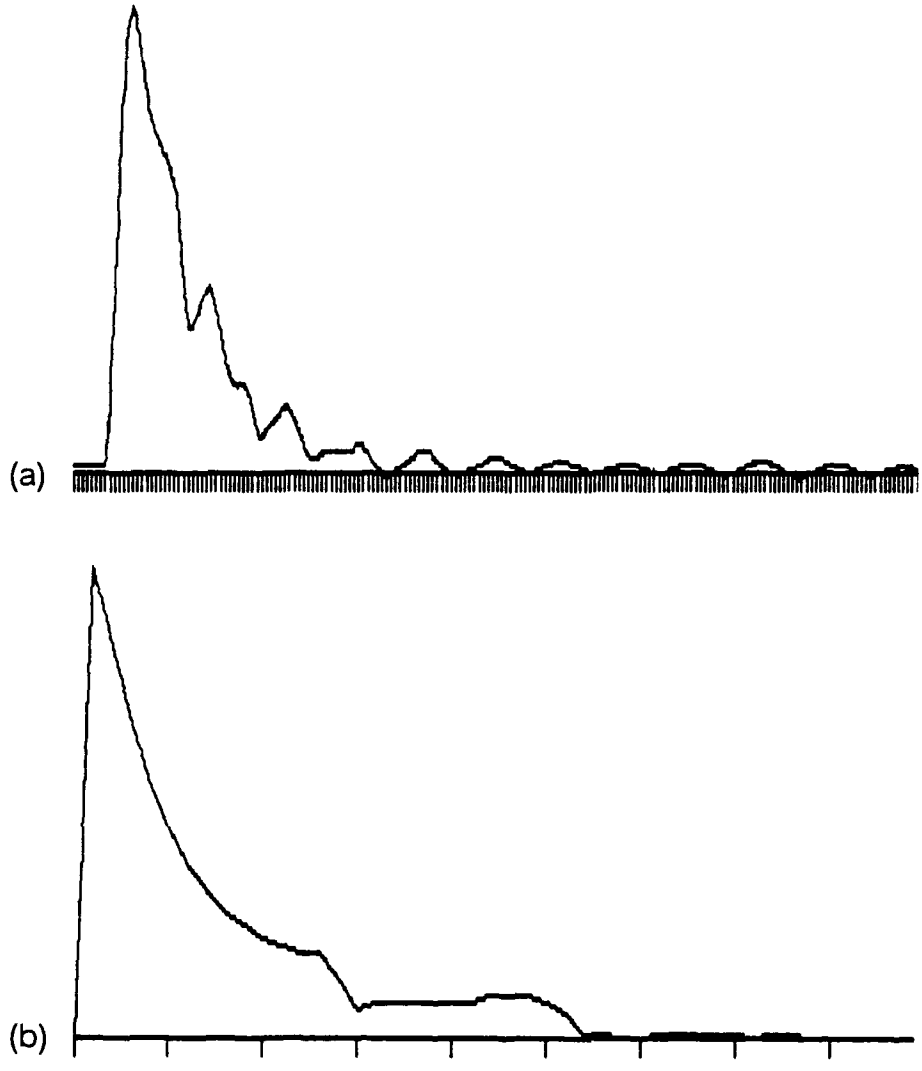

FREQUENCY	AMPL.
1.95E+05	75
3.91E+05	63
5.86E+05	51
7.81E+05	41
9.77E+05	34
1.17E+06	28
1.37E+06	24
1.56E+06	20
1.76E+06	18
1.95E+06	16
2.15E+06	15
2.34E+06	14
2.54E+06	14
2.73E+06	10
2.93E+06	5
3.13E+06	6
3.32E+06	6
3.52E+06	6
3.71E+06	6
3.91E+06	6
4.10E+06	6
4.30E+06	7
4.49E+06	7
4.69E+06	7
4.88E+06	6
5.08E+06	4
5.27E+06	1
5.47E+06	1
5.66E+06	0
5.86E+06	0
6.05E+06	1
6.25E+06	1
6.45E+06	1
6.64E+06	1
6.84E+06	1
7.03E+06	0
7.23E+06	1
7.42E+06	1
7.62E+06	0

Scale factors for (a): amplitude is linear, time scale is 200 ns per major division.
Scale factors for (b): amplitude is linear, frequency scale is 1 MHz/division.

Fig. 2.23. (a) First sensing-tap response, 100- by 500-ns wave. (b) Fast Fourier transform of this response and tabulated frequency and amplitude values.

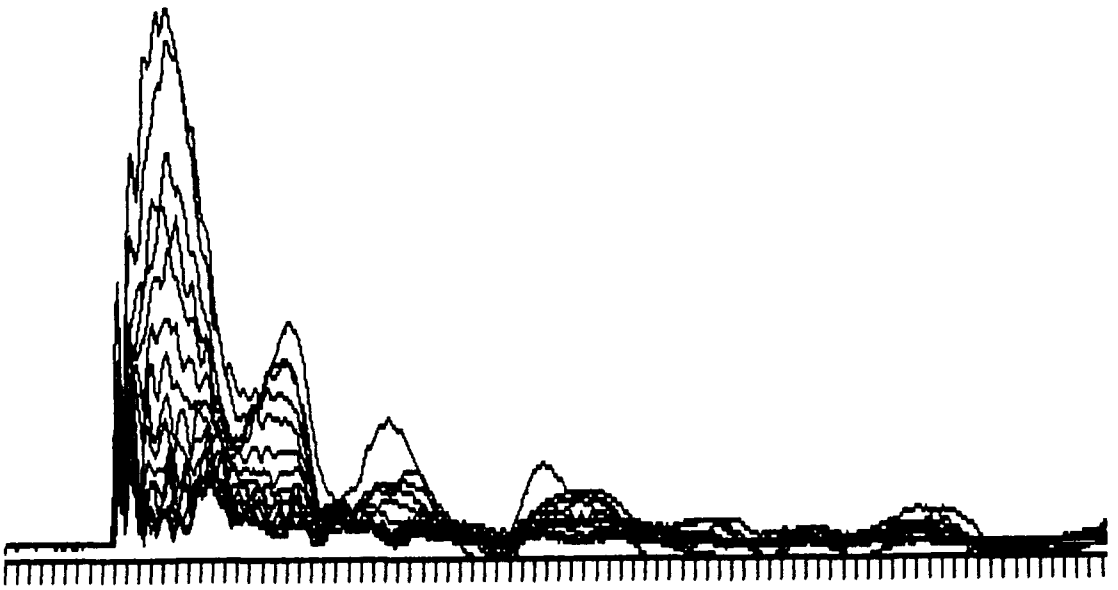

Fig. 2.24. Superimposed traces from the first fifteen sensing taps for the 10- by 150-ns wave.

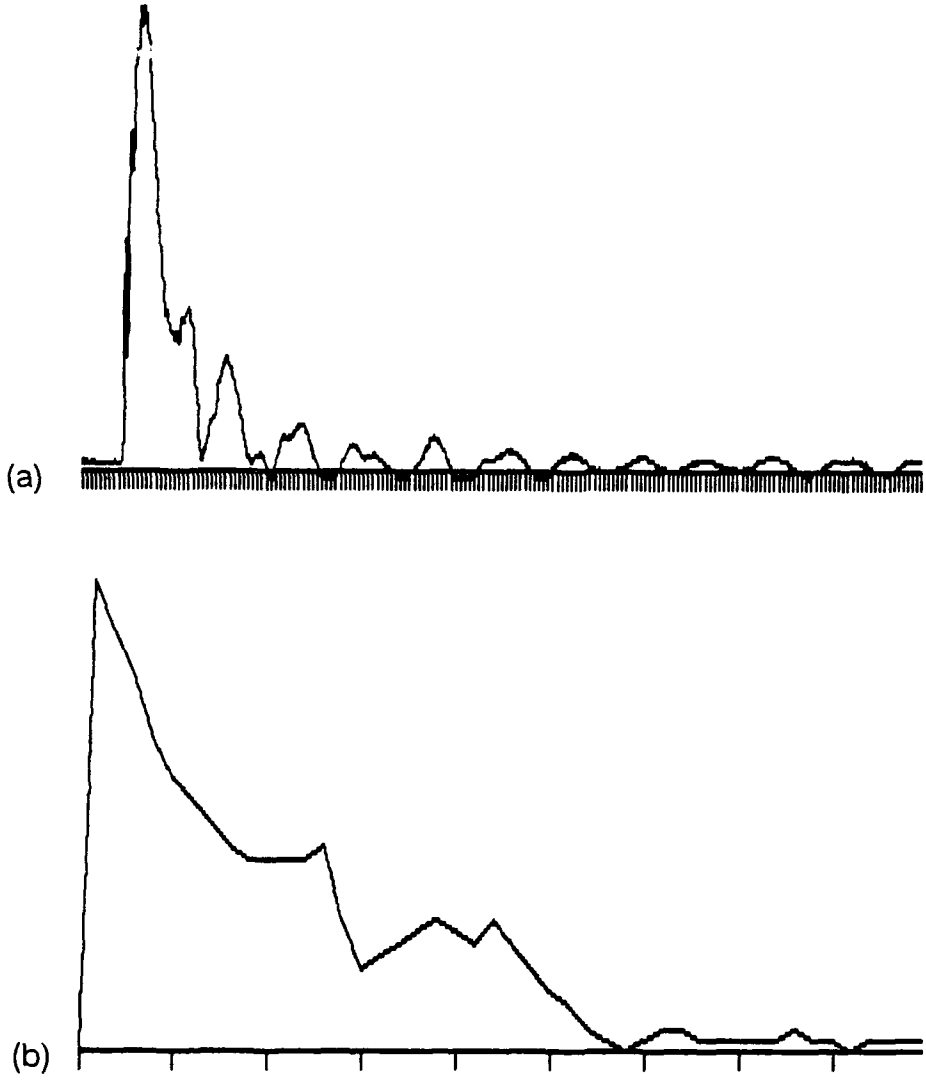

FREQUENCY	AMPL.
1.95E+05	39
3.91E+05	35
5.86E+05	31
7.81E+05	26
9.77E+05	23
1.17E+06	21
1.37E+06	19
1.56E+06	17
1.76E+06	16
1.95E+06	16
2.15E+06	16
2.34E+06	16
2.54E+06	17
2.73E+06	11
2.93E+06	7
3.13E+06	8
3.32E+06	9
3.52E+06	10
3.71E+06	11
3.91E+06	10
4.10E+06	9
4.30E+06	11
4.49E+06	9
4.69E+06	7
4.88E+06	5
5.08E+06	4
5.27E+06	2
5.47E+06	1
5.66E+06	0
5.86E+06	1
6.05E+06	2
6.25E+06	2
6.45E+06	1
6.64E+06	1
6.84E+06	1
7.03E+06	1
7.23E+06	1
7.42E+06	2
7.62E+06	1
7.81E+06	1
8.01E+06	0

Scale factors for (a): amplitude is linear, time scale is 200 ns per major division.
Scale factors for (b): amplitude is linear, frequency range is 1 MHz/division.

Fig. 2.25. (a) First sensing-tap response for the 10- by 50-ns wave. (b) Fast Fourier transform of this response and tabulated frequency and amplitude values.

Resonances are observed in Fig. 2.20. For the 1.2- by 50-μs wave, a maximum voltage difference occurs at approximately 2.7 μs between sensing taps 7 and 8. This voltage, however, is measured across four disks rather than two disks as is the case for sensing taps 1 through 6. Adjacent sensing taps 7 through 14 each span four disks. Sensing taps 14 and 15 are on either side of the tap changer, set on position A.

The largest voltage differences measured at any given time appear between sensing points 5 and 6 at approximately 1.4 μs and between 3 and 4 at approximately 0.4 μs.

Figure 2.22 displays the superimposed trace from the first fifteen sensing taps for the 100- by 500-ns wave. Figure 2.23(a) shows a 2.7-MHz oscillation in the first sensing-tap signal. An FFT of the signal detected at the first tap is shown in Fig. 2.23(b), as are tabulated values of the resulting frequencies and their amplitudes. Resonances occur at 2.5 MHz and 4.3 MHz. The latter resonance had not previously been observed, and contributes to a greater than 1/unit magnitude measured at sensing tap points 2 and 3. The maximum voltage difference observed is between sensing taps 4 and 5 in the time span of 70 150 ns.

Figure 2.24 displays the superimposed traces from the first fifteen sensing taps for the 10- by 150-ns wave. A damped 5.4-MHz oscillation can be observed. By far the greatest voltage difference appears between sensing taps 1 and 2, the first four disks of the primary. Higher-frequency resonances that have been excited can be observed in the FFT, Figs. 2.25(a) and (b), and can be identified in the tabulated frequencies and amplitudes. Resonances are found at 2.5 MHz, 3.7 MHz, and 4.3 MHz.

Those regions with the greatest voltage difference are expected to be the location of insulation system breakdown when they are subjected to high-voltage impulses.

2.4.4 Results of the Low-Voltage Impulse Distribution Analysis of a 138-kV Condenser-type Power-Apparatus Bushing Core

This core used 31 foils separated by (typically) 11 layers of kraft sheet. A potential-tap lead was attached to foil 30 and brought out through a hole in foil 31 to the normally shorted-to-ground potential-tap connector. The dielectric system therefore consisted of 31 concentric foils separated by a number of layers of insulating paper, with a length of flexible small-diameter wire connected from foil 30 to ground, and with foil 31 grounded through a short length of flexible lead.

Figure 2.26 displays the impulse voltage distribution for each of the three waves. It will be noted that all of the curves do not start at 100%. The output of the low-voltage source used for these measurements was maintained at a constant value corresponding to 100% for the 1.2- by 50-μs wave. The necessarily long lead between the source and the specimen resonated with the specimen capacitance to produce the observed increase in voltage at the specimen terminal.

The impulse voltage distribution is governed almost entirely by the distributed capacitances of the bushing, the distributed inductance having little effect. Because only the relative response of the bushing to each waveform is important, and wave-to-wave comparisons are not performed, no impact is made on the analysis. For the 1.2- by 50-μs surge test, minor deviations from a uniform voltage distribution occur among foils 4 to 12. The greatest voltage difference, 5%, occurs between foils 12 and 13. This voltage difference is of little significance.

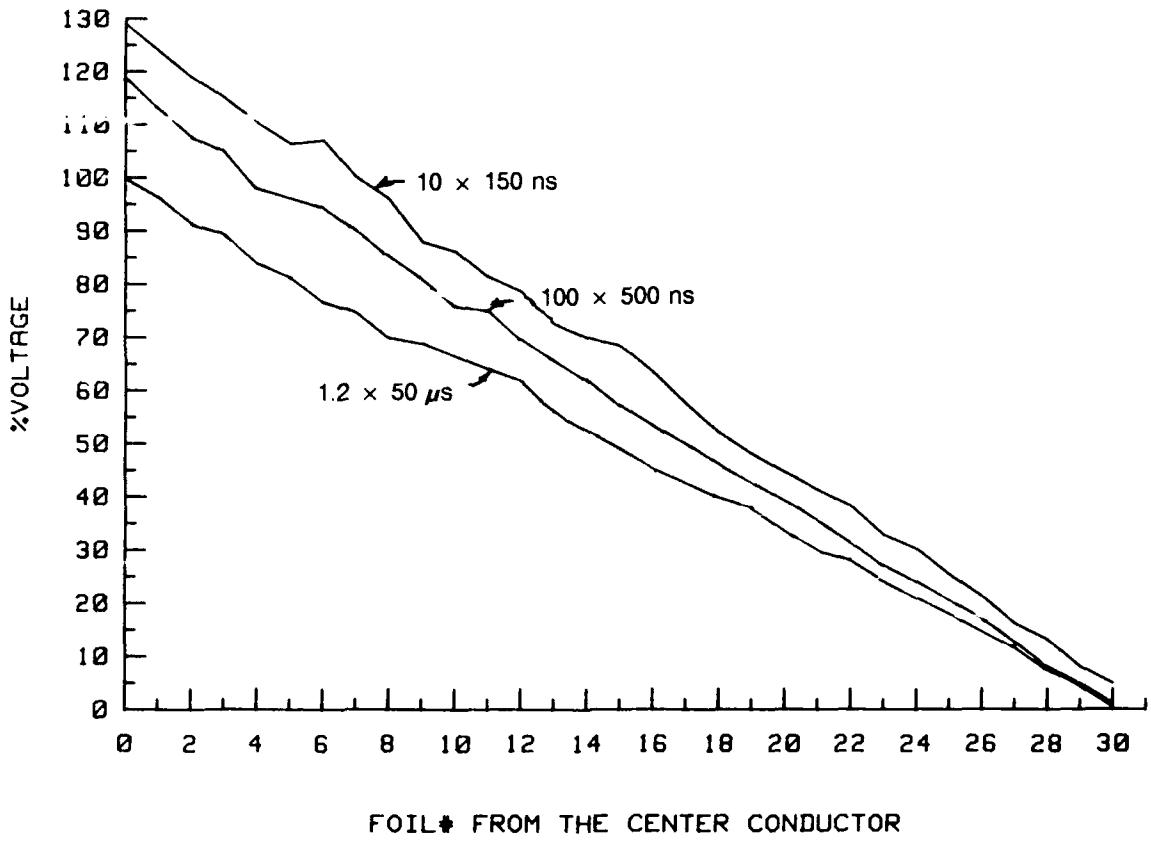

Fig. 2.26. Impulse-voltage distribution for the three waves on a 115-kV, 800-A, 550-kV-BIL power-apparatus bushing core.

The impulse-voltage distribution for the 100- by 500-ns wave also shows essentially uniform voltage distribution except for the drop across the connecting lead between foils 30 and 31. Minor deviations from uniform distribution occur among foils 3 to 11. The maximum foil-to-foil voltage difference is approximately 5.5%, occurring between foils 3 and 4.

The impulse-voltage distribution for the 10- by 150-ns wave also shows minor deviations from a uniform distribution for foils 5 to 14. There is, however, a pronounced increase in the voltage drop across the lead from foil 30 to ground. The maximum foil-to-foil voltage difference is 5.5% between foils 8 and 9.

Collectively, minor deviations from uniform voltage distribution appear on foils 3 to 15 for all three waves. Foils 1, 2, and 16 to 30 have essentially uniform voltage distribution independent of waveshape. The voltage drop across the flexible lead from foil 30 to ground varies directly with the frequency and amplitude of the applied wave.

These low-voltage impulse distribution analyses were later used to evaluate specimens subjected to high-voltage impulses.

3. IMPULSE ONLY: MODELS, EXPERIMENTS, AND RESULTS

3.1 WAVESHAPES

Upon completion of the low-voltage impulse testing of distribution transformers, power transformers, and power apparatus bushings, a series of high-voltage impulse tests were conducted at McGraw-Edison Technical Center and at Maxwell Laboratories in San Diego. These tests again used the nominal waveshapes discussed earlier, but the tests were performed with sufficient voltage and energy levels to produce insulation damage. Primary emphasis was on conducted rather than radiated waves.

We wanted to use the same three waveshapes on these full-size specimens as we used for the low-voltage impulse distribution experiments. Little difficulty was encountered in establishing 1.2- by 50-μs waves in the laboratories. However, the capacitance of the specimens was large enough to affect the shape of the 100- by 500-ns wave and seriously affect the shape of the 10- by 150-ns wave. The effects are most noticeable on the wavefronts, where the desired 100-ns front ranged from 100 to 200 ns and the desired 10-ns front ranged from 25 to 100 ns, depending on the specimen and the test site. The range of the 500-ns tail was 500 to 600 ns. The range of the 150-ns tail was 200 to 600 ns, particularly where circuits producing 1000 kV were used.

The major impact of these faster waves on the insulation systems is more closely related to the steepness of the wavefronts. However, the duration of the wave tail can have a lesser impact.

High-voltage experiments were performed at two magnitude ranges. The lower of these ranges, 120-400 kV, was used to provide critical impulse flashover (CIFO) data for correlation between SFSD-impulse and lightning-impulse behavior.

The higher range, 800-1100 kV, was dictated by NEMP considerations abstracted from literature in the public domain.

3.2 FACILITIES

The majority of the 1.2- by 50-μs lightning-impulse work and some of the 100- by 500-ns and 10- by 150-ns work was conducted in the high-voltage laboratory at the Thomas A. Edison Technical Center. An overview of this facility is shown in Fig. 3.1. Capabilities include a conventional 2100-kV, 34-kJ Marx generator; wave-shaping components; instrumentation; and adequate space to permit evaluation of the largest specimens. The normal instrumentation was supplemented by the high-speed data-acquisition system that was discussed in Section 2.1.3.

The majority of the 10- by 150-ns impulse work was performed at Maxwell Laboratories in San Diego, California, using a HEMP simulator modified to accept specimens of the size required by this project. A layout of this laboratory is shown in Fig. 3.2. The fundamental design is that of a completely shielded source—an oil-insulated Marx generator—inside a shielded generator chamber that directly abuts a totally shielded test cell. A small 400-kV, 10-kJ, 1.2- by 50-μs Marx generator (Hipotronics) was also available at this facility. Available instrumentation consisted primarily of a number of oscilloscopes with liquid-resistor voltage dividers or liquid-resistor shunts. These oscilloscopes were

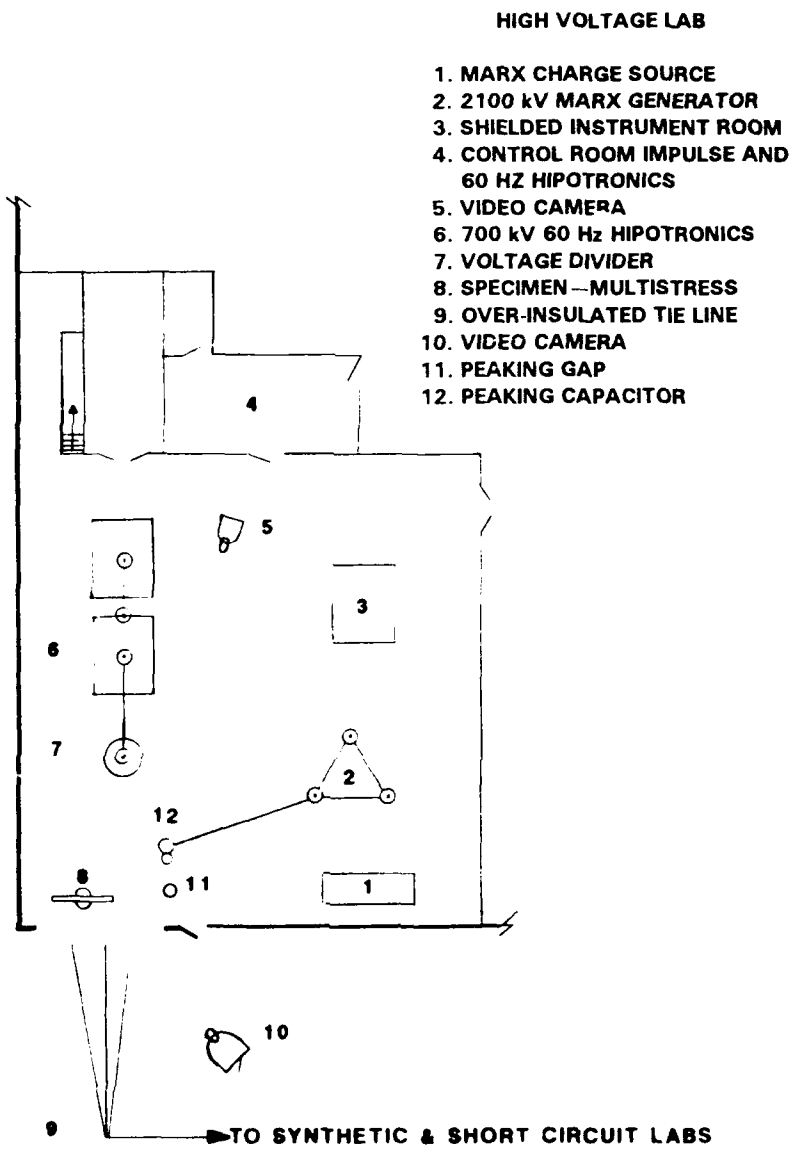

Fig. 3.1. Overview of the McGraw-Edison Technical Center as arranged for the impulse testing.

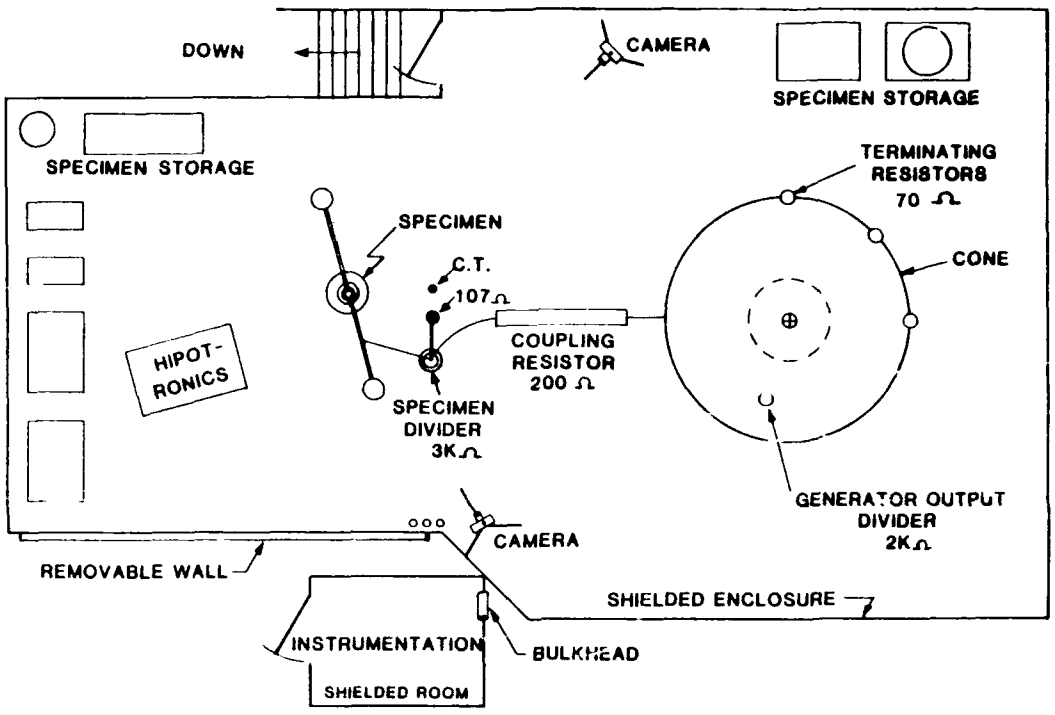

Fig. 3.2. Steep-front short-duration impulse laboratory layout at Maxwell Laboratories.

housed in a separate shielded room. This equipment was supplemented by the high-speed instrumentation equipment that was previously discussed and by several photographic cameras. The test circuit is shown in Fig. 3.3. In situ calibrations were performed using 25-cm spheres and standard sphere-gap calibration curves.[2] For calibration of the faster impulses, information from ref. 3 was used.

3.3 DISTRIBUTION TRANSFORMERS

Five pole-mount, oil-insulated, 75-kVA, 14.4/24.9-kV→120/240-V, shell-form distribution transformers having 125-kV basic insulation levels (BILs) were selected as representative samples of the oil/paper/enamel insulation system. (See Fig. 3.4.) The windings were of the LO-HI-LO type, using design voltage stresses at the high end of the range of present practice. The number of samples was limited by available funding; until the sample failed, however, a large number of tests were performed on each sample.

These transformers were subjected to a series of 125–130-kV 1.2- by 50-μs impulses to verify the ability of the unit to withstand 100% of rated BIL and to determine the neutral current characteristics.[4] The neutral current characteristics helped detect failure during the evaluation.

STEEP FRONT SHORT DURATION
IMPULSE GENERATOR SCHEMATIC

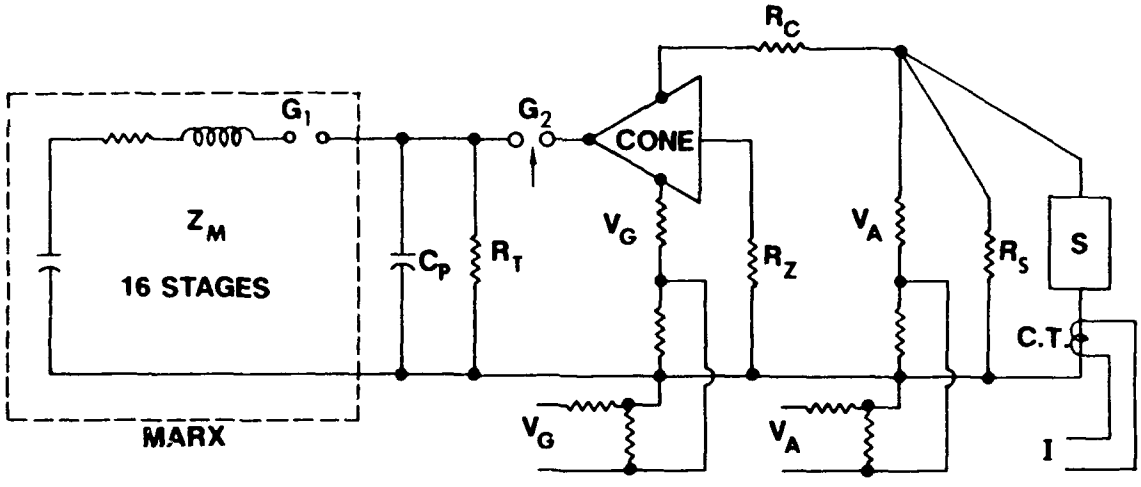

Z_M = MARX IMPEDANCE
G_1 = MARX GAPS
C_P = PEAKING CAPACITOR
R_T = TAIL RESISTOR
G_2 = OUTPUT SWITCH
C.T. = MINIATURE CURRENT XMFR
CONE = MONOCONE ANTENNA

V_G = GENERATOR OUTPUT VOLTAGE DIVIDER
R_Z = TERMINATING RESISTANCE
R_C = COUPLING RESISTANCE
V_A = SPECIMEN VOLTAGE DIVIDER
R_S = SHUNT RESISTANCE
S = SPECIMEN

Fig. 3.3. Steep-front short-duration impulse generator and test-circuit schematic.

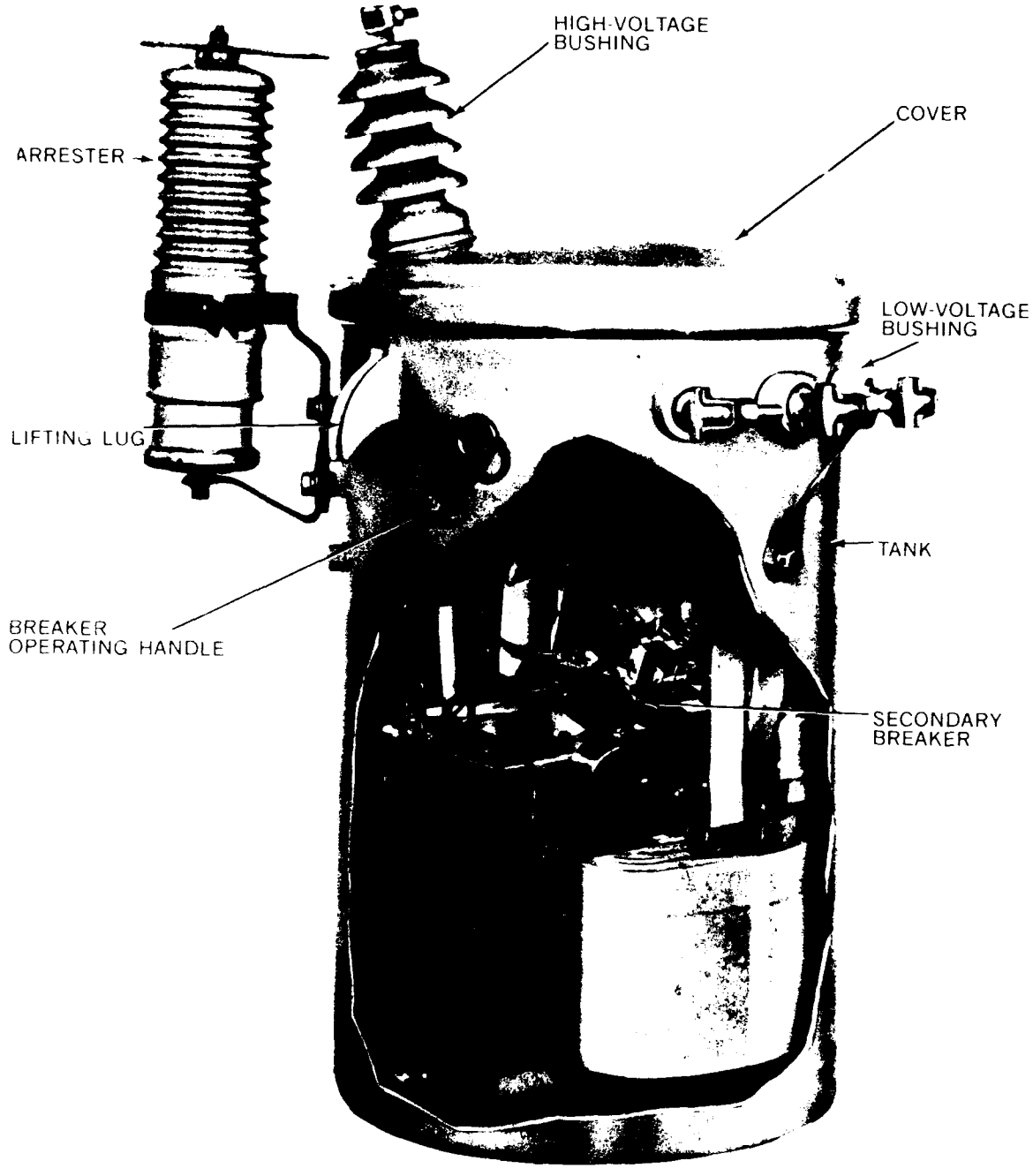

Fig. 3.4. Cutaway of pole-mount 75-kV distribution transformer with a tank-mounted externally gapped arrester.

All five of the transformers of this group successfully passed the 125-kV full-wave BIL tests. Subsequently, in combination with an 18-kV distribution-class lighting arrester, each of these transformers was to be subjected to 1100-kV impulses of each of the three waveshapes, first with the lightning arrester tank-mounted and direct-connected. If the transformer was not damaged or did not fail after having been exposed to a total of 20 shots, an external gap was inserted between the arrester and the transformer's high-side terminal, and the transformer was then subjected to a maximum of another 20 shots. Unless otherwise noted, these shots were taken in 4 groups of 5 shots, alternating impulse polarity for each successive group of 5 shots. If there again was no failure of the transformer, the arrester was removed from the tank, mounted on a cross-arm, and connected to the transformer tank ground and high-side terminal with a lead of about 3 m. See Fig. 3.5 for distribution transformers with various mounting arrangements for lighting arresters.

The summary data for the 1.2- by 50-μs BIL tests can be found in Appendix B.1.

3.3.1 Results of 1.2- by 50-μs Impulse Tests on Distribution Transformers

All specimens passed the 125-kV full-wave BIL without arresters. Specimen 2 subsequently failed at 126 kV while a series of neutral current tests were being made.[4] The failure started near the corner of the winding, went from the outer edge of the outer layer of the primary (there being a preexisting tear in the margin of the primary-layer insulation), and then crossed the primary-secondary barrier to the adjacent edge of the innermost turn of the outer secondary winding. The preexisting tear, which apparently occurred during manufacture, reduced the FO path from primary to secondary by approximately 1 cm, or approximately 25% of the design path. Consequently, insulation strength was reduced and a failure occurred at this point. No other failures, either turn-to-turn or layer-to-layer, were found.

3.3.2 Results of 100- by 500-ns Impulse Tests on Distribution Transformers

For this simple distribution transformer subjected to multiple shots of 100- by 500-ns impulses, no failures were observed during 20 shots with the lightning arrester tank-mounted and direct-connected. Subsequently, no failures were observed during 29 shots with an external gap between the tank-mounted arrester and the transformer terminal.

In a final test series performed with no arrester, this transformer failed on the fourth negative-polarity shot at a crest voltage of 229 kV. One failure was a puncture through the layer margin between the first-to-second-layer transition and the adjacent edge of the third layer near a winding corner. This failure was a combination of puncture of the layer insulation and a multiplicity of tracks across the layer margin. A second failure occurred between the last and next-to-last winding layers at approximately the midpoint of the second-from-last layer. (See Fig. 3.6.) Both of these locations are high electrical stress regions as determined by the low-voltage impulse distribution analysis. There is no immediate explanation for multiple failure locations in this sample.

3.3.3 Results of 10- by 150-ns Impulse Tests on Distribution Transformers

For this simple distribution transformer, only negative 10- by 150-ns impulses were used. No failures were observed during the 20 shots with the lightning arrester tank-mounted and direct-connected.

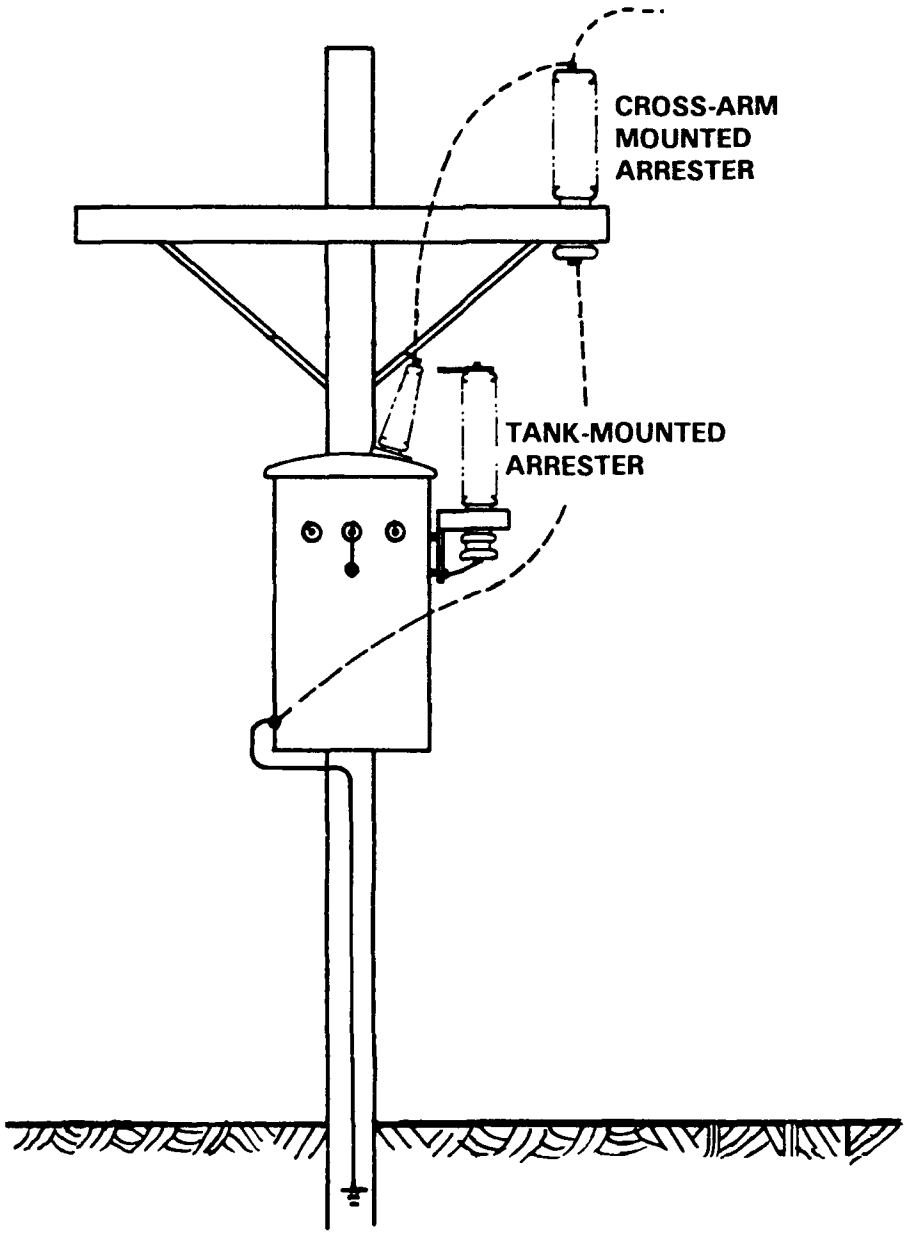

Fig. 3.5. Gapped tank-mounted arrester and crossarm-mounted arrester, typical of field installations. For tank-mounted, direct-connected applications, the gap between the transformer bushing and the arrester is shorted out.

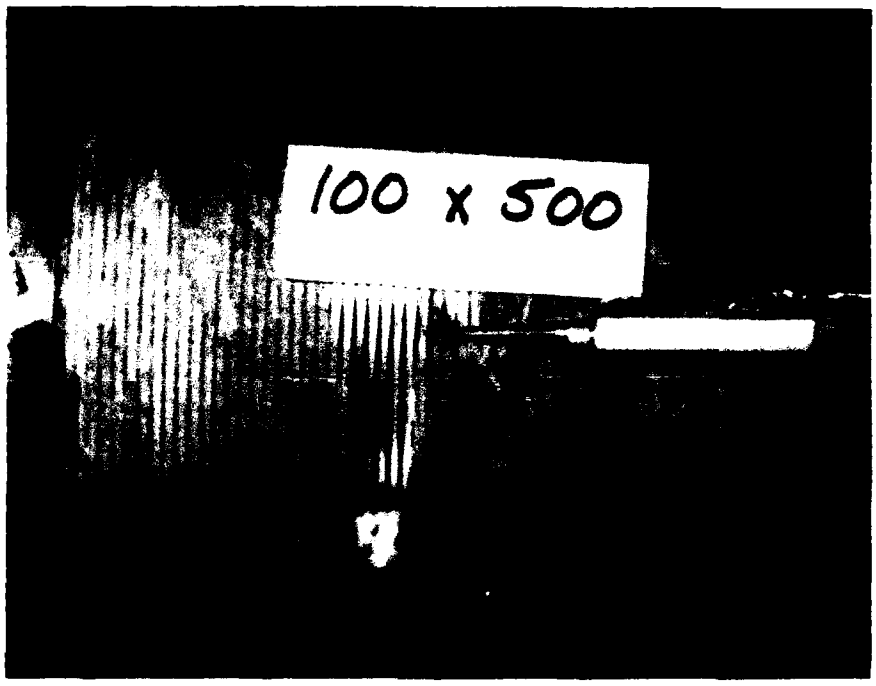

Fig. 3.6. Failure of 75-kVA distribution transformer at the approximate midpoint between the second-to-last and last layers, caused by 100- by 500-ns impulse.

With the arrester tank-mounted and externally gapped, a failure was encountered on the tenth shot. The failure occurred at a crest voltage of 205 kV, the fifth shot of the second 5-shot sequence. This failure involved both turn-to-turn and layer-to-layer failures. The turn-to-turn failure involved the first three turns of the primary at a location one-half turn from the high-side input lead near a corner of the winding. Layer-to-layer puncture also occurred here. On closer examination, an additional failure was found at the transition from layers 1 and 2 to the adjacent edge of layer 3. The barrier insulation was not punctured in this failure. Figure 3.7 shows the location of the punctured layer insulation. These failures occurred in the high-stress region as predicted by the low-voltage impulse distribution analysis. Again, no immediate explanation for the multiple failures is readily available.

3.4 LIGHTNING ARRESTERS

Lightning arresters perform a major role in the protection of transmission and distribution systems. Little has been published about the response of lightning arresters to the SFSD impulses involved in this program.

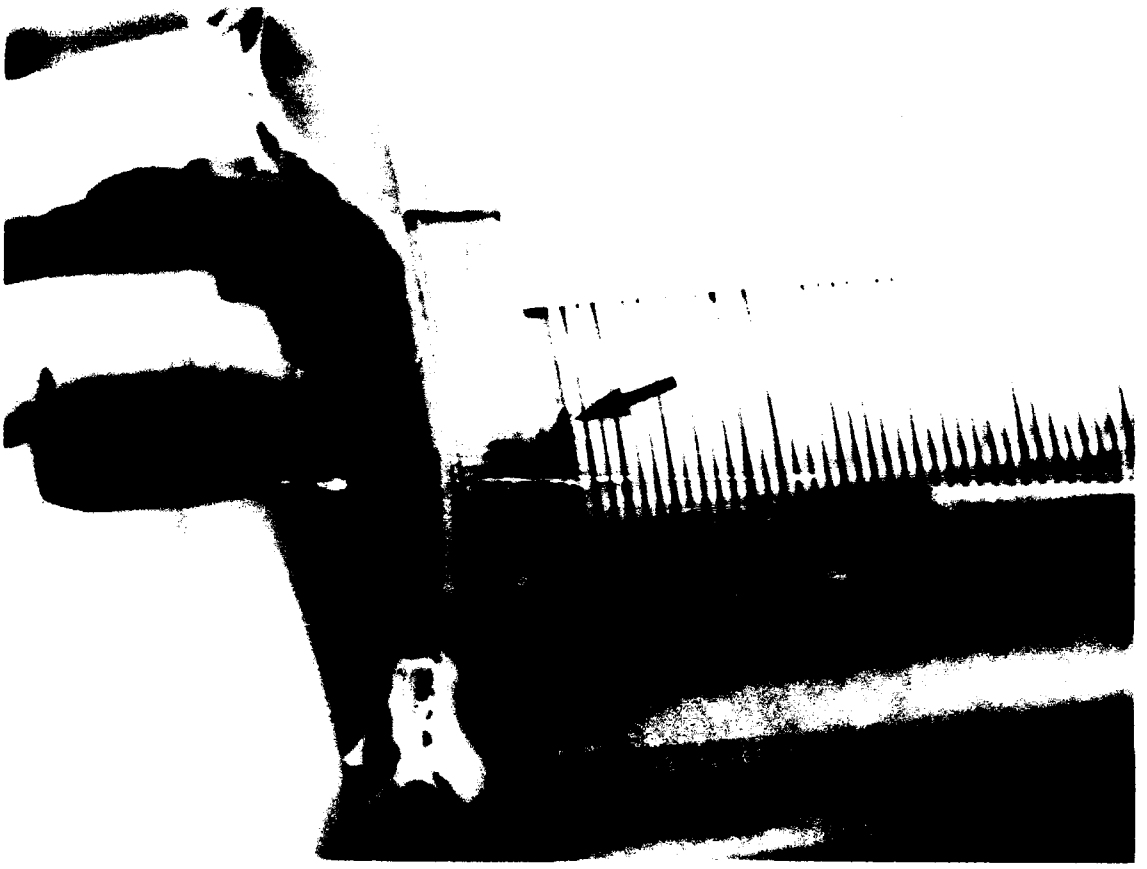

Fig. 3.7. Punctured layer insulation in 75.0-kVA transformer.

Approximately 98% of all the lightning arresters installed are of the bonded silicon carbide (SiC) type with graded internal gaps that are either lumped or distributed. External gaps are sometimes used in addition. Metal-oxide varistor (MOV) arresters, which are approximately 2% of all installed arresters, may use external gaps, internal shunting gaps, or no gaps. The no-gap version is by far the most popular. These MOV arresters have supplanted the SiC units as the standard.

Accordingly, specimens representative of those installed on transmission and distribution lines were exposed to impulses of the three waveshapes at each of two levels. The lower of the two levels yields the critical impulse sparkover (CISO). The higher level yields the FOWFO. Additional full-wave impulse measurements were made following the steep-front impulses to determine if any degradation had occurred. Little effort was expended on the distribution-class MOV arrester.

The same proviso relative to the achieved waveshapes for the three waves, as stated previously (see Section 3.1), also applies here, i.e., the capacitance of the test specimen alters the waveshape.

Although the level of protection of the arresters is found to be higher for SFSD impulses, the insulation strength of the transformer also rises with SFSD impulses. The degree of protection is

determined by the response characteristics of the insulation and the arrester. Direct-connected arresters provided protection for all tests and for all waveshapes tested, but failures occurred with both gapped and remotely placed arresters.

3.4.1 Station-Class Arresters

Figure 3.8 shows 96 kV on SiC arresters with distributed, graded, internal gaps and no external gap. Test results are given in Table 1. The results of tests on 96-kV MOV arresters having no gaps are shown in Table 2.

3.4.2 Distribution-Class Lightning Arresters

Typical distribution-class arresters are shown in Figs. 3.9 and 3.10. Impulse test results for 30-kV internally gapped SiC arresters and 30-kV MOV arresters without gaps are shown in Tables 3 and 4. The FOW values vs time to crest are plotted in Fig. 3.11.

3.5 LINE INSULATION

Porcelain components have been used for structural line insulation for many years, with service life frequently exceeding 60 years. Once installed, the porcelain components normally remain in service until some external influence causes electrical and/or mechanical failure. Wet-process porcelain provides the backbone structural insulation and has done so for the last 30 to 40 years. Prior to that time, dry-process porcelain was used. Dry-process porcelain proved to be susceptible to electrical puncture failures from the transients on the power system. This was confirmed by standard full-wave and chopped-wave impulse tests commonly used for evaluation and quality control.

Porcelain components are used at all voltage levels. Higher-voltage insulation is frequently achieved by stacking lower-voltage-rated units. Representative types of porcelain structural insulating members are post, pin, cap-and-pin, and suspension insulators.

For this project all specimens were representative of structural insulating components presently in use on utility systems. The specimens chosen were removed from service and were free of any visible electrical or mechanical damage.

To the extent possible, all specimens were evaluated in physical configurations identified in applicable ANSI/IEEE standards. Five samples of each of the following four types of porcelain/air structural-insulation devices were used.

- Apparatus, post-type insulator, 95-kV BIL, ANSI C29.9-1983. See Fig. 3.12. Construction: Electrical-grade wet-process porcelain column with metal attachment fittings on both ends. The porcelain/fitting interface is filled with a low-melting-point metal alloy.

- Pin-type insulator, Radio Freed, class 55-6, 150 radio-influence voltage BIL, ANSI C29.1-1982. See Fig. 3.13. Construction: Electrical-grade wet-process porcelain with integral porcelain-threaded socket. Mounted on a "lead-head" pin.

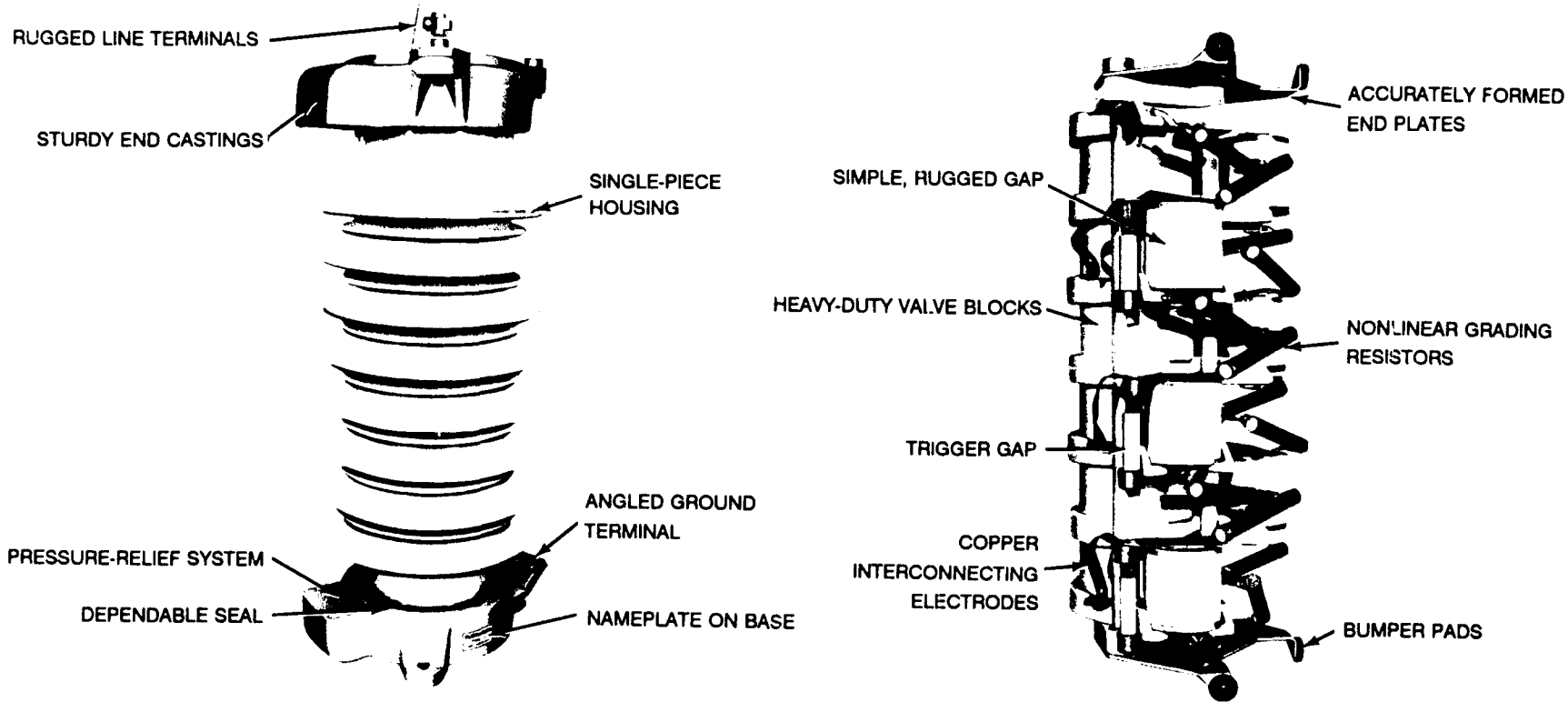

Fig. 3.8. (a) Overview and (b) cutaway of a silicon-carbide type station-class lightning arrester representative of those in service. The type of nonlinear grading resistor and gap construction varies among different manufacturers.

Table 1. Results of tests on 96-kV SiC station-class arresters

WAVEFORM	INITIAL CISO[a] (kV)	FOW SPARK-OVER (kV)	1.2 × 50 μs CISO AFTER SFSD[b] (kV)	RATIOS	
				$\frac{\text{CISO(SFSD)}}{\text{CISO(1.2×50)}}$	$\frac{\text{FOW(SFSD)}}{\text{FOW(1.2×50)}}$
1.2 × 50 μs	190	219	N/A	N/A	N/A
100 × 500 ns	294	333	184	1.6	1.5
10 × 150 ns	314	918	191	1.6	4.2

[a]Initial: Tests of CISO prior to SFSD impulse tests.
[b]After: Tests of CISO using 1.2- by 50-μs impulse after SFSD impulse to test for degradation.

NOTE: The data summary can be found in Appendix B, Section B.3.1.

Table 2. Results of tests on 96-kV MOV station-class arresters

WAVEFORM	INITIAL CISO[a] (kV)	FOW SPARKOVER (kV)	1.2 × 50 μs CISO AFTER SFSD[b] (kV)	RATIOS	
				$\frac{\text{CISO(SFSD)}}{\text{CISO(1.2×50)}}$	$\frac{\text{FOW(SFSD)}}{\text{FOW(1.2×50)}}$
1.2 × 50 μs	170	208	N/A	N/A	N/A
100 × 500 ns	202	---	172	1.2	---
10 × 150 ns	248	685	162	1.5	3.3

[a]Initial: Tests of CISO prior to SFSD impulse tests.
[b]After: Tests of CISO using 1.2- by 50-μs impulse after SFSD impulse to test for degradation.

NOTE: The data summary can be found in Appendix B, Section B.3.2.

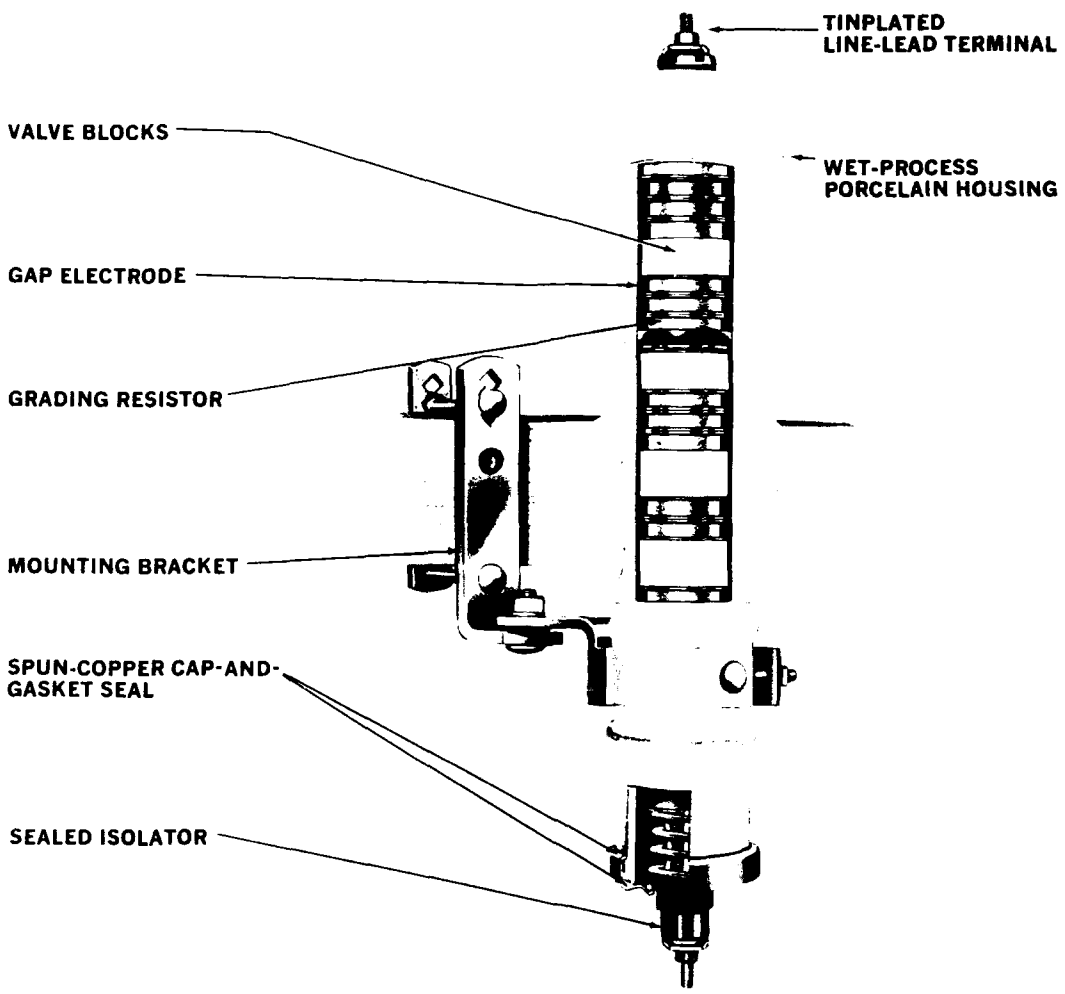

Fig. 3.9. Cutaway of a silicon-carbide distribution-class arrester having distributed groups of nonlinear resistor-graded internal gaps.

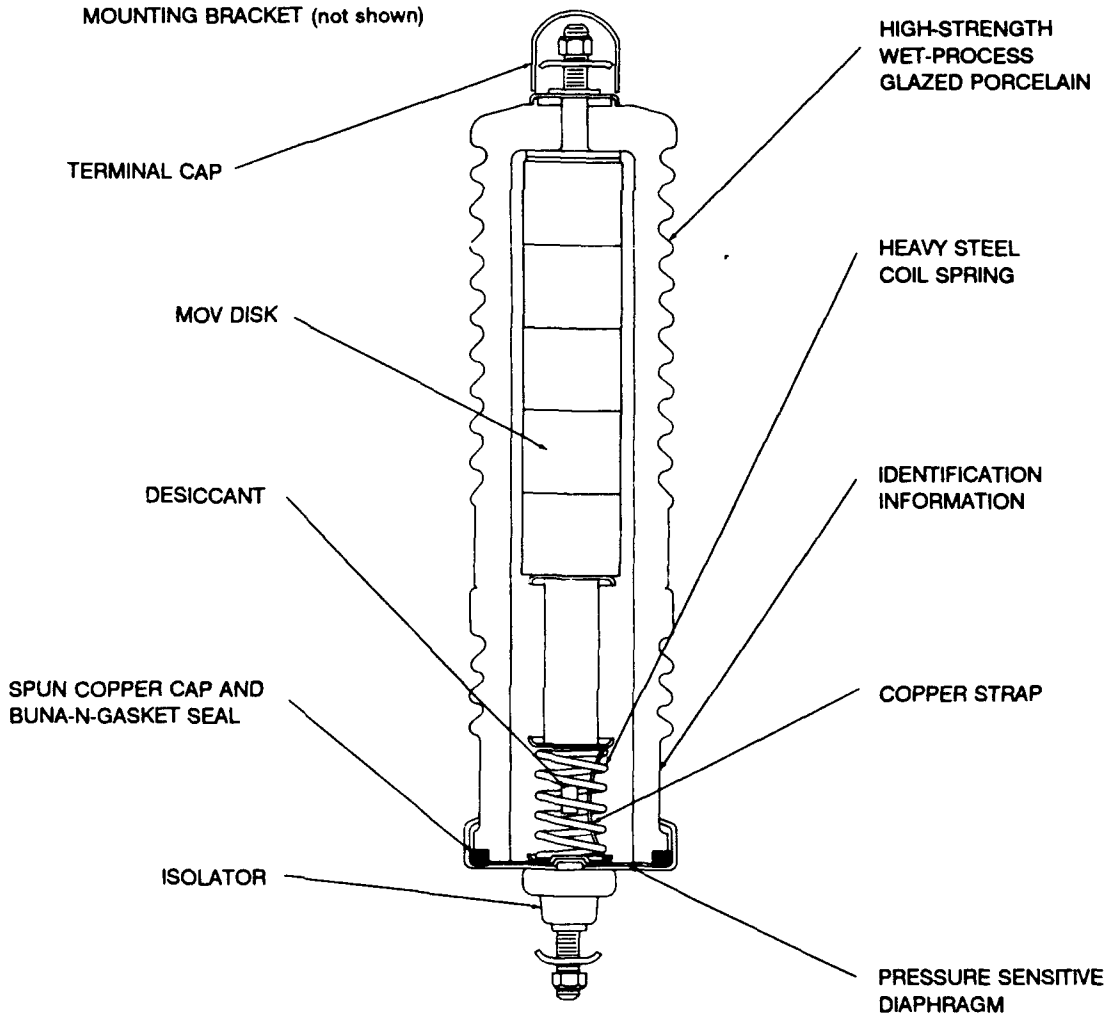

Fig. 3.10. Cutaway of a metal-oxide varistor distribution-class lightning arrester representative of those currently being installed. This arrester has no internal gaps.

Table 3. Results of tests on 30-kV SiC distribution-class arresters

WAVEFORM	INITIAL CISO[a] (kV)	FOW SPARKOVER (kV)	1.2 × 50 μs CISO AFTER SFSD[b] (kV)	RATIOS	
				$\frac{\text{CISO(SFSD)}}{\text{CISO(1.2×50)}}$	$\frac{\text{FOW(SFSD)}}{\text{FOW(1.2×50)}}$
1.2 × 50 μs	75	81	N/A	N/A	N/A
100 × 500 ns	85	187	76	1.1	---
10 × 150 ns	148	483	76	2.0	6.0

[a]Initial: Tests of CISO prior to SFSD impulse tests
[b]After: Tests of CISO using 1.2- by 50-μs impulse after SFSD impulse to test for degradation.

NOTE: The data summary can be found in Appendix B, Section B.2.1.

Table 4. Results for 30-kV MOV arrester with no gaps

WAVEFORM	EQUIV. CISO	EQUIV. FOW	RATIO
			$\frac{\text{FOW(10×150)}}{\text{CISO(1.2×50)}}$
1.2 × 50 μs	80 kV	---	5.5
10 × 150 ns	---	436 kV	

NOTE: The data summary can be found in Appendix B, Section B.2.2.

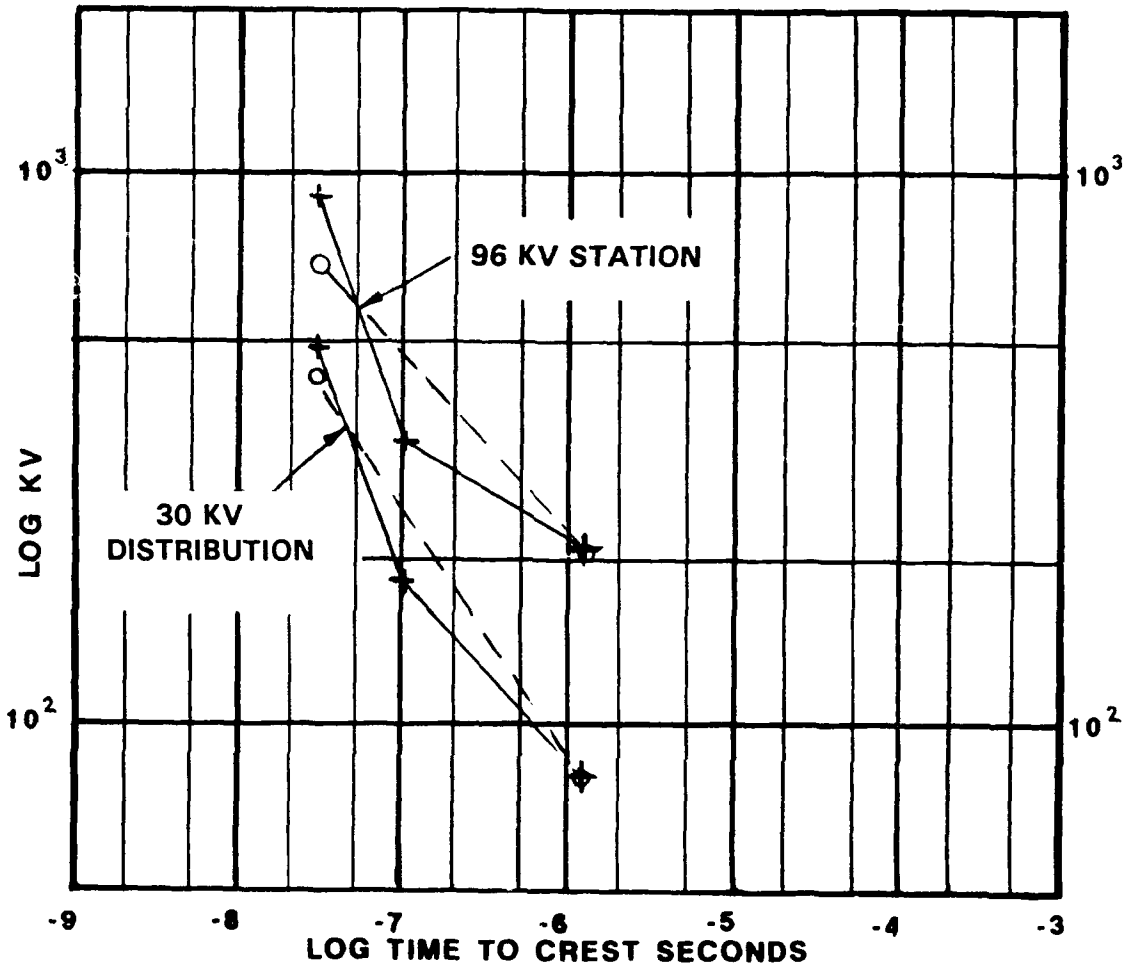

Fig. 3.11. Front-of-wave sparkover for 30-kV silicon-carbide and MOV distribution-class arresters, and 96-kV silicon-carbide and metal-oxide varistor station-class arresters vs time-to-crest.

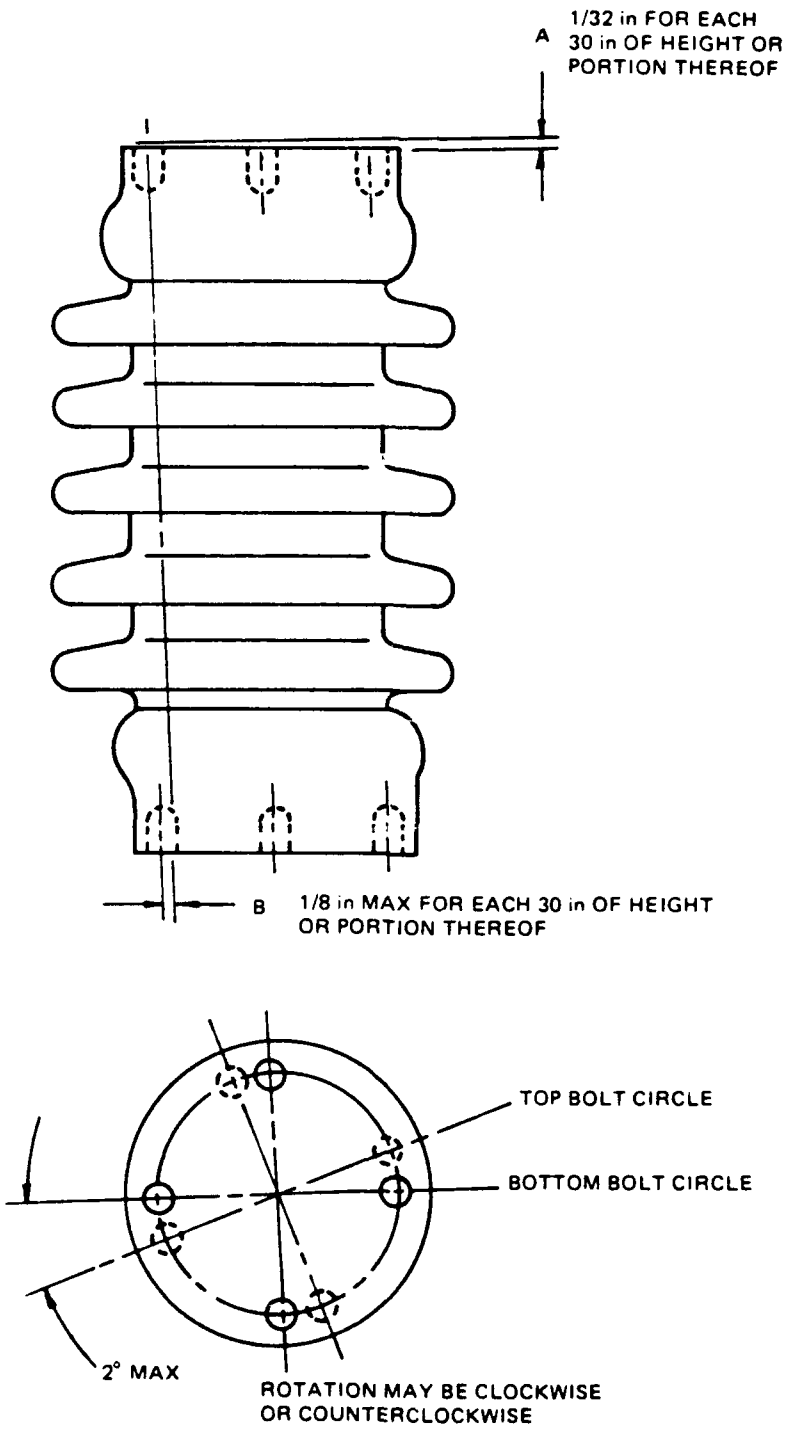

NOTES:
(1) All dimensions are measured at bolt circle.
(2) Tolerance applies to individual units.

Fig. 3.12. Outline of post-type apparatus insulators, per ANSI C29.9-1983, used for this project. (a) Side view and (b) top view.

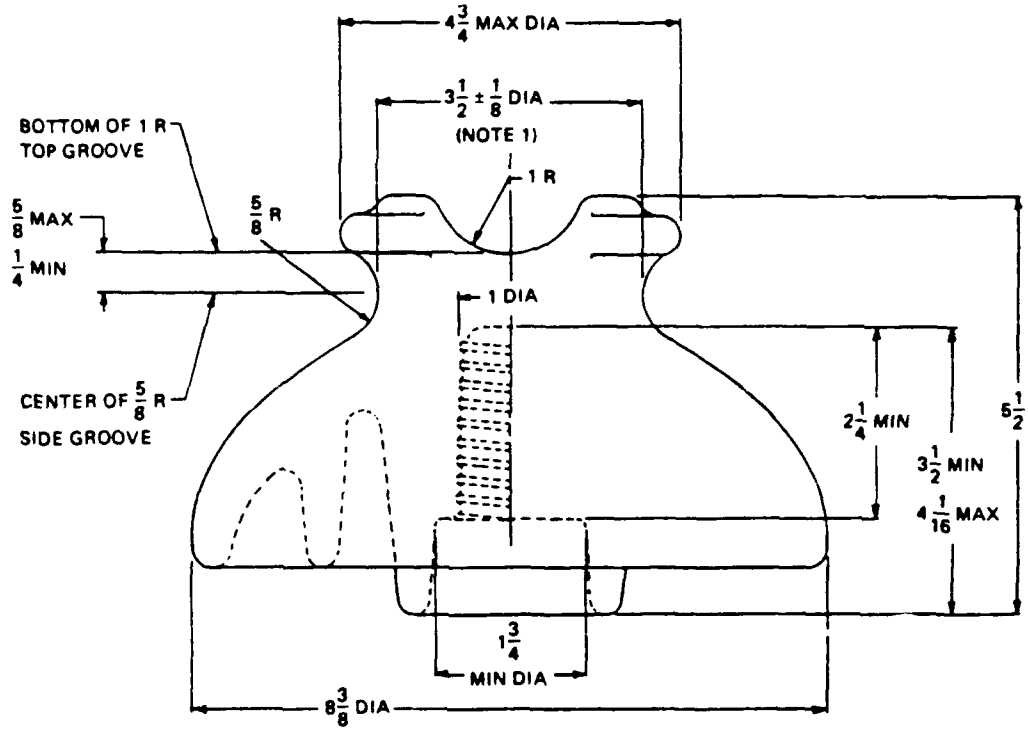

NOTES:

(1) "J" neck.

(2) All dimensions are in inches.

(3) If high-resistance coatings are applied to the insulator, such coatings shall be considered as effective leakage surfaces, and the distance over them shall be included in the leakage distance.

(4) The side-wire groove shall seat a mandrel with a diameter of 1-1/8 inches but shall not seat a mandrel with a diameter of 1-7/16 inches. The top-wire groove shall seat a mandrel with a diameter of 1-3/4 inches.

	Rating	See American National Standard C29.1-1982, Section:
Dimensions		
Leakage distance, inches	15	2.5.2
Dry-arcing distance, inches	8	2.5.3
Minimum pin height, inches	7-1/2	–
Mechanical Values		
Cantilever strength, pounds (kilonewtons)	3000 (13)	5.1.3
Electrical Values		
Low-frequency dry flashover, kilovolts	100	4.2
Low-frequency wet flashover, kilovolts	50	4.3
Critical impulse flashover, positive, kilovolts	150	4.7
Critical impulse flashover, negative, kilovolts	170	4.7
Low-frequency puncture voltage, kilovolts	135	4.11
Radio-Influence Voltage Data		
Low-frequency test voltage, rms to ground, kilovolts	22	4.9
Maximum RIV at 1000 kHz		
Radio freed, microvolts	100	4.9
Plain, microvolts	8000	4.9

Fig. 3.13. (a) Outline and (b) specifications for ANSI class 55-6 pin-type insulators used.

- Apparatus, cap-and-pin type, 125-kV BIL, ANSI C29.8-1980. See Fig. 3.14. Construction: Electrical-grade wet-process porcelain shell with metal cap and metal mounting pin. Both metal/porcelain interfaces are composed primarily of Portland cement.

- Suspension-insulation class 52-3, ball-and-socket type, and class 52-4, clevis-and-pin type. 125-kV BIL, ANSI C29.2-1983. See Fig. 3.15. Construction: Electrical-grade wet-process porcelain shell with socket cap-and-ball or clevis-and-pin suspension hardware. Both metal/porcelain interfaces are primarily Portland cement.

3.5.1 Tests

The post and cap-and-pin insulators were mounted on a 10-in. by 16-in. aluminum channel that was mounted in turn on a wooden crossarm. The simulated conductor was fastened appropriately to the insulator top (see Fig. 3.16). The pin insulators were mounted directly on the crossarm. The suspension insulators were hung inverted, with appropriate hardware and the simulated conductor, using the floor of the shielded enclosure as the reference plane.

Lightning impulses having a nominal waveshape of 1.2 by 50 μs were applied at discrete voltage levels to establish and/or confirm the BIL value. See Fig. 3.17 for a typical lightning-impulse wave. See Fig. 3.18 for specimen traces. Steep-front short-duration impulses were then applied to determine the withstand/FO value. Lightning impulses were again applied to determine the change, if any, in that characteristic. Five specimens of each type were used.

Open-shutter Polaroid photographs of the specimens were taken on all 1100-kV SFSD impulses and on most but not all low-level SFSD "BIL" impulses. Simultaneous voltage and current oscillographic traces were taken to confirm FO and/or puncture.

The FOs for the lightning and low-SFSD impulse waves occurred either at crest voltage or shortly thereafter. All FOs for the 1100-kV SFSD impulse occurred on the wavefront for the post, pin, single-disk suspension, and cap-and-pin insulator specimens.

All insulator specimens used a 10-ft length of 3/4-in. thin-wall conduit terminating in 12-in.-diam spheres to simulate the presence of an installed conductor.

All instrumentation leads from the EMP impulse generators and specimen voltage and current sensors were routed to a common bulkhead in the wall of the shielded instrumentation room. (See Fig. 3.2.) The instrumentation itself was the LeCroy package consisting of 6880 and TRB828C Digitizers, 6103 Amplifier, MM8104 Memory, and 6010 Controller, connected to a Compaq™ Portable Computer with a plotter/printer. This equipment was described in Section 2.2.1. It was supplemented by the multi-oscilloscope installation.

Steep-front short-duration voltage sensing was accomplished by using copper-sulfate dividers. Current sensing was achieved by using 2-ns- and 5-ns-risetime miniature current transformers.

A schematic of the testing circuit excluding connections for the Hipotronics 1.2 by 50 μs Impulse Generator was displayed in Fig. 3.3.

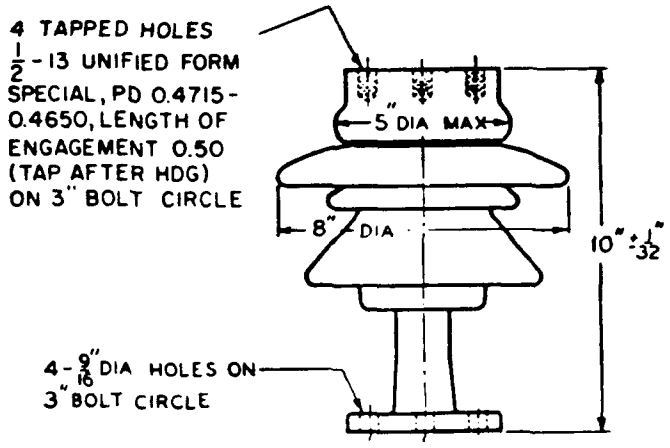

TECHNICAL REFERENCE NO. 4

	Rating	See American National Standard C29.1-1976 Section :
Dimensions		
Leakage distance, in.	12	2.5.2
Mechanical Values		
Cantilever strength–upright, lb	2000	5.1.4.1
Cantilever strength–underhung, lb	1000	5.1.4.1
Tensile strength, lb	5000	5.1.4.3
Torsional strength, in.-lb	7000	5.1.4.2
Compression strength, lb	10 000	5.1.4.4
Tension proof, lb	1250	7.2.2
Electrical Values		
Critical-impulse flashover, positive, kV	125	4.7
Low-frequency wet withstand, kV	45	4.5
Impulse withstand, kV	110	4.8
Low-frequency puncture, kV	115	4.11
Radio-Influence-Voltage Data		
Low-frequency test voltage, kV	10	4.9
Maximum riv at 1000 kHz, μV	50	4.9

NOTE: If high-resistance coatings are applied to the insulator, such coatings shall be considered as effective leakage surfaces, and the distance over them shall be included in the leakage distance.

Fig. 3.14. (a) Outline and (b) specifications for ANSI C29.8-1980 cap-and-pin type apparatus insulators used on this project.

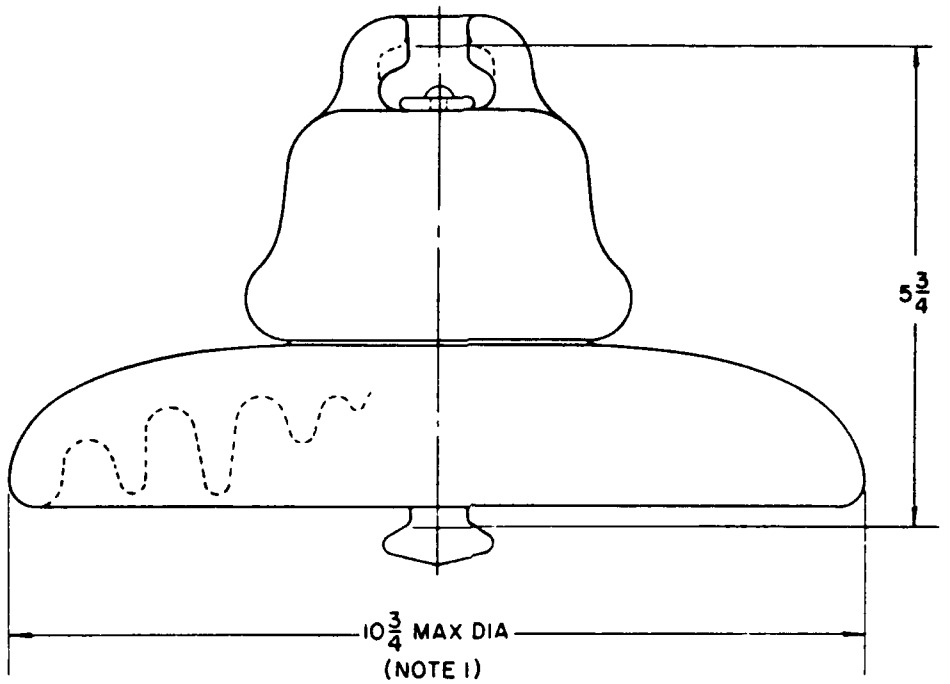

NOTES:

(1) For specific diameter and tolerance, see manufacturer's drawings.

(2) All dimensions are in inches; for metric equivalents, see Table 1.

(3) The connecting length of a string of six insulators selected at random shall be equal to 6 times the nominal spacing of the insulators ± 3/4 in (± 19.1 mm).

(4) Dimensions and tolerances shall be determined, after galvanizing (where applicable), by the ball and socket gages in Fig. 12 and 13.

(5) Connecting hardware parts defined by gages in Fig. 12 and 13 are designated as Type B.

	Rating	See ANSI C29.1-1982, Section:
Dimensions		
Leakage distance, inches (mm)	11-1/2 (292)	2.5.2
Mechanical Values		
Combined mechanical and electrical strength, pounds (kN)	15 000 (67)	5.2
Mechanical impact strength, inch-pounds (N·m)	55 (6.0)	5.1.2.2
Tension proof, pounds (kN)	7 500 (33.5)	7.2.1
Time load, pounds (kN)	10 000 (44)	5.3
Electrical Values		
Low-frequency dry flashover, kilovolts	80	4.2
Low-frequency wet flashover, kilovolts	50	4.3
Critical impulse flashover, positive, kilovolts	125	4.7
Critical impulse flashover, negative, kilovolts	130	4.7
Low-frequency puncture, kilovolts	110	4.11
Radio-Influence Voltage Data		
Low-frequency test voltage, rms to ground, kilovolts	10	4.9
Maximum RIV at 1000 kHz, microvolts	50	4.9

Fig. 3.15. (a) Outline and (b) specification for ANSI class 52-3 suspension insulators used on this project. Class 52-4 supervision insulators using pin-and-clevis suspension hardware but otherwise identical to the 52-3 units were also used.

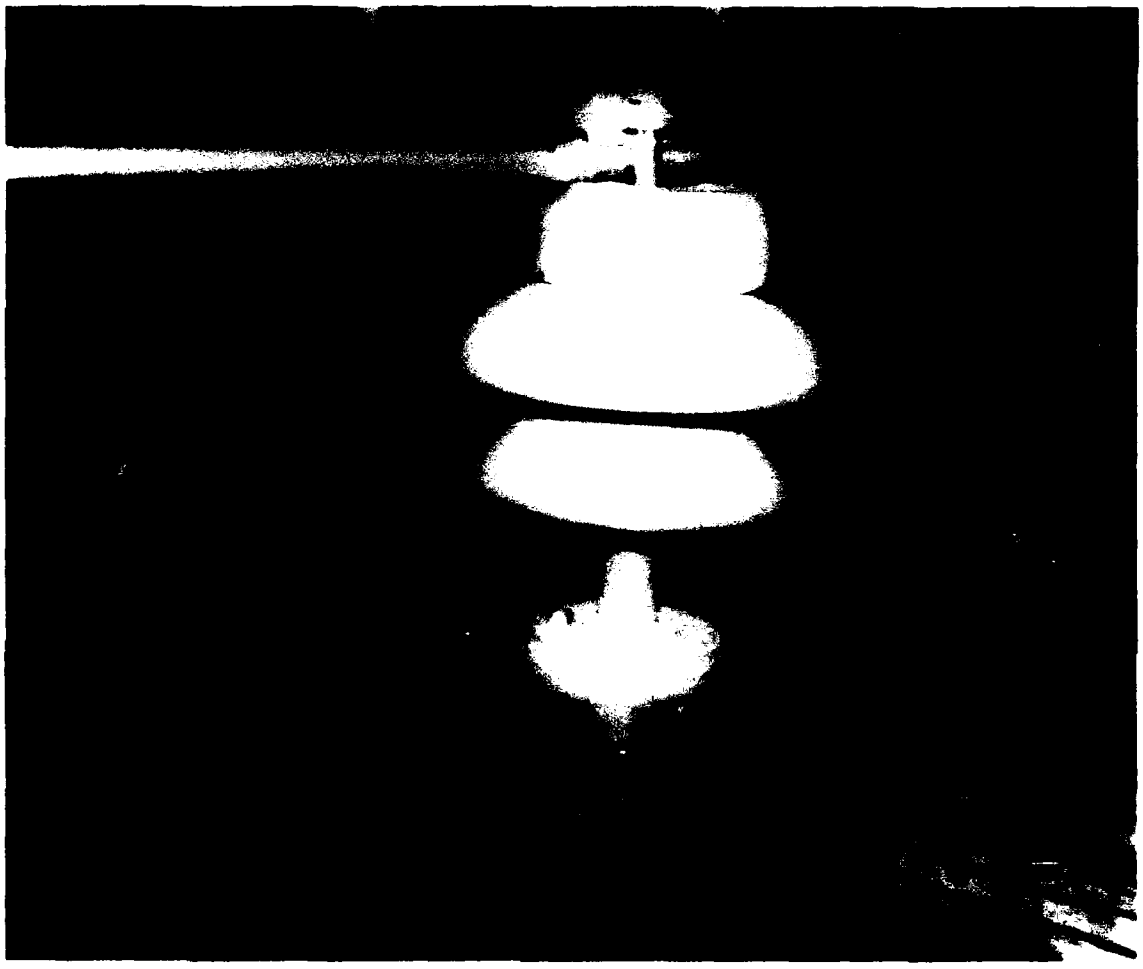

Fig. 3.16. Cap-and-pin insulator with simulated conductor mounted on aluminum channel for impulse testing.

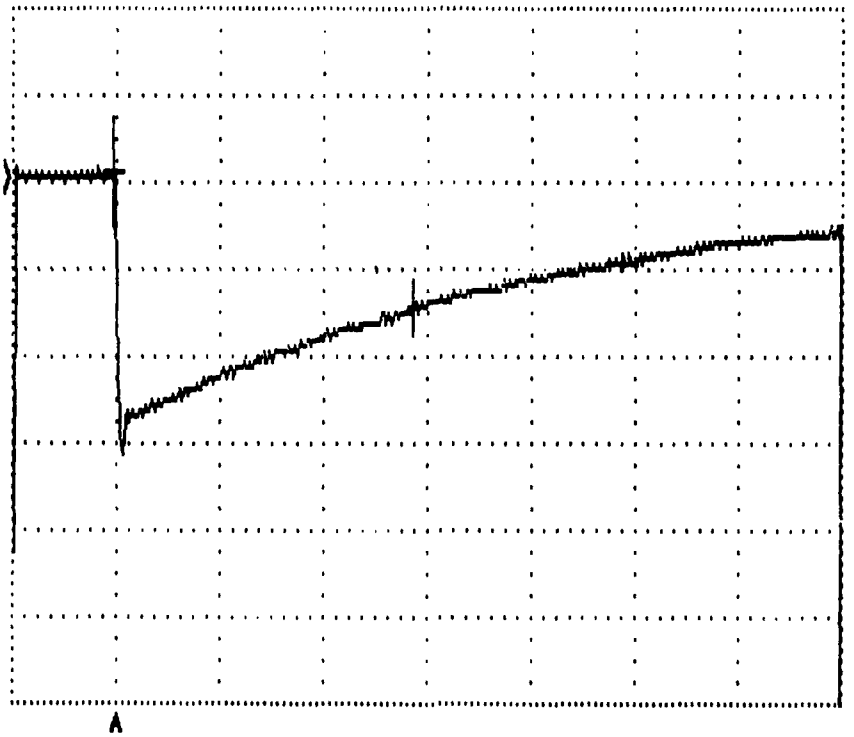

Scale factors: 48.5 kV and 20 μs per major division.

Fig. 3.17. Typical full-wave lightning impulse as applied to a pin-type insulator.

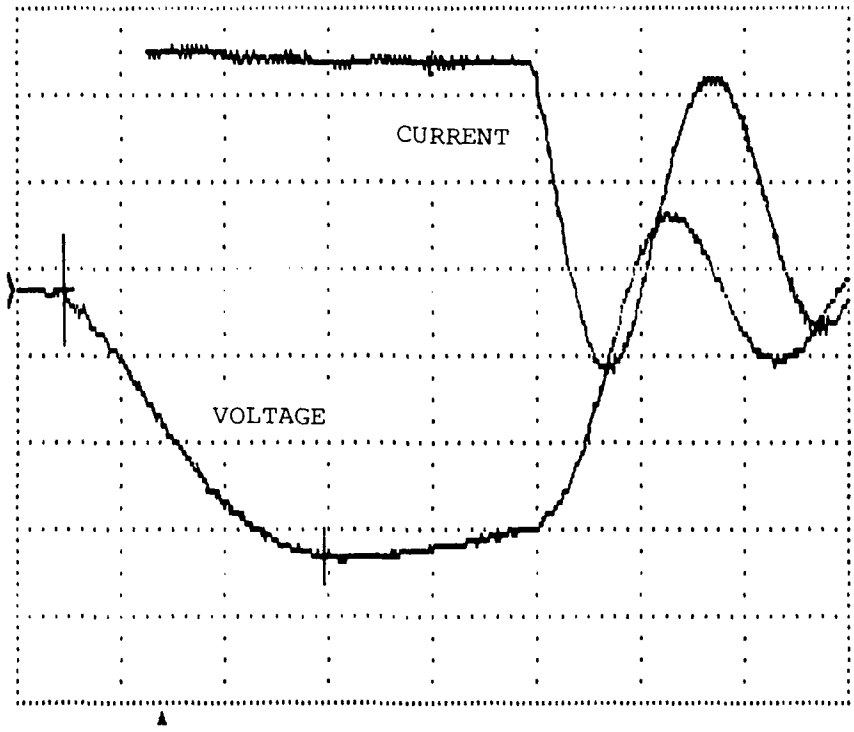

Scale factor for current (upper trace): 814 A per major division.
Scale factor for voltage (lower trace): 32.2 kV per major division.
Time base for both traces is 500 ns per major division.

Fig. 3.18. Full-wave lightning impulse voltage and current traces for a single suspension disk, showing flashover occurring approximately 1 μs after voltage crest.

Significant differences from other applications for this facility are:

- The addition of RT, a 100-Ω resistor, to decrease the time to half-crest on the wave tail.
- The addition of RC, a 200-Ω resistor that, in conjunction with a reduced value of R_Z = 60 Ω, limits the available current at 1100 kV to ≤4230 A.
- The addition of RS, a 107-Ω resistor that, when required for voltage at the specimen, gives ~140 kV to ~400 kV. Electromagnetic-pulse generator output was reliably controllable between 400 kV and 1.1 MV.

Calibration of the Hipotronics Marx lightning-impulse generator was achieved by using 25-cm sphere gaps, the data being corrected for atmospheric conditions as described in ref. 2.

The output level of the EMP generator was verified by the concurrence of the voltage signals from the generator output divider, the specimen divider, and a B-dot field sensor not shown on the schematic, in conjunction with the signal from the calibrated miniature current transformer. Overall calibration of the generator was achieved using sphere-gap volt-time data as described in ref. 3.

The insulator results are listed in Tables 5 and 6. The FO values for these insulators are plotted vs time-to-crest voltage in Fig. 3.19.

3.5.2 Test Results

Subsequently, three of the same specimens used in developing the data in Table 5 were subjected to a 1100-kV SFSD wave for five or six shots of the same polarity. One pin insulator and four suspension disks were punctured. The number of shots, FO voltage, time to crest, and comments are shown in Table 6.

Subsequently, a string of eight suspension disks was hung inverted above the reference plane using suitable hardware and the simulated conductor. Five attempts were made to cause FO of this insulator string using the 1100-kV SFSD impulse. No FOs were observed. Six of the above eight suspension disks were similarly individually subjected to the 1100-kV SFSD impulse. Again, no FOs were observed. Finally, four of the six tested suspension disks were similarly subjected to the 1100-kV SFSD impulse. Flashover was observed for all four disks on each of the first five shots. One disk was punctured on the sixth shot, with the other three disks flashing over. The measured wave was 1110 kV, 40 by 600 ns. See Figs. 3.20, 3.21, and 3.22. For reference, a value of 10 kV/disk is used in uncontaminated applications. See Appendix B, Section B.4.5, for the Data Summary.

Heavy corona was observed for all 1100-kV SFSD-impulse applications. Figure 3.23(a) shows a cap-and-pin insulator, and Figure 3.23(b) shows the string of four suspension disks. Both photographs display the corona encountered in a single discharge.

Pin insulator. The porcelain was punctured along a line essentially parallel to the insulator axis from the center top to the "lead head" mounting pin. Spalling of the porcelain body occurred at both the entrance and exit points of the puncture, with radial cracks up to 2 in. long emanating from the puncture location. Failure occurred on the fifth shot of the test sequence, which used an applied waveform of 15 by 500 ns at a 1110-kV crest (see Data Summary B.4.2 in Appendix B).

Table 5. Summary of test results for pin, cap-and-pin, and suspension insulators

SPECIMEN PARAMETERS	SPECIMEN TYPE			
	PIN	POST	CAP AND PIN	SUSPENSION
No. of specimens	5	5	5	5
Average lightning-impulse FO (kV)	155[a]	166	203	141
Lightning-impulse waveshape	----------0.94 μs × 57 μs----------			
Average low-SFSD impulse FO (kV)	325	262	360	286
SFSD voltage waveshape	35 × 325 ns [b]	33 × 500 ns	37 × 430 ns	38 × 750 ns
Average lightning-impulse FO after low-SFSD impulse (kV)	150	166	195	139
Ratio of average low-SFSD impulse FO to average lightning-impulse FO	2.10	1.58	1.77	2.03
No. of specimens, 100 × 500 ns	3	3	3	3
Impulse FO (kV) (FOW)	323	318	368	319[c]

[a]The lightning-impulse FOs averaged 186 kV when the pin insulators were mounted on the 10-in. by 16-in. channel, which was grounded. All averages are simple numerical averages.
[b]The applied SFSD-impulse waveshape without a specimen in place was 42 by 600 ns. Each type of specimen modified the wave.
[c]One specimen punctured on the fifth shot.

NOTE: Data Summary is in Appendix B, Sections B.4.1 through B.4.4.

Table 6. Results of 1100-kV SFSD impulse test on porcelain/air insulation

SPECIMEN PARAMETERS	SPECIMEN TYPE			
	PIN	POST	CAP AND PIN	SUSPENSION
No. of specimens	3	3	3	3
Average lightning-impulse FO before 1100-kV SFSD impulse (kV)	150	166	195	139
Average 1100-kV SFSD impulse (kV)	827[a]	740	819	747[b]
Average lightning-impulse FO after 1100-kV SFSD impulse (kV)	149	157	199	---
Applied SFSD impulse waveshape	----------40 ns × 600 ns----------			

[a]One pin insulator punctured at 620 kV on the wavefront. All averages are numerical averages.
[b]All three suspension disks punctured: one on the wavefront at 420 kV, the other two on the wave tail.

NOTE: Data Summary is in Appendix B, Sections B.4.1 through B.4.4.

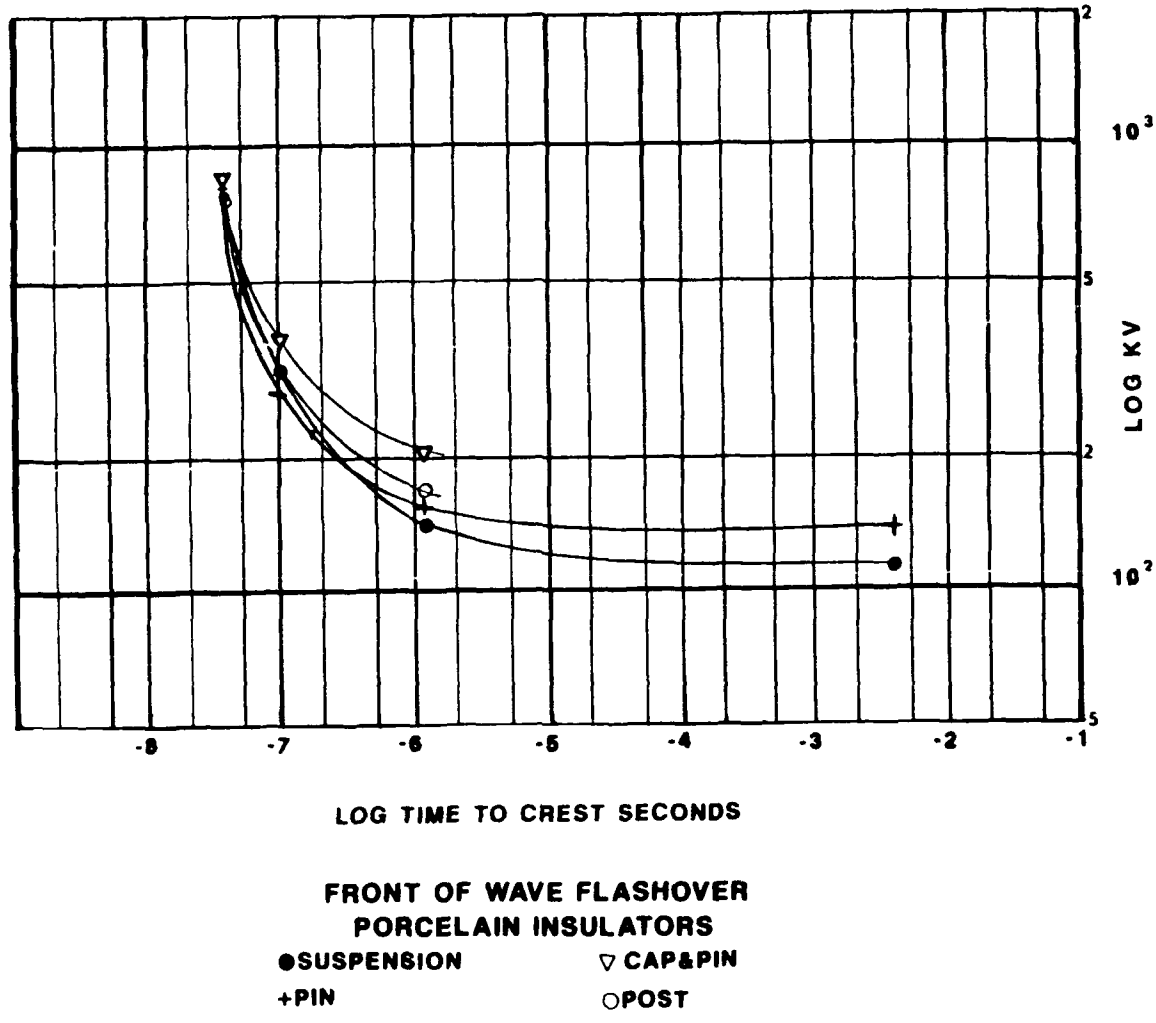

Fig. 3.19. Time to crest for front-of-wave breakdown on pin (+), post (o), cap-and-pin (v), and suspension disk (•) insulators.

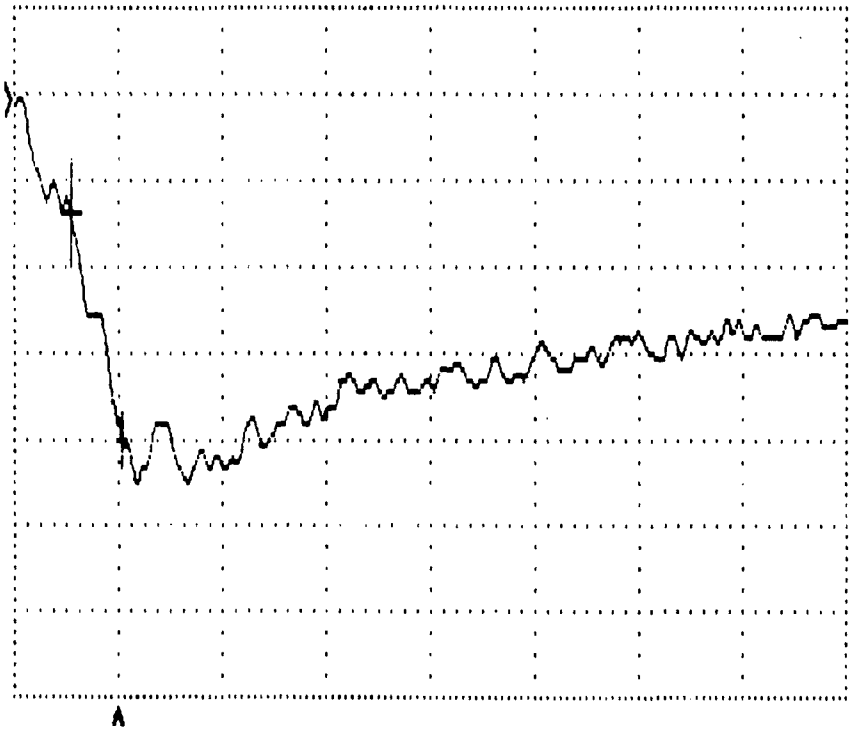

Scale factor for vertical axis: 256 kV per major division.
Scale factor for horizontal axis: 50 ns per major division.
Crest voltage: 1152 kV.

Fig. 3.20. Typical 110-kV steep-front short-duration impulse as applied to a string of four suspension insulators.

Scale factor for vertical axis: 256 kV per major division.
Scale factor for horizontal axis: 10 ns per major division.

Fig. 3.21. Time-expanded portion of the front of the wave shown in Fig. 3.20. The cursors are placed at the 30% and 90% amplitude points, yielding a rise time of 42 ns from zero to crest. The first peak at 10 ns is caused by the coupling of the EMP-generator radiated wave to the specimen and to the voltage measuring divider.

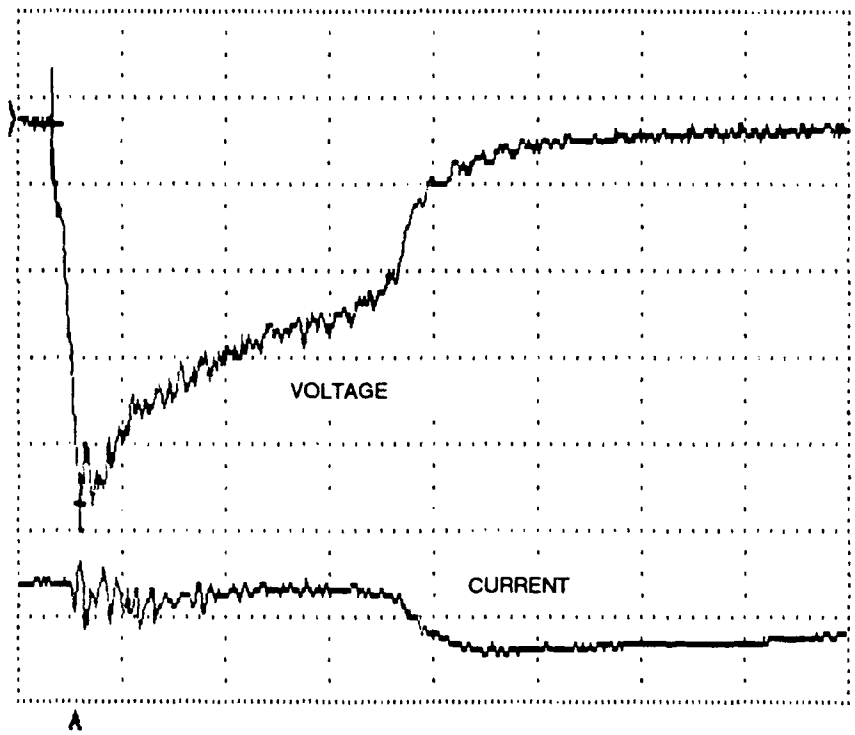

Scale factor for vertical axis: 256 kV per major division for the upper trace and
1875 A per major division for the lower trace.
Scale factor for horizontal axis: 200 ns per major division.

Fig. 3.22. Typical voltage and current traces showing flashover of a string of four suspension disks at 600 ns after voltage crest. Peak voltage is 1110 kV. Peak current is 1500 A.

(a)

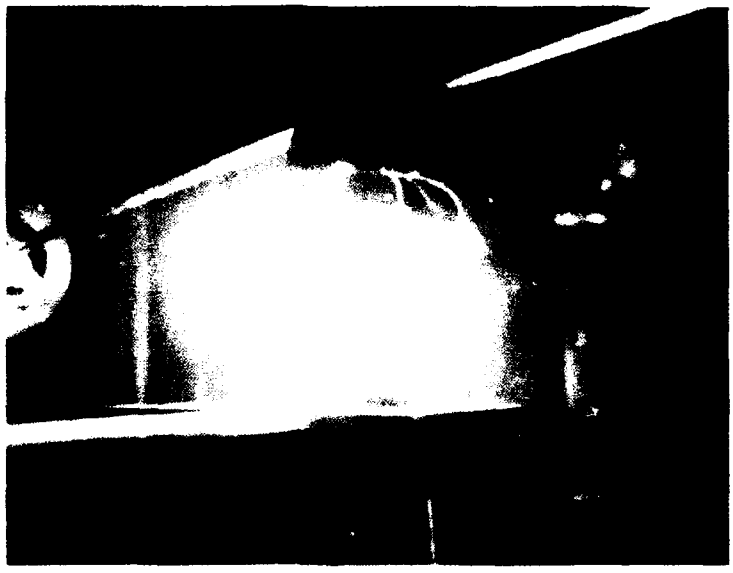

(b)

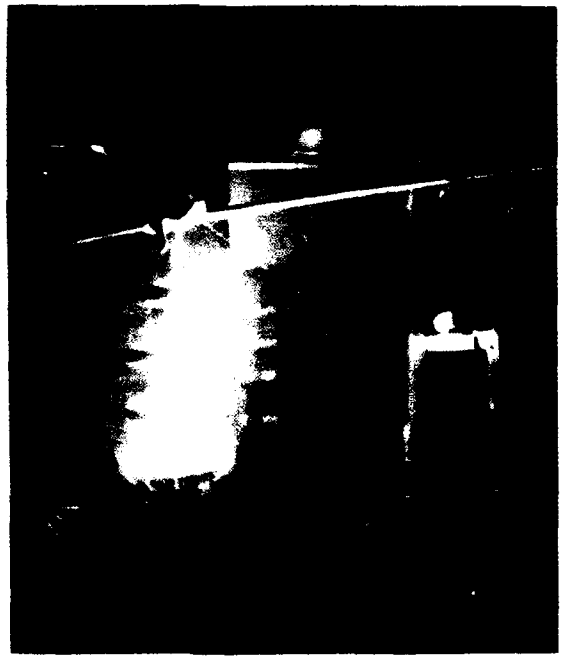

Fig. 3.23. (a) Corona and flashover for a single SFSD impulse on a cap-and-pin insulator, and (b) corona and flashover for a single SFSD impulse on a string of four insulators.

Suspension insulator. One suspension disk in a string of four was punctured on the sixth shot of the test sequence using the 1110-kV-crest HEMP wave. The puncture occurred between the head of the suspension ball pin and the suspension cap (see Data Summary B.4.5, Part 1, in Appendix B).

Three suspension disks tested individually under the same conditions also were punctured in essentially the same location as was the one disk in the string of four (see Fig. 3.24). Structural integrity was not lost (see Data Summary B.4.4 in Appendix B).

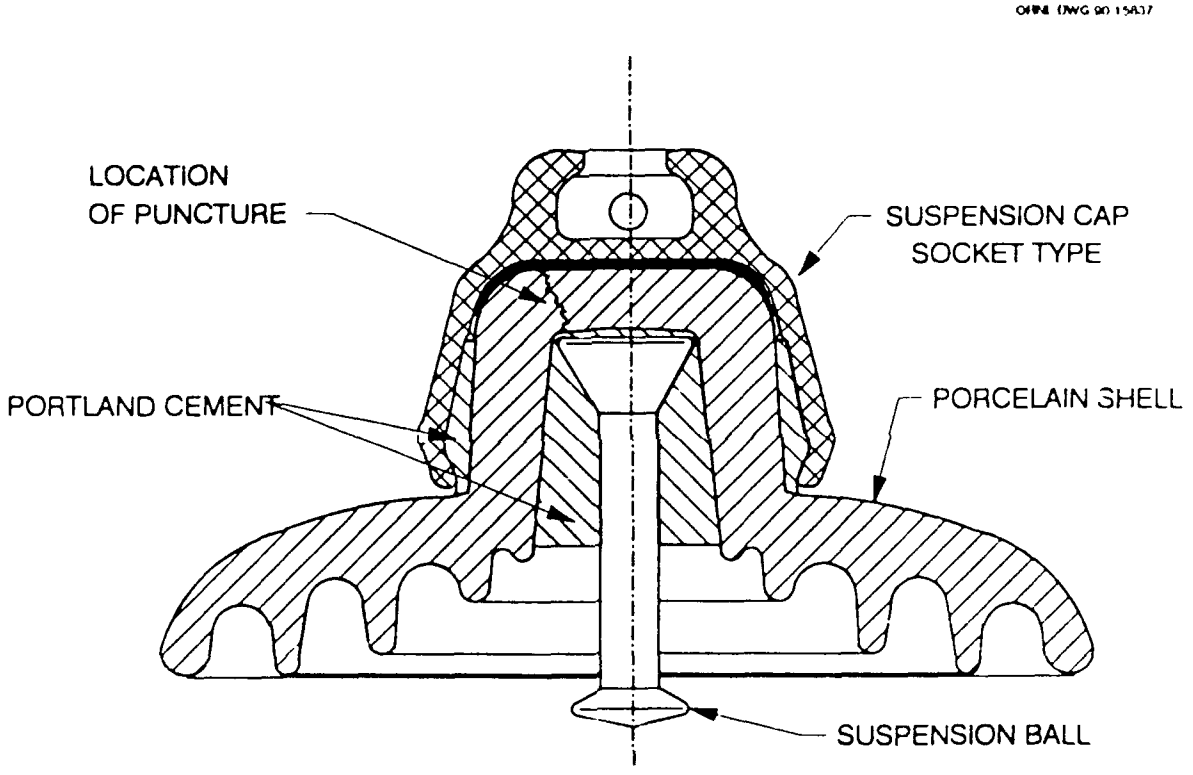

Fig. 3.24. Cross-section view of a class 52-3 suspension disk showing the location of the typical SFSD impulse-caused puncture. The puncture is generally associated with the presence of voids in the interfacial materials.

The punctures in the structural insulation are generally associated with voids in the interfacial materials that reduce the insulation strength and provide internal paths for arcing. The size of the void appears to affect the materials' ability to withstand follow current.

In a subsequent stress evaluation of the combined suspension insulators, using a 110-kV, ~300- by 2000-ns, 4200-A impulse (with a 10.1-kV, 60-Hz, 2000-A impulse available) and a tensile load of 800 lb, one of these punctured suspension disks failed structurally and all load support was lost. A second SFSD-punctured disk failed structurally with the 10.1-kV, 60-Hz, 800-lb load applied before the 300- by 2000-ns impulse.

3.6 POWER-TRANSFORMER PRIMARY WINDING

This section discusses specimen selection and preparation and results of impulse testing for the primary winding of the core-form power transformer.

3.6.1 Specimen Selection and Preparation

The low-voltage impulse distribution analysis showed that for the steep-fronted impulse, the highest stresses appeared in the region of the windings at the high-side input. This occurrence is well known in the industry. Characteristically, the amount of insulation applied to the conductors in this region is greater than that used in the rest of the primary winding. The increased amount of insulation typically decreases the distributed winding capacitances in this region, thereby aggravating the voltage stress distribution. Hence, simply adding insulation does not solve the problem. The stress distribution may be beneficially modified by interlacing the sections of the first several winding pancakes.

Economics and logistics dictated that only the critical segments of the primary winding be evaluated on the high-voltage, steep-front impulse waves rather than an entire primary winding. Accordingly, the primary windings of the 16.4-MVA power transformer used for the low-voltage impulse distribution evaluation were removed from the transformer intact. Each winding was split at the midpoint, the high-side input connection. The first 16 winding pancakes on both sides of the midpoint were then removed as a unit.

The first ten pancakes in each of these sections had heavier insulation than did the remaining six. The remaining six pancakes had the same insulation as did the rest of the primary winding.

The 16-pancake segment of the winding mounted on its insulating core was placed in a test tank capable of providing the necessary vacuum impregnation cycle for the reestablishment of the dielectric properties of the insulation system. Subsequently, a metallic cylindrical shell simulating the presence of the transformer core leg was placed inside the coil. The impulse was applied to the desired point on the winding segment through a 115-kV power-class bushing mounted in the tank top. The connections were made at the transitions between the outer edges of each pair of pancakes.

Figure 2.9 provided an overall view of the primary winding. Figure 3.25 shows a 16-pancake segment of the winding. Figure 3.26 displays the winding segment in place with the hollow metal cylinder that simulated the presence of the transformer core. Voltage dividers were connected from the input lead to the tank and from the low side of the specific pancake(s) to the tank.

Three such specimens were prepared, one for each of the three impulse waves. We were interested in the insulation system used in this winding. Accordingly, impulses were applied to the first six disks, using disks 7 and 8 as a pair and disks 9 and 10 as a pair. All these disks had heavier insulation (13 layers of cellulose paper) than did the remaining disks, which had 9 layers. If supplemental specimens were required, pairs of disks with the lesser insulation were used. Connections were made at the transitions between disks.

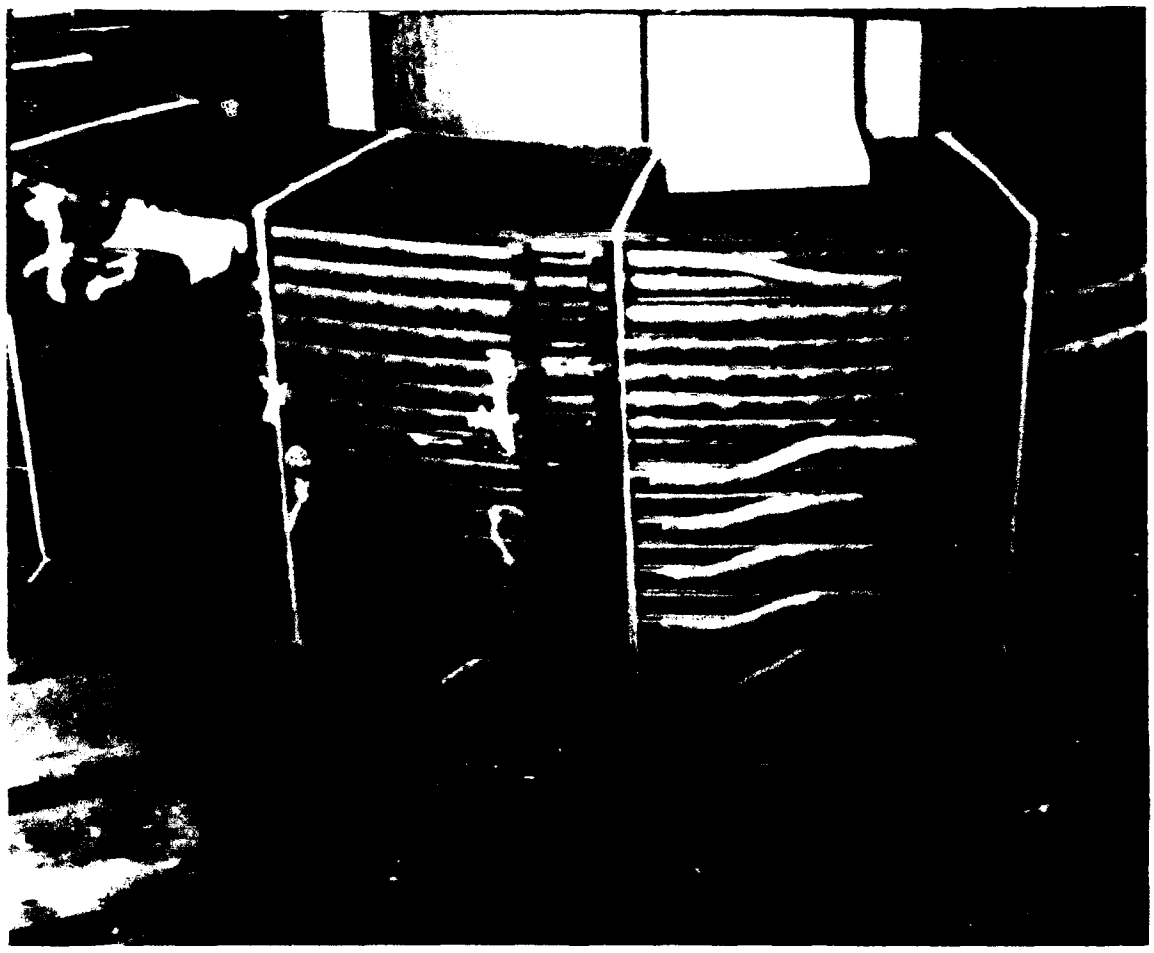

Fig. 3.25. Sixteen-disk segment of the core-form primary winding as prepared for evaluation.

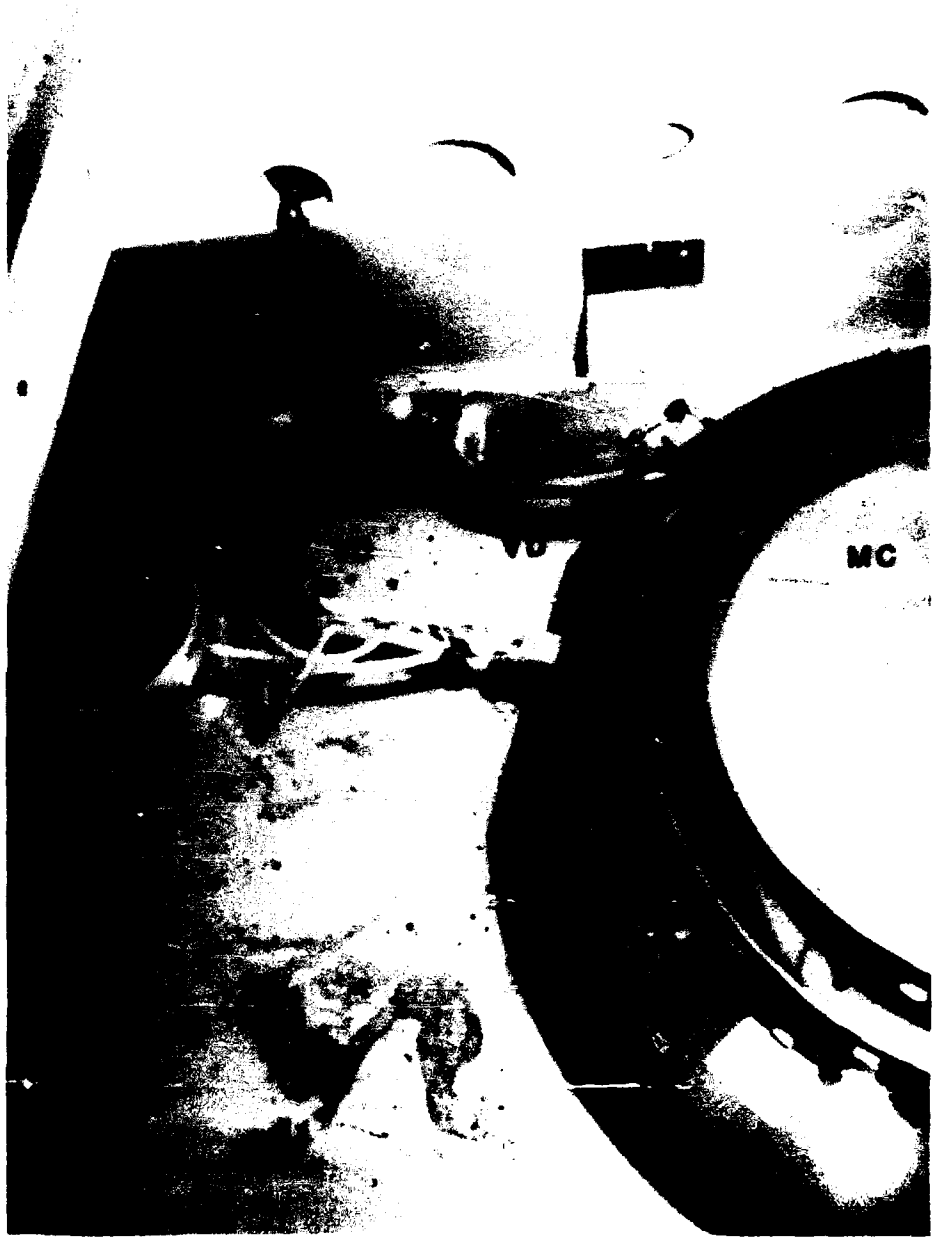

Fig. 3.26. Sixteen-disk segment in place, including the connecting lead, two copper-sulfate voltage dividers (VD), and hollow metal cylinder (MC), simulating the transformer core.

3.6.2 Results of Impulse Testing of Segments of the Primary Winding of the Core-Form Power Transformer

Severe problems were encountered in impulse-testing segments of the primary winding of the core-form power transformer using both of the two faster waves. Breakdowns detected during the testing program proved upon subsequent disassembly of the specimens to be strongly related to the connectors used for the conducting interface between the test lead and the transition point on the disks. Because of this, the results obtained in this case are more a function of the oil gap than of the cellulose insulation. The breakdown paths through the multiple layers of cellulose surrounding the conductors could be clearly identified. However, the breakdown path through the oil, which was influenced by the presence of the test lead connectors and was probably significantly longer than the disk-to-disk separation, could not be determined with much certainty. In the case of the 1.2- by 50-μs impulse, the breakdowns on the more heavily insulated disks involved the outermost turn near a radial spacer.

Figure 3.27 shows the location of such a breakdown. The deformation seen in the upper surface of the disk was caused by the axial compressive force applied during manufacture. This force prevents telescoping of the winding under fault conditions. This perturbation in the insulation system was not modeled.

Failure caused by the 1.2- by 50-μs impulse on the lesser-insulated disks occurred in the center of the disks, as is shown in Fig. 3.28. In each case the initial failure is turn-to-turn. Subsequent additional failures occurred between the adjacent faces of these two disks. The combination of turn-to-turn and disk-to-disk failure occurred at voltage magnitudes 4 to 8 times that normally involved in routine impulse testing of the complete transformer.

3.7 POWER-APPARATUS BUSHING

The insulation system used in condenser-type power-apparatus bushings is similar to that used in transformers. However, in the condenser bushing, broad areas of conducting foil and insulating paper/oil are involved, resulting in substantial capacitance between the central conductor and the ground sleeve.

Power-apparatus bushings rated at 115 kV, 550-kV BIL, 800 A were selected as specimens for high-voltage evaluation. These specimens, except for their voltage rating, are alike in that they use the same insulating materials and have the same construction as do the 138-kV, 650-kV-BIL bushing core utilized for the low-voltage impulse distribution analysis. The relative insulation stresses are the same for the two designs, as are the construction techniques. Figure 2.13 showed a cutaway drawing of a typical power-apparatus bushing. Figure 3.29 shows the bushing installed in the test tank ready for impulse tests.

Three specimens were obtained, one for each of the three impulse waves. These specimens were tank-mounted with capacitors in series between the central conductor and the tank. The capacitors and the associated connecting leads effectively simulated a transformer to which this bushing would be connected.

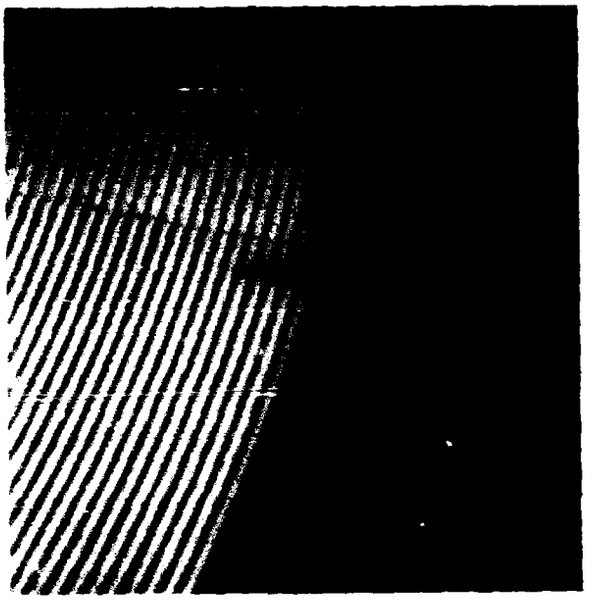

Fig. 3.27. Location of failure caused by 1.2 by 50 μs impulse on outer turn of the first disk.

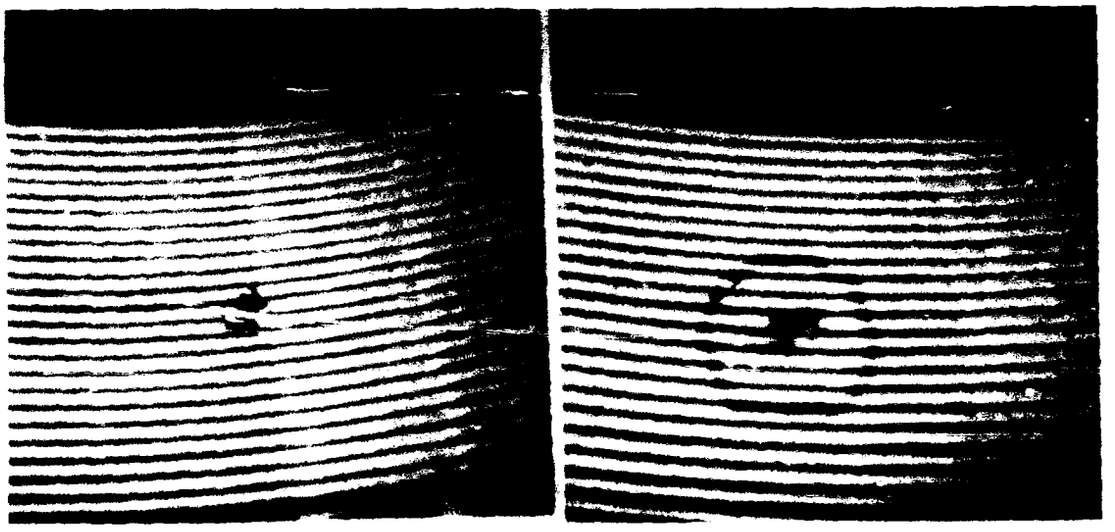

Fig. 3.28. Locations of failures caused by 1.2- by 50-μs impulse on disk pairs (a) 11 and (b) 12. Turn-to-turn and subsequent disk-to-disk failures are identified.

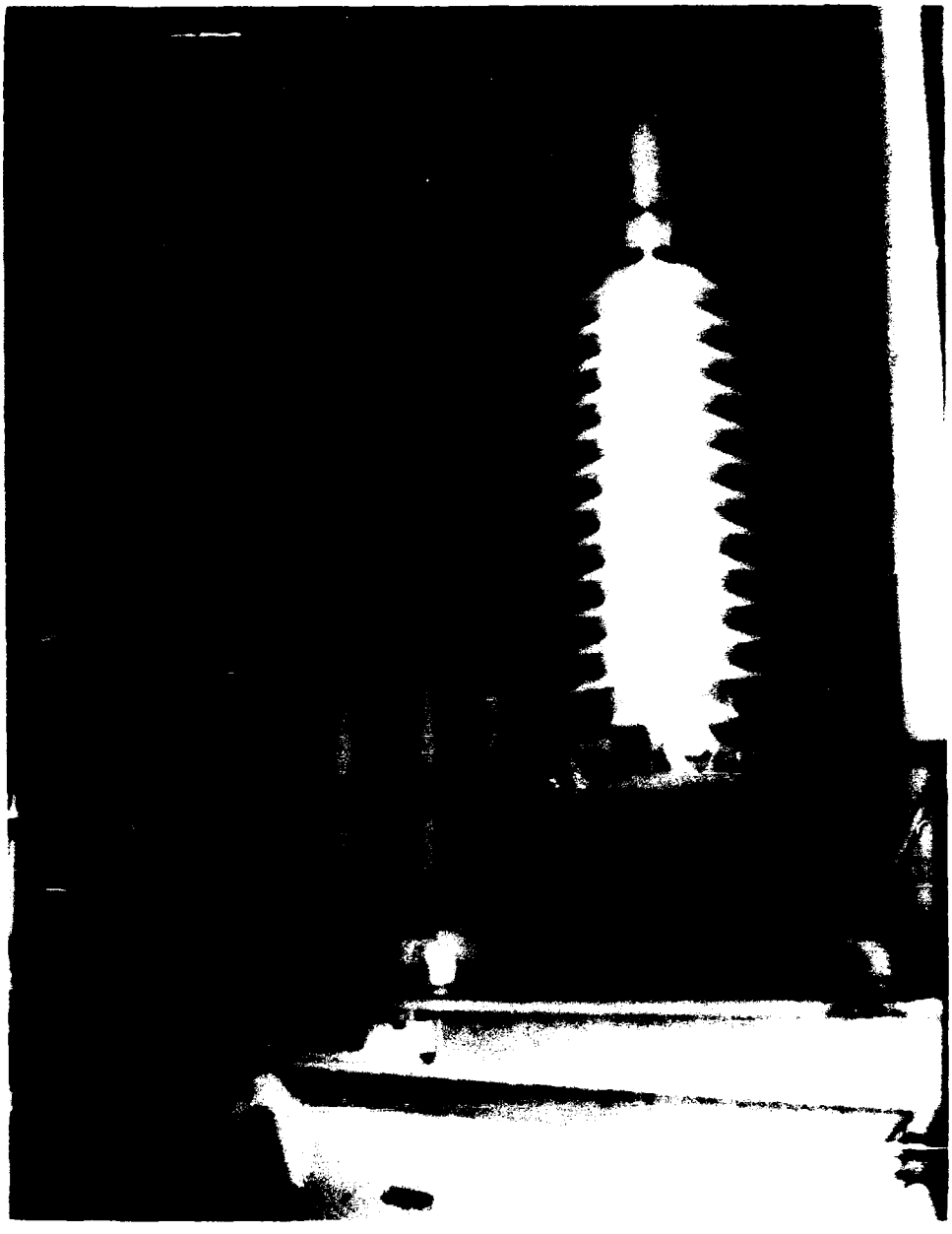

Fig. 3.29. Power-apparatus bushing (115 kV) mounted in tank ready for application of steep-fronted wave.

3.7.1 Power-Apparatus Bushing Test Results

The capacitance of the bushing adversely affected the FOW rise time for the steepest wave. For the applied wave with a 30-ns rise time, the resulting rise time measured on the bushing was ~100 ns. Rise times for the other two waves were as described earlier. The impulse current magnitudes ranged from 4.6 to 7.6 kA.

Critical impulse flashover, as well as FOWFO, was determined for the specimen dedicated to the 1.2- by 50-μs lightning impulse. Neither CIFO nor FOWFO could be determined for the other specimens with the two faster waves. A limit of 1200 kV was reached without FO for the 10- by 150-ns and 100- by 500-ns wave specimens. After the 10- by 150-ns tests were performed, CIFO measurement at 1.2 by 50 μs on specimen 2.7 indicated that no measurable degradation had occurred.

However, specimen 3.5 underwent a catastrophic failure at the 900-kV level on the 100- by 500-ns wave test. Table 7 summarizes the impulse testing on the power-apparatus bushings.

Table 7. Impulse testing on power-apparatus bushings

SPEC. NO.	WAVESHAPE	CIFO +KV	CIFO −KV	FOW +KV	FOW −KV
1.6	1.2 × 50 μs	775[a]	641[a]	1130[b]	1120[b]
2.7	100 × 500 ns	---	---	---	900[c]
3.5	30 × 350 ns	---	>1099[d]	---	>1099[d]
3.5	1.2 × 50 μs	747[a]	694[e]	---	---

[a]Peak voltage recorded. Flashover occurred at crest or shortly thereafter.
[b]1000 kV/μs rate of rise. Average of 5 shots of each polarity.
[c]Cumulative total shots with negative polarity = 28. Cumulative total shots with positive polarity = 12. Specimen underwent catastrophic failure on the fifth shot at the 900-kV level.
[d]CIFO and FOWFO not achieved. Maximum applied voltage limited to 1100 kV. Cumulative total shots with negative polarity = 20. Cumulative total shots with positive polarity = 13.
[e]Performed after the 30- by 350-ns testing.

NOTE: See Data Summary in Appendix B, Section B.6.

Photographic monitoring of each shot taken on specimens 2.7 and 3.5 revealed that there was a significant amount of corona on the specimens for all shots of 550 kV and above, increasing dramatically as the impulse voltage increased.

Figure 3.30 displays the corona occurring during a single 1100-kV impulse on a 115-kV bushing. Figure 3.31 shows the specimen and associated circuit components from the same angle of view as that of Fig. 3.32. In order to achieve ~1100 kV at the specimen, it was necessary to charge the generator to ~2400 kV, with approximately one-half the voltage being dropped across the series resistor. See Figs. 3.2 and 3.3 for the laboratory layout and test-circuit schematic.

In spite of the copious corona, no FO occurred for the bushing subjected to the 30- by 350-ns wave.

Subsequent disassembly of bushing no. 3.5, used on the 30- by 350-ns wave, revealed no signs of degradation. The oil dielectric properties met the "as new" specification. There was no evidence of discharges anywhere within the bushing.

Fig. 3.30. Heavy corona caused by a single steep-fronted impulse on the bushing/specimen shown in Figs. 3.29 and 3.31. Figures 3.30 and 3.31 have similar angles of view.

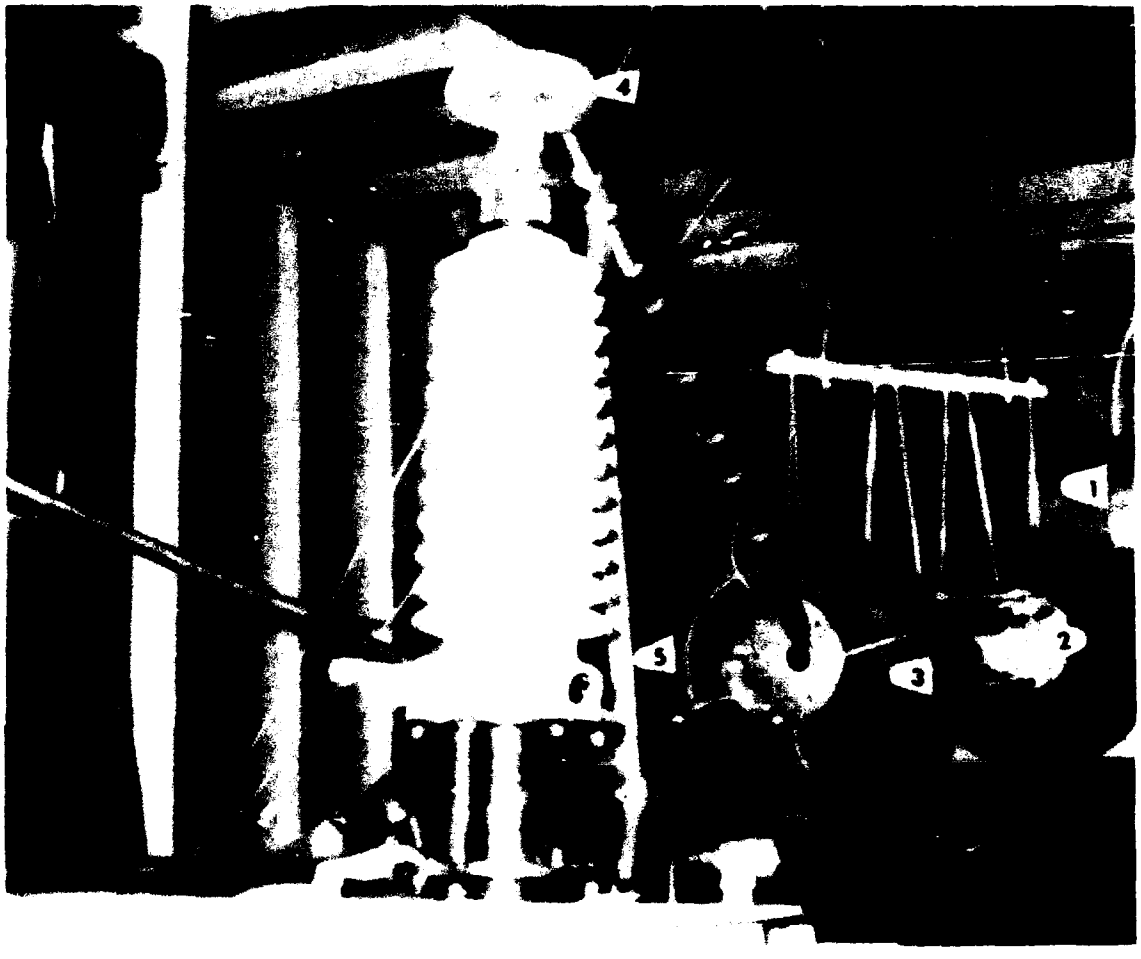

Fig. 3.31. Power-apparatus bushing (115 kV) in EMP simulation laboratory. (1) Corona shield at the generator output, (2) and (3) corona rings at the ends of the coupling resistor, (4) corona ring at bushing top, and (5) specimen voltage sensing divider.

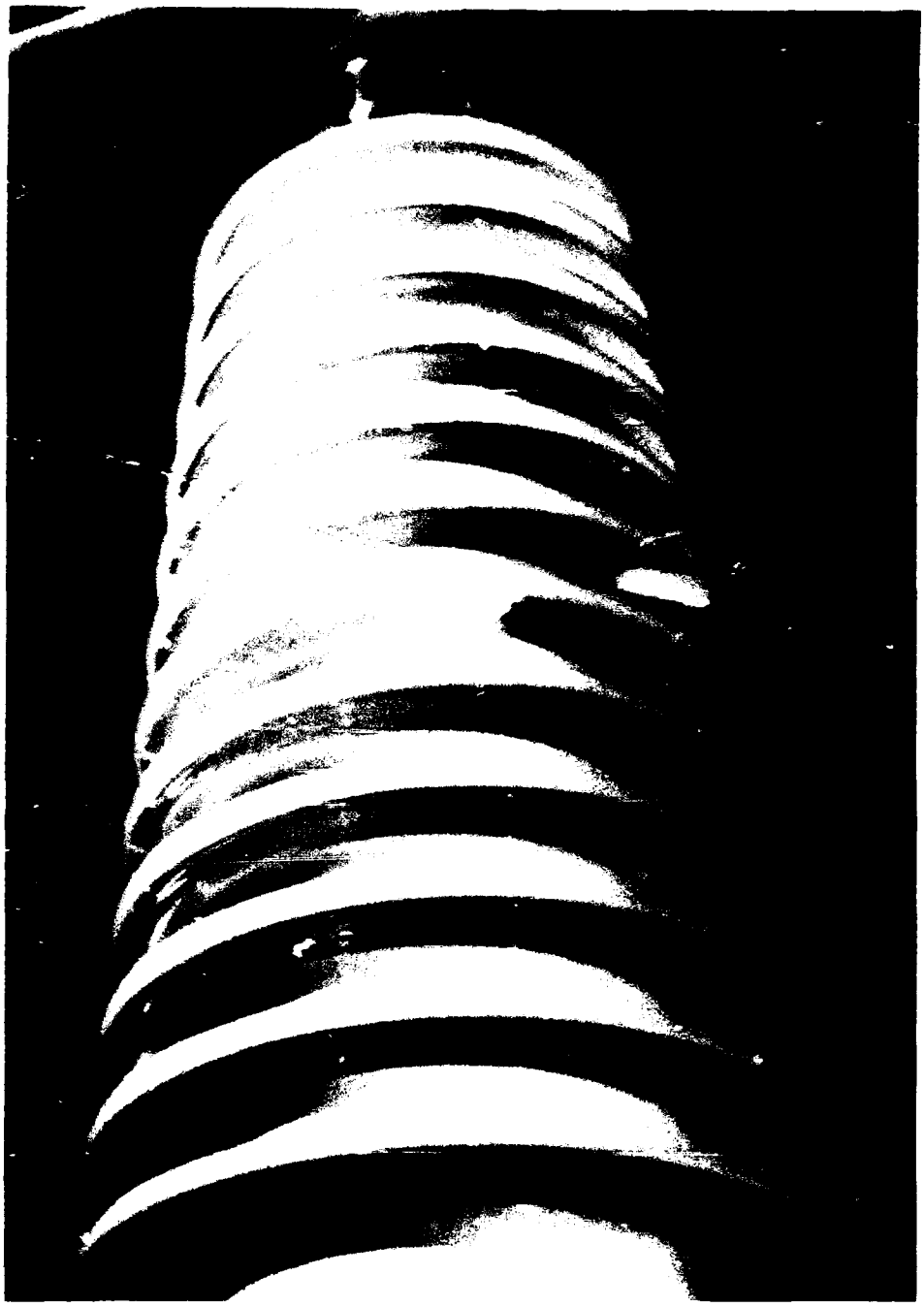

Fig. 3.32. Damage resulting only from steep-front impulse to the 115-kV power-apparatus bushing. Not visible are two longitudinal cracks in the upper portion of the weathershed.

Examination of specimen no. 2.7, used on the 100- by 500-ns wave, revealed that the upper segment of the two-piece weathershed of the porcelain had cracked longitudinally in two places, accompanied by loss of two segments of the skirts. (See Fig. 3.31.) Upon fracture, the oil level quickly drained down to the junction between the upper and lower sections of the weathershed.

Subsequent disassembly of the bushing showed that the failure originated between the outermost first and second foils (the ground foil and the potential-tap foil) and then propagated toward the entrance end of the bushing, eventually involving a total of 16 of the 27 foils in this bushing design. Figures 3.33 and 3.34 display some of the tracking evidence on the bushing core, clearly involving the entire length of the tapered section. The joint between the upper and lower segments of the weathershed, relative to the core, is adjacent to and below the tapered portion of the bushing core.

It is concluded, therefore, that the cumulative degradation of the bushing core's insulation system resulted in an internal arc, creating a shock wave that fractured the upper section of the weathershed. The precise part played by the bushing potential tap and its associated leads is not completely clear. At the di/dt's (time rates of change of the current) involved for these fast-fronted waves, conductor voltage drops of 75 to 100 kV/m/kA are realizable. The total lead length associated with the potential tap is about 1/3 to 1/2 m. Currents of about 3 to 5 kA may pass through the bushing insulation system. The voltage stress in this region under these steep-front impulse conditions may be 4 to 6 times as high as the stress under lightning impulse conditions. The bushings tested with the 1.2- by 50-μs impulse wave showed no indication of damage. Hence, the probability of failure was increased by the SFSD impulse, and these impulses are likely candidates for causing anomalous failures.

3.7.2 Bushing Potential-Tap Measurements

Attempts were made to utilize the bushing potential tap as a signal source for monitoring the transient performance of the power-apparatus bushing. Breadboard-type experiments indicated that with the addition of a suitable shunting capacitor and terminating resistors, measurements might be made at frequencies substantially higher than the normal 60 Hz application. An adapter containing the desired components was fabricated from a heavy-wall capped pipe and inserted in the bushing potential-tap well. This combination could be calibrated, yielding acceptable results on the 1.2- by 50-μs impulse wave, but proving to be unworkable on the 100- by 500-ns and faster waves. This concept was therefore discarded. Reliable measurements were obtained using conventional impulse dividers. Figure 3.35 displays the schematic circuit and the adapter.

Fig. 3.33. Tracking on the upper tapered section of the power-apparatus bushing core assembly.

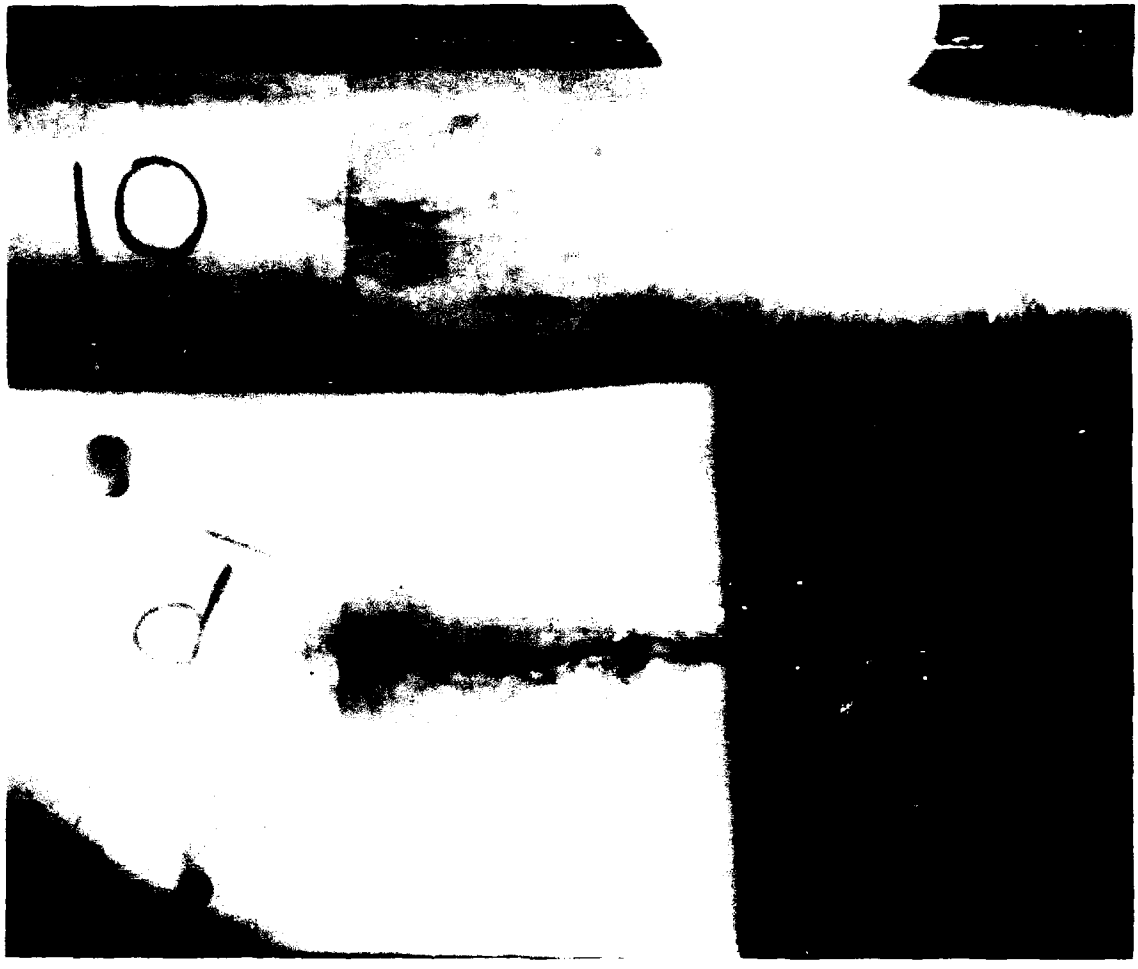

Fig. 3.34. Tracking between layers of cellulose paper insulation, starting at the edge of the potential tap foil.

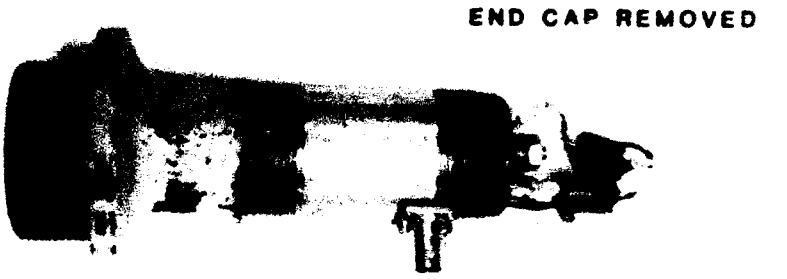

(a)

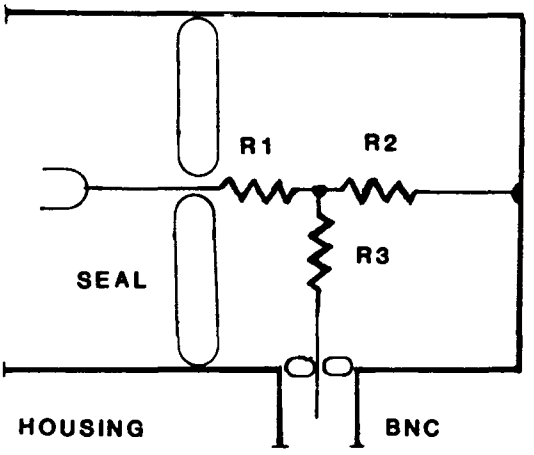

(b) R1=4300 OHMS R2=2.6 OHMS R3=45 OHMS

Fig. 3.35. Overview of the bushing potential-tap adapter. (a) Photo of adapter and (b) schematic of adapter.

4. COMBINED 60-HZ AND SFSD IMPULSE TESTS

4.1 INTRODUCTION

The majority of the evaluations performed for this project involved conducted impulse waves only. Suspension insulators, pin insulators, and distribution transformers were identified as possible weak links in the transmission and distribution systems.

This section addresses the behavior of suspension disks and distribution transformers with lightning arresters under stresses imposed by the simultaneous application of 60-Hz, steep-front impulses, and, where appropriate, mechanical load.

The specimens were mounted on a wood power pole in a manner similar to that of an actual utility installation, so as to simulate a distribution-line installation height of 10 m, with a pole-mounted ground lead. A maximum of 20 shots were to be made unless the specimen failed sooner. Positive-polarity impulses were to be applied at the negative 60-Hz crest and negative-polarity impulses at the positive 60-Hz crest, with a polarity change for each group of 5 shots. Specimens were energized either at 14.4 kV or 34.5 kV, 60 Hz. As an alternative, the insulators were energized at 20 kV or 49 kV dc in a circuit resonating at 60 Hz upon FO or failure. Unless otherwise noted, the available fault current was a maximum of 1000 A for all circuits.

The suspension-insulator strings were mechanically loaded with an axial tensile force of ~360 kg (800 lb).

4.2 TEST FACILITY

This experimental program was performed at the Thomas A. Edison Technical Center of Cooper Industries, combining the capabilities of the High Voltage Complex and the Short Circuit and Synthetic Laboratories. The test specimens were located in the High Voltage Complex, with the laboratory instrumentation facilities supplementing the LeCroy data acquisition system as well as the steep-fronted impulse. The Short Circuit Laboratory provided the 60-Hz source, which was connected to the specimens via an overinsulated tie line that was ~140 m (460 ft) long. The same tie line was used when the Synthetic Laboratory supplied 60 Hz to the RLC (resistance/inductance/capacitance) circuits. Impulse blocking equipment was placed between the specimen and the tie-line from the Short Circuit and Synthetic Laboratories. Figure 4.1 gives an overall view of the combined facilities.

4.3 SPECIMEN INSTALLATION

All the specimens, whether transformers or insulators, were mounted on a wood pole and/or wood crossarm per the test specifications. Under normal installation conditions, the distribution line would have an approximately 10-m mounting height, resulting in a ground-lead length of 10–12 m. For our laboratory purposes, this lead length was split into two segments—roughly one-half on the source side of the installation and one-half on the ground side. This represents the tightest coupling of the specimen to the generator that could be realistically achieved.

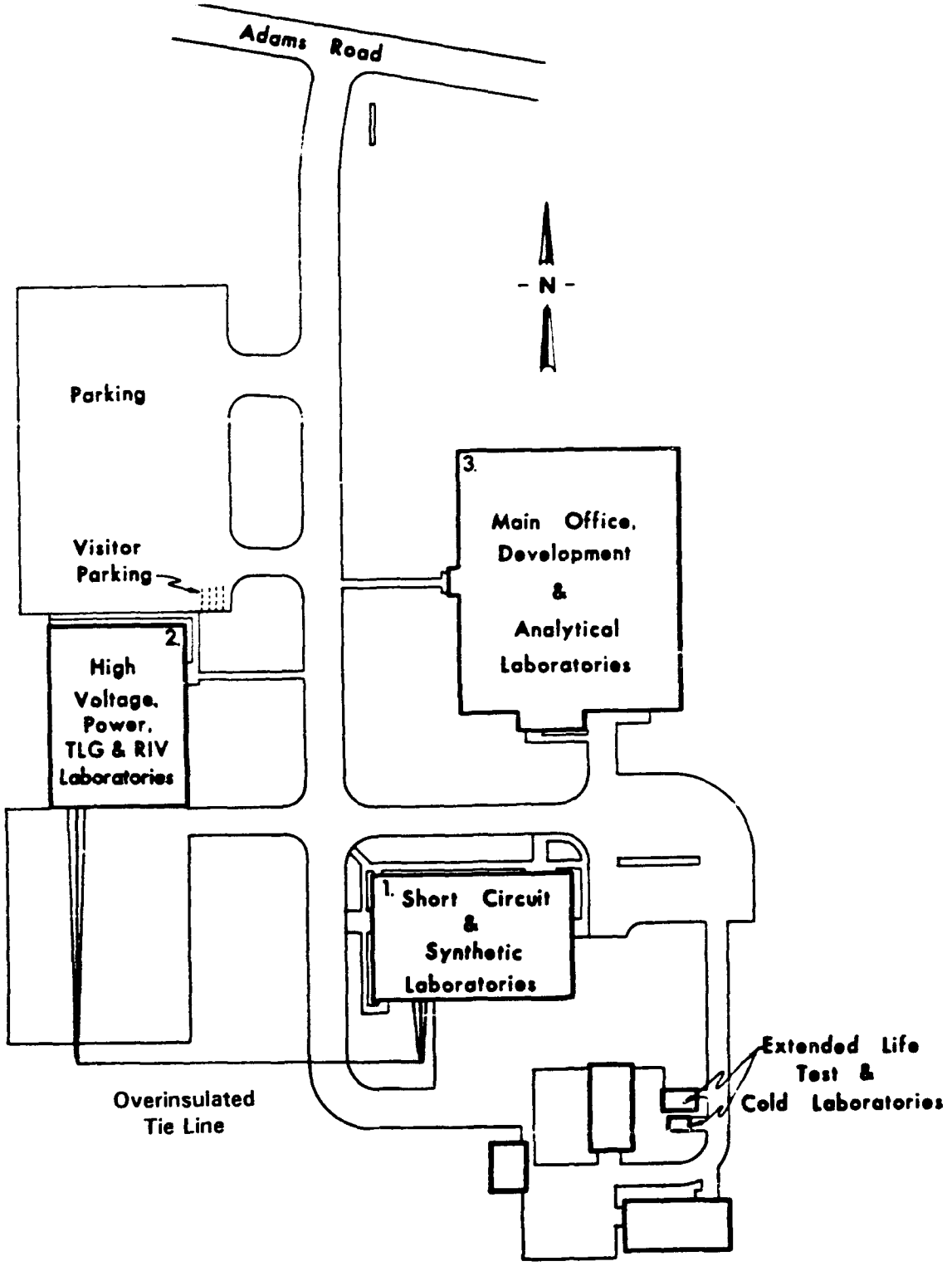

Fig. 4.1. Multistress evaluation test facility at the McGraw-Edison Power Test Laboratories.

A copper-sulfate impulse-voltage divider was tied to the source end of the approximately 5-m-long lead and to the same ground point as the grounded end of the other segment of the lead, also approximately 5 m long. The voltage measured by the voltage divider, therefore, is a combination of the IX (circuit reactance) drop of these leads and the specimen. Open-circuit voltages in the range of 800 kV to slightly over 900 kV were the norm. The specimen FO (insulators) or lightning arrester/transformer sparkover operation limited the maximum voltage during a shot to approximately 650 kV or less.

The necessity of the approximately 2-m spacing between the specimen source end-connection and the specimen ground reference-connection, combined with the tall, oil-insulated peaking capacitor and the long-peaking air gap, contributed to the approximately 90-ns impulse-wave rise time, which was somewhat slower than desired. A schematic of the test circuit including the instrumentation for the transformer/arrester portion of the test is shown in Fig. 4.2. Figure 4.3 shows the specimen, peaking capacitor, peaking air gap, and impulse-voltage divider.

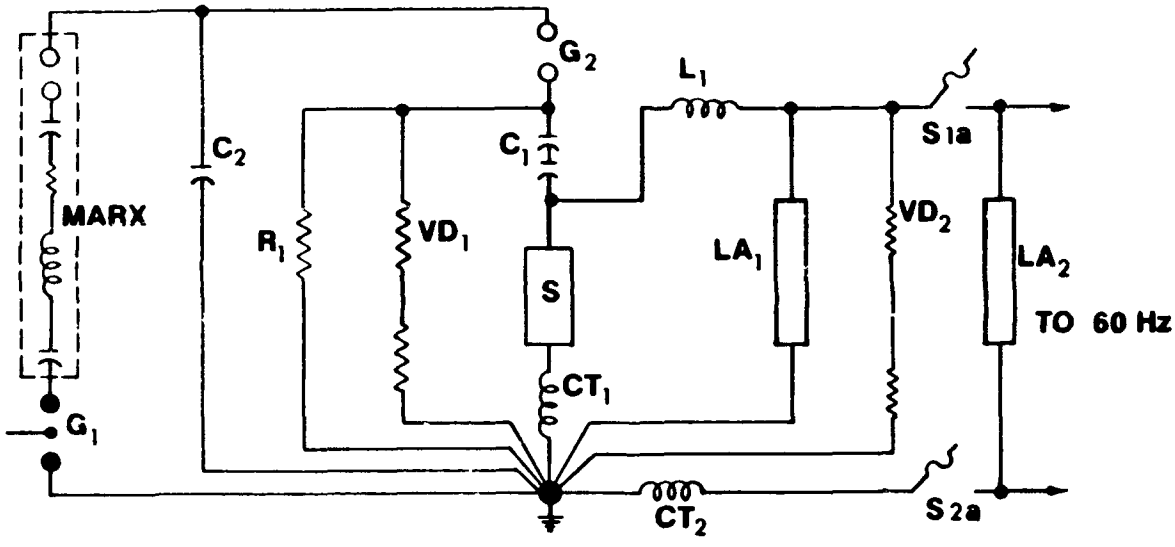

MARX = 11 STAGES .13μF/STAGE
4800Ω TOTAL
G_1 = PLASMA GAP, TRIGGER
G_2 = PEAKING GAP
C_1 = BLOCKING CAPACITOR 0.025μF
C_2 = PEAKING CAPACITORS 0.2 nF
L_1 = IMPULSE BLOCKING REACTOR
R_1 = 1KΩ

CT_1 = IMPULSE CURRENT
CT_2 = 60 Hz CURRENT
VD_1 = IMPULSE VOLTAGE DIVIDER
VD_2 = 60 Hz VOLTAGE DIVIDER
LA_1 = 36 KV DISTRIBUTION ARRESTER
LA_2 = 54 KV DISTRIBUTION ARRESTER
S = SPECIMEN

Fig. 4.2. Combined 60-Hz and steep-front test circuit used for the suspension insulator and distribution transformer evaluations.

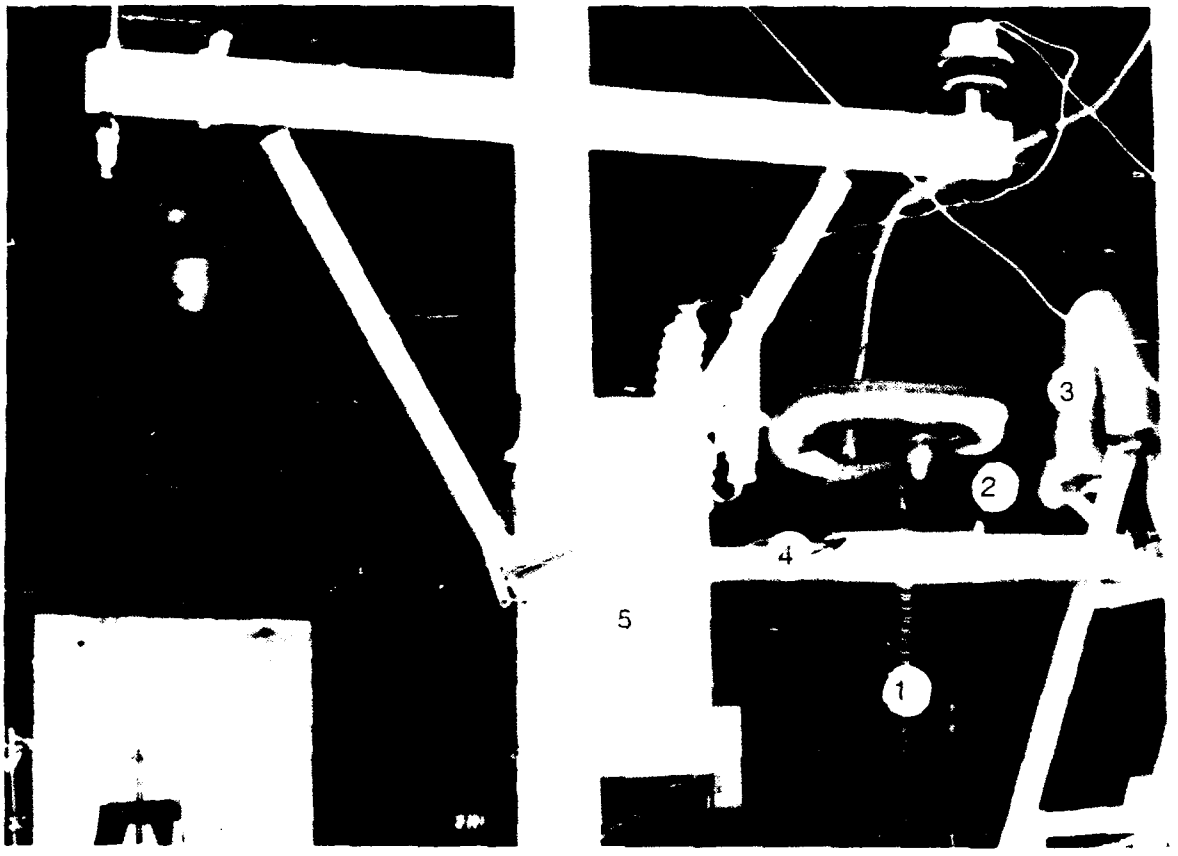

Fig. 4.3. Installation of (1) peaking capacitor, (2) peaking gap, (3) impulse-voltage divider, (4) blocking capacitor, and (5) specimen for the multistress test.

Simultaneous specimen impulse voltage, specimen impulse current, 60-Hz voltage, and 60-Hz current were recorded for each shot. Normal-speed video was used to monitor virtually all shots. A D-dot sensor was used to confirm waveshape.

4.4 EVALUATION OF TRANSFORMERS WITH ARRESTERS

This section discusses specimen characteristics and results of testing for transformers with arresters.

4.4.1 Specimens

The transformers selected for this evaluation were 25-kVA, 14.4-kV→120/240-V, single-phase, single-bushing, pole-mounted, shell-form transformers with LO-HI-LO winding construction and with an internal weak-link fuse and secondary breaker. The arrester, which was either tank-mounted and direct connected, tank-mounted with an external gap, or crossarm mounted, was an 18-kV, SiC distribution-class device.

Figure 4.3 shows the installation with the direct-connected arrester. Transformer secondary-load resistors are visible immediately adjacent to the left side of the transformer tank. Visible in the right background are the peaking air gap (between spheres), peaking capacitor, and gap/voltage-divider/blocking-capacitor connection. The blocking capacitor (see Figs. 4.2 and 4.4) prevented 60 Hz from damaging the copper-sulfate impulse-voltage divider.

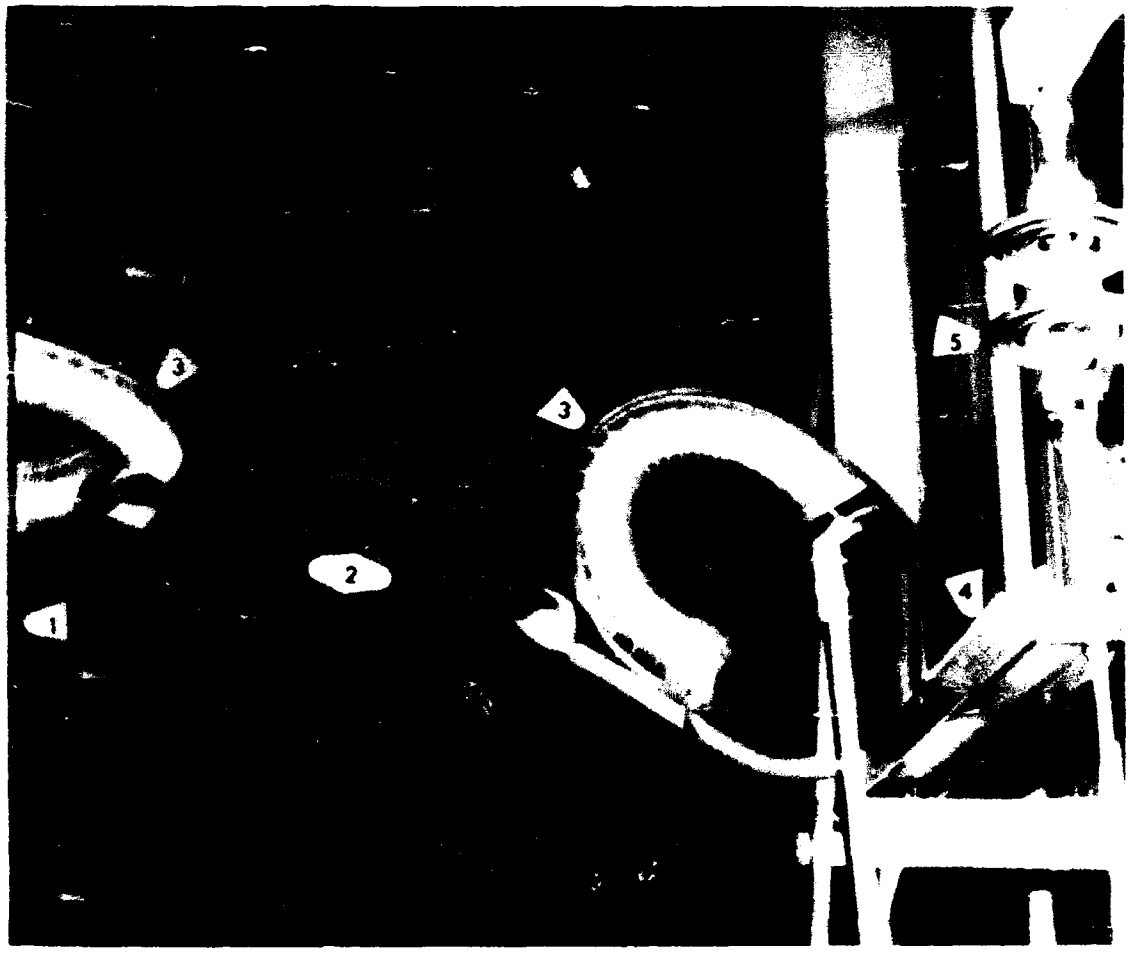

Fig. 4.4. Part of the impulse circuit consisting of the (1) peaking capacitor, (2) peaking gap, (3) gap grading rings, (4) 60-Hz blocking capacitor and support, and (5) suspension-disk specimen.

The transformer installation with the arrester crossarm mounted is also shown in Fig. 4.5. The lead identified as "to 60 Hz" connects to the impulse blocking apparatus, which includes a remotely operated oil switch and fused disconnect switches (see Fig. 4.6) for 60-Hz energization and fault-current interruption in the event of catastrophic specimen failure.

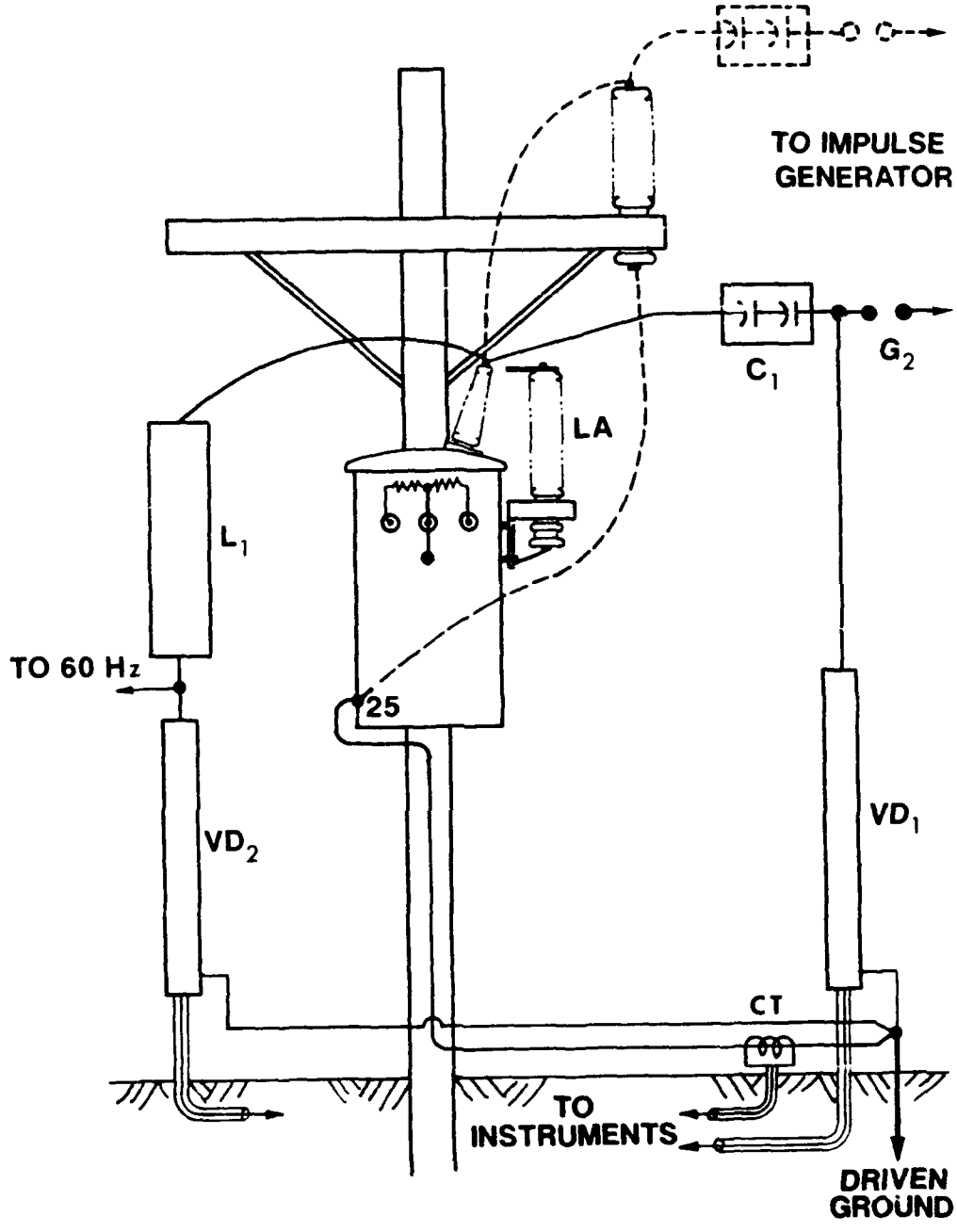

Fig. 4.5. Schematic of the distribution transformer in the test circuit with the associated lightning arrester shown in its several positions. Shorting out the external gap at the top of the arrester LA produced the tank-mounted direct-connected version.

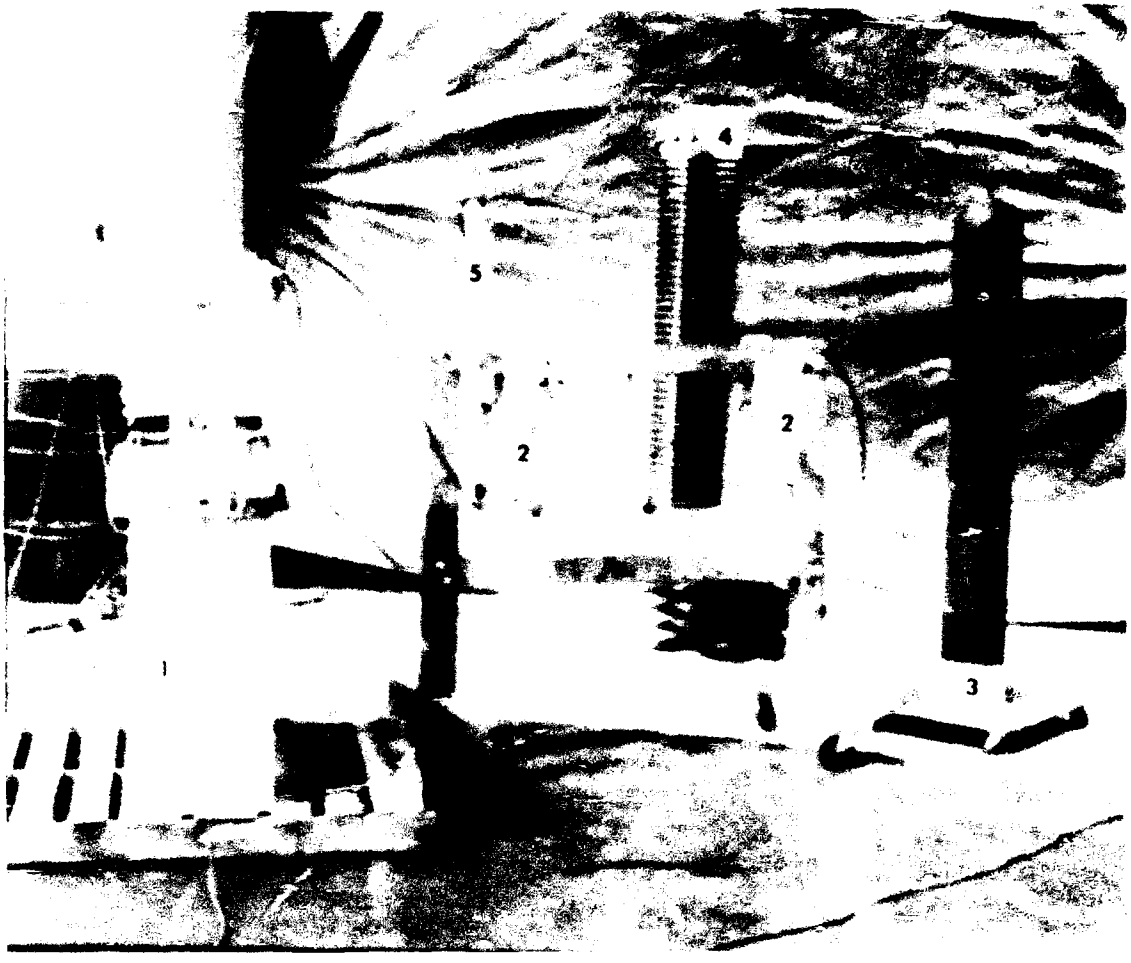

(1) oil switch
(2) fused disconnect switches
(3) potential divider
(4) air core reactor
(5) arrester

Fig. 4.6. Impulse-blocking equipment between the test specimen and the short-circuit generator.

For the test, the 60-Hz voltage was applied to the transformer primary for a minimum of 30 s (typically 1 min) prior to the application of the impulse. This 30-s-plus time interval was required to stabilize the charge distribution within the transformer. The voltage was also maintained on the specimen for 1 min following the impulse application to allow any insulation damage to evolve into a fault. In the event that the transformer survived a total of 20 impulses applied with 60 Hz, a neutral-current test was performed and compared with the neutral-current measurement made prior to the 20-shot sequence. If no failure was detected, the same transformer was subjected to another set of 20 shots with the arrester connection changed to one of the alternatives. The impulse polarity was reversed for each group of 5 shots of the 20-shot sequence as was done previously. Unless failure occurred, the process was repeated for each alternative configuration.

4.4.1.1 Transformer/arrester specimen no. 3.9

The first test sequence used transformer no. 3.9 with an 18-kV MOV lightning arrester that was tank-mounted and direct-connected. The available fault current was approximately 1000 A rms and was supplied by the Short Circuit Lab. The 60 Hz was applied for a minimum of 30 s prior to the application of the impulse. This transformer/arrester combination survived 20 shots, with shots made in groups of 5 with alternating polarity between each group. The same specimen was subjected to a similar sequence with an external 15/16-in. gap between the arrester and the transformer bushing. The combination again survived 20 shots. The 15/16-in. gap was observed flashing over on each shot. The arrester was then mounted on a crossarm with a total of approximately 3 m of lead from the transformer bushing through the arrester to the ground connection on the transformer tank. This combination was subjected to 20 shots and again was not damaged.

4.4.1.2 Transformer/arrester specimen no. 6.9

A second transformer was tested using an 18-kV SiC arrester that was tank-mounted and direct-connected. Then it was tested using a series with an external 15/16-in. gap between the arrester and the transformer bushing, and again tested using the crossarm-mounted arrester as had been done for the first transformer. This transformer/arrester combination took a total of 60 shots without failure (20 shots from each test sequence).

4.4.1.3 Transformer/arrester specimen no. 4.0

For the third transformer with an 18-kV SiC arrester, the sequence of test conditions was reversed. The first sequence of 20 shots was taken with the arrester mounted on the crossarm with a normal 3-m lead between the arrester and the bushing and transformer tank. This combination failed. Failure was evidenced by an increase of approximately 30% in the neutral-current test performed following the twentieth shot, compared with the neutral-current measurement prior to any shots. No external display was observed.

No detectable fault current flowed at any time during this test sequence, and no change in exciting current could be detected.

4.4.2 Results

Table 8 summarizes the results of the transformer-arrester testing

Table 8. Results of transformer-arrester testing

SPEC. NO.	ARRESTER CONNECTION	NO. OF SHOTS		CHANGE IN NEUTRAL CURRENTS
		+IMPULSE	−IMPULSE	
2.9	direct[1]	10	10	none
	gapped[2]	10	10	none
	crossarm	10	10	none
3.9	direct[1]	10	10	none
	gapped[2]	10	10	none
	crossarm	10	10	none
4.0	crossarm	10	10	30% increase

[1]Tank-mounted and direct-connected
[2]Tank-mounted with 15/16-in. external gap

NOTE: The data summary is in Appendix C, Section C.1.

Typical impulse-voltage traces for the lead transformer and arrester combinations are shown in Fig. 4.7. These traces are for a negative impulse on a positive 60-Hz crest. A substantial portion of the impulse voltage is the lead drop. For the externally gapped arrester configuration, the maximum voltage appearing across the transformer ranges from 125 to 150 kV, as was evidenced by visual and photographic observation of the gap sparking over on each shot.

Figure 4.8 displays the positive impulse voltage on negative 60-Hz voltage for specimen no. 4.0 for the first and twentieth shots. The perturbation at the A in Fig. 4.8 indicates insulation system failure.

The neutral-current data traces taken before and after the 20-shot sequence are similar to those shown in Fig. 4.9. The neutral-current trace before testing is self explanatory. The neutral-current trace AFTER testing involved a significant increase in the current, exceeding the signal clipping level. The failure was NOT permanent. A second neutral-current injection failed to show the damage.

Disassembly of this transformer revealed both turn-to-turn and layer-to-layer insulation damage at the edge of the outermost layer of the primary winding near a corner. The damage was not severe enough to cause an evolving 60-Hz fault. Figure 4.10 shows the location of the failure with slight discoloration and extremely slight degradation of the outer wrap of layer insulation. Figure 4.11 shows the degradation of the layer insulation between the two outer layers of the primary winding. The failure of the third transformer (no. 4.0) cannot be immediately explained. Although efforts were made to reduce the "conditioning" effects of repeated shots, such conditioning of the samples may have occurred in the first and second samples (nos. 3.9 and 2.9, respectively). Placing the arrester on the crossarm earlier in the test sequence for the third transformer (no. 4.0) may have subjected it to higher stress earlier in the sequence. Trapped charge may be one possible cause of this "conditioning" phenomenon.

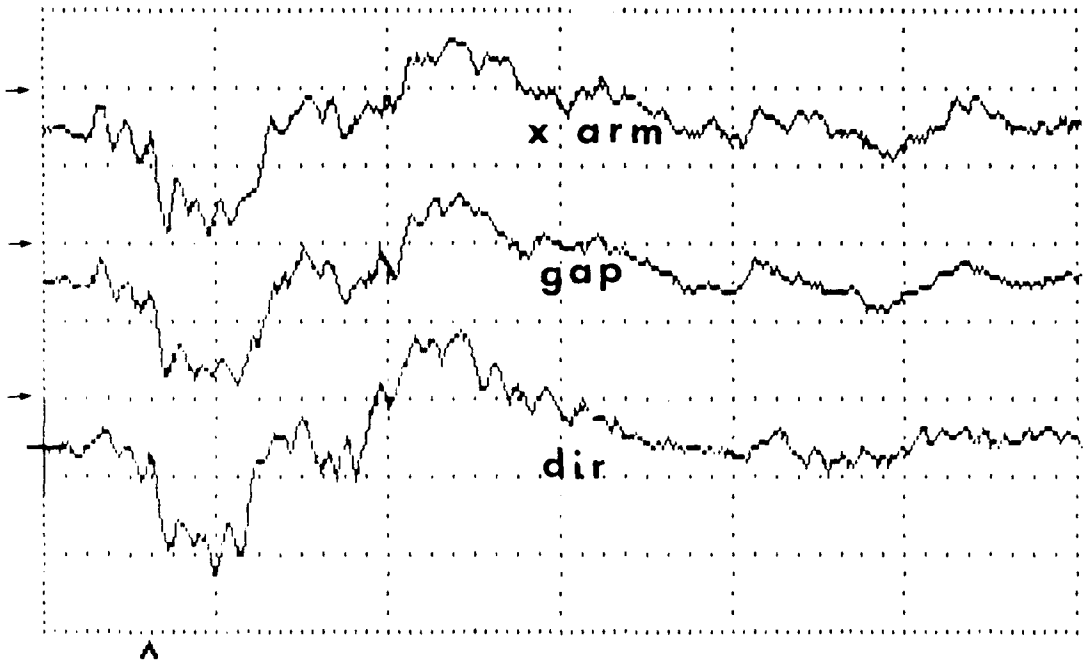

Scale factor for vertical axis (all th ee traces): 270 kV/division.
Scale factor for horizontal axis (all three traces): 200 ns/division.

Fig. 4.7. Negative impulse voltage on positive 60-Hz voltage for each of the three transformers with arrester configurations. The zero lines for each of the traces are at the arrows.

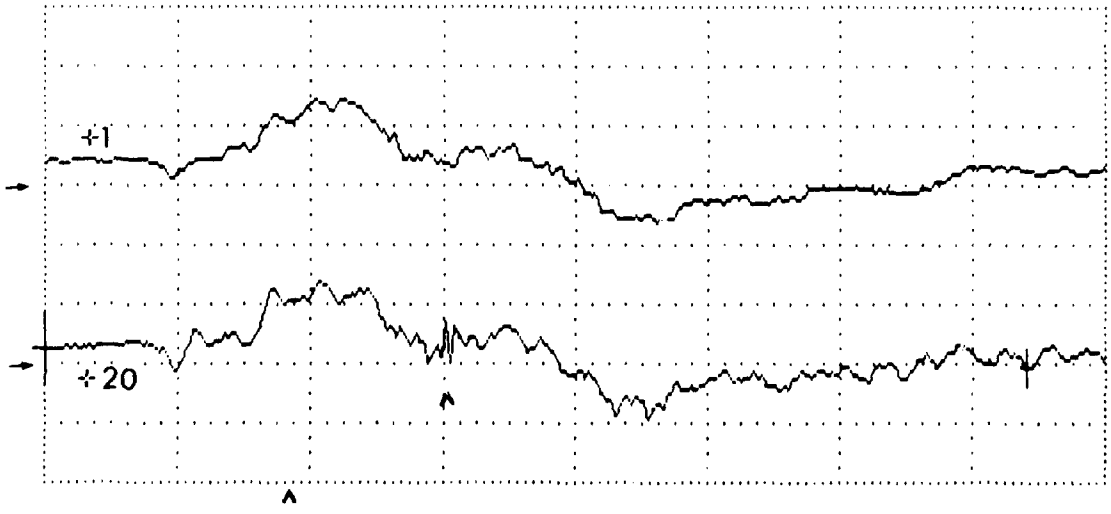

Scale factor for vertical axis: 270 kV/division.
Scale factor for horizontal axis: 100 ns/division.

Fig. 4.8. Positive impulse voltage on negative 60-Hz voltage traces for the first and twentieth shots. The arrows indicate the zero line positions for the two traces.

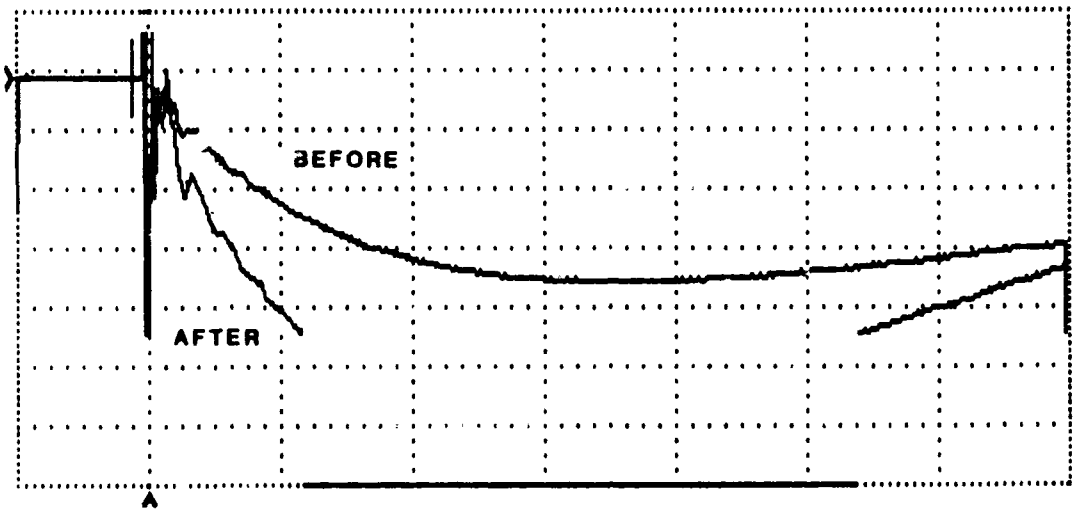

Scale factor for vertical axis: 20 A/division.
Scale factor for horizontal axis: 20 μs/division.

Fig. 4.9. Neutral-current injection traces before and after the failure of specimen under impulse only. The "after" signal exceeded the signal clipping level. Independent instrumentation yielded a peak current of 114 A as compared with the "before" magnitude of 69 A.

Fig. 4.10. Failure at the edge of the outer layer of the primary winding. The outer section of the secondary winding has been removed.

Fig. 4.11. View showing degradation of the layer insulation between the two outermost layers of the primary winding.

4.5 SUSPENSION INSULATORS

We obtained used suspension insulators conforming to ANSI class 52-3 and 52-4 specification (see Fig. 3.14). These insulators, which were obtained from utility serviceable stores, were manufactured in 1968–69 and had been in utility service for an indeterminate period. They were hung from the pole-mounted wooden crossarm using conventional suspension hardware and were loaded with a 360-kg weight. This weight, a small fraction of the rated tensile strength of the insulator, is representative of the mechanical loading of these insulators on distribution lines. Two line configurations were used. The first configuration simulated a horizontal distribution line by using a 3-m (10-ft) length of 1-in. (trade size) electrical conduit terminated in 30-cm (12-in.) spheres lying horizontally in the suspension saddle. The second configuration simulated dead-end construction using an axial load only. The suspension hardware fastened to the crossarms was grounded (60-Hz pole ground lead) for most of the program. A number of shots, however, were taken with this hardware ungrounded, using an intentional 20-cm (8-in.) gap on the crossarm between the hardware and the closest ground connection. Figure 4.12(a) shows the configuration used for the mid-line specimens. The 20-cm gap, if used, provides approximately 100 kV of insulation strength when subjected to 1.2- by 50-μs impulses. Figure 4.12(b) shows the configuration used for the dead-end specimens. The dead weight was spaced off the floor to maintain axial tensile force during a shot or sequence of shots. The behavior of the specimens was monitored by using normal-speed video recording.

4.5.1 Suspension-Insulator Tests

The specimens using two suspension disks in series with grounded hardware were tested first, with the nominal 60 Hz supplied from the Synthetic Lab. Available fault current was approximately 1000 A on the first loop, decaying to approximately 400 A on the third loop. (A loop corresponds to one-half cycle.) Two of these specimens survived all 20 shots, which were made in groups of five and changed polarity for each group. One of the insulators on one of the three specimens punctured and carried 60 Hz, but did not fracture or catastrophically fail. A 500-V megohmmeter gave a zero resistance measurement on the punctured disk. This specimen failed on the sixth shot, which was the first application of a positive impulse following five applications of negative impulse. The same specimen was subsequently tested under similar conditions with 1000 A available from the Short Circuit Laboratory. Similar specimens were tested using a 20-cm gap between the suspension hardware and ground along the wood crossarm. While these specimens could be flashed over on every shot with impulse only, they could not be flashed over on every shot when the Synthetic Laboratory's FO follow-current system was connected to the specimen. The 60-Hz circuit from the Synthetic Laboratory effectively reduced the output of the impulse generator such that the series insulation combination of porcelain and wood could not be flashed over.

Several specimens of single suspension disks were inserted in a tightly coupled impulse circuit having rise times substantially less than 90 ns (some rise times on the order of 20 ns were recorded). All such single insulator specimens on this circuit were punctured within two to seven shots. These punctured insulators were subsequently tested in series with other good insulators. In all cases, the punctured insulators subjected to impulse with 60 Hz fractured. In several instances, the suspended lines did not drop even though all of the skirts were blown off the two-disk combinations, and half of one of the skirts was blown off a second two-disk combination. For this sequence of tests, the available 60-Hz fault current was raised to approximately 2500 A rms in the first loop, decaying to approximately 1000 A rms on the third loop of current flow.

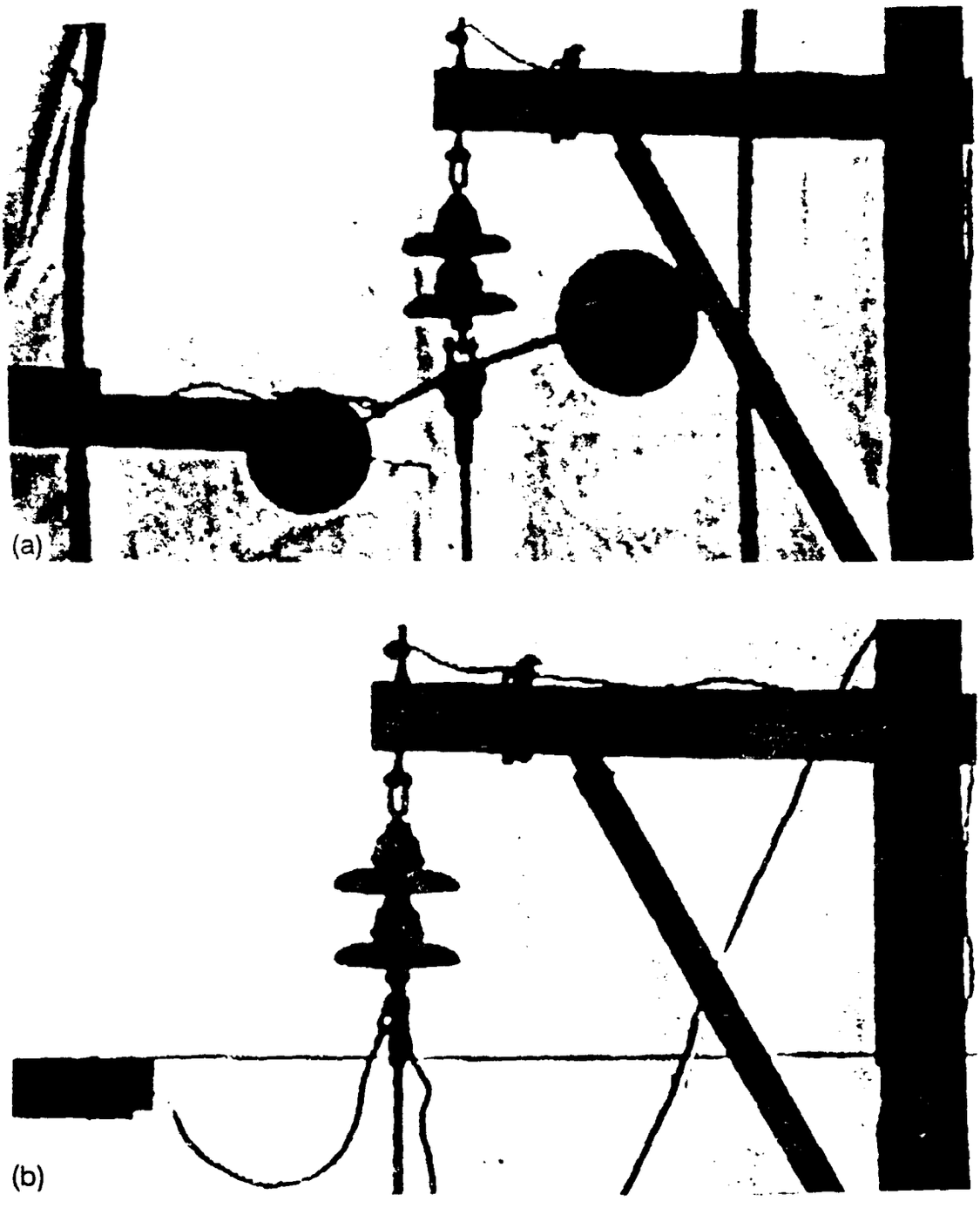

Fig. 4.12. (a) Suspension-insulator specimen simulating midline construction, and (b) simulated dead-end construction.

Figure 4.13 shows typical upper-surface damage to the suspension disks as the result of the exposure to the multistress environment. Figure 4.14 shows the underside damage to the insulators. Figure 4.15 shows the severe damage incurred when the specimen fractured but did not drop the line. Figure 4.16(a)-(e) is a sequence of frames from the video recording that displays FO and follow-current flow without the line dropping. Figure 4.17(a)-(e) shows a similar sequence of frames with FO, fault-current flow, and suspension-disk fracture followed by line dropping.

Fig. 4.13. Damage to the upper surface of the suspension disks resulting from fault-current flow initiated by a steep-fronted impulse.

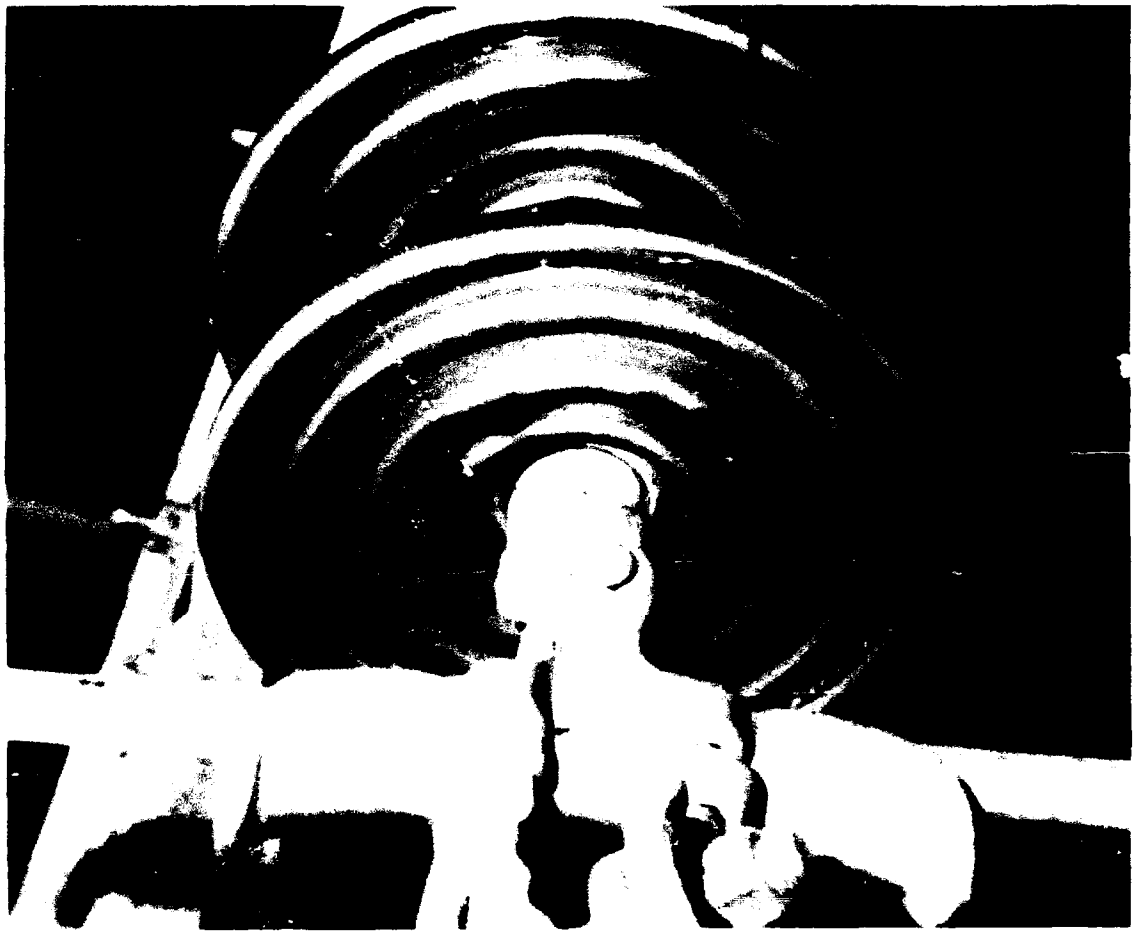

Fig. 4.14. Damage to the lower surfaces of the suspension disks resulting from fault-current flow initiated by a steep-fronted impulse.

Fig. 4.15. Severe damage to the suspension-disk specimens without the line dropping.

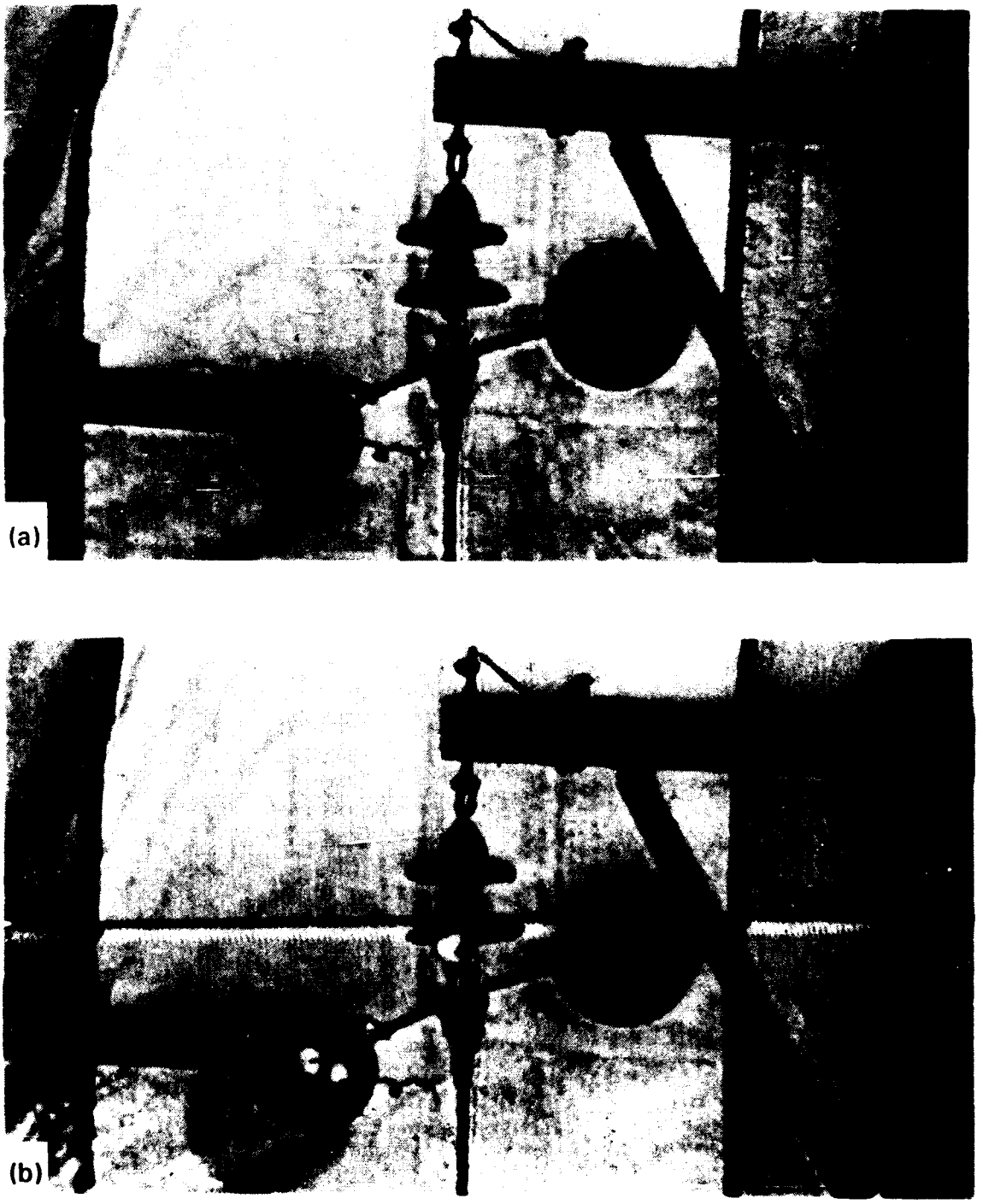

Fig. 4.16. Sequence of video frames showing flashover and fault current arcing without the line dropping: (a) prior to test, (b) initial flashover.

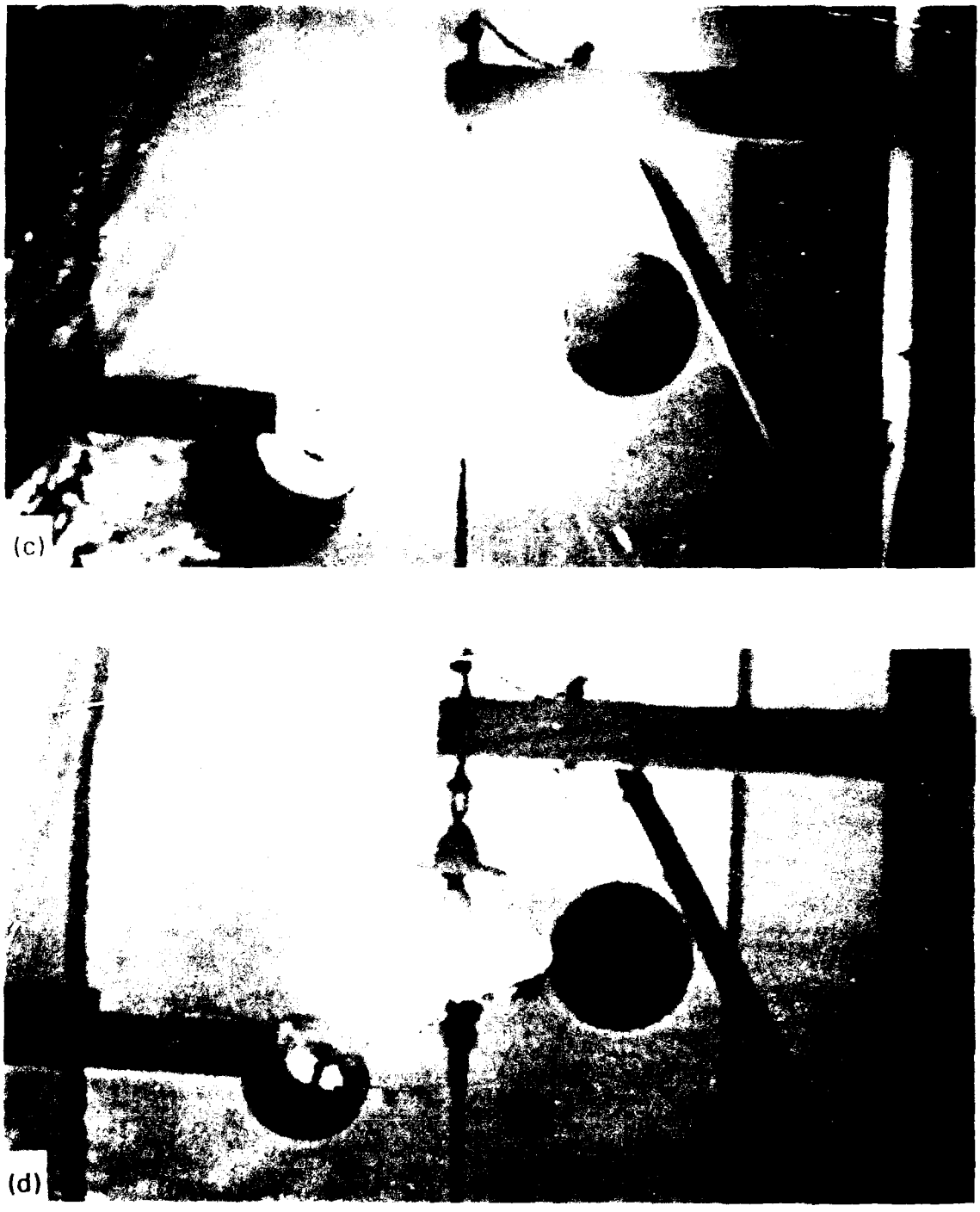

Fig. 4.16. (c) Maximum power follow, (d) decaying arc.

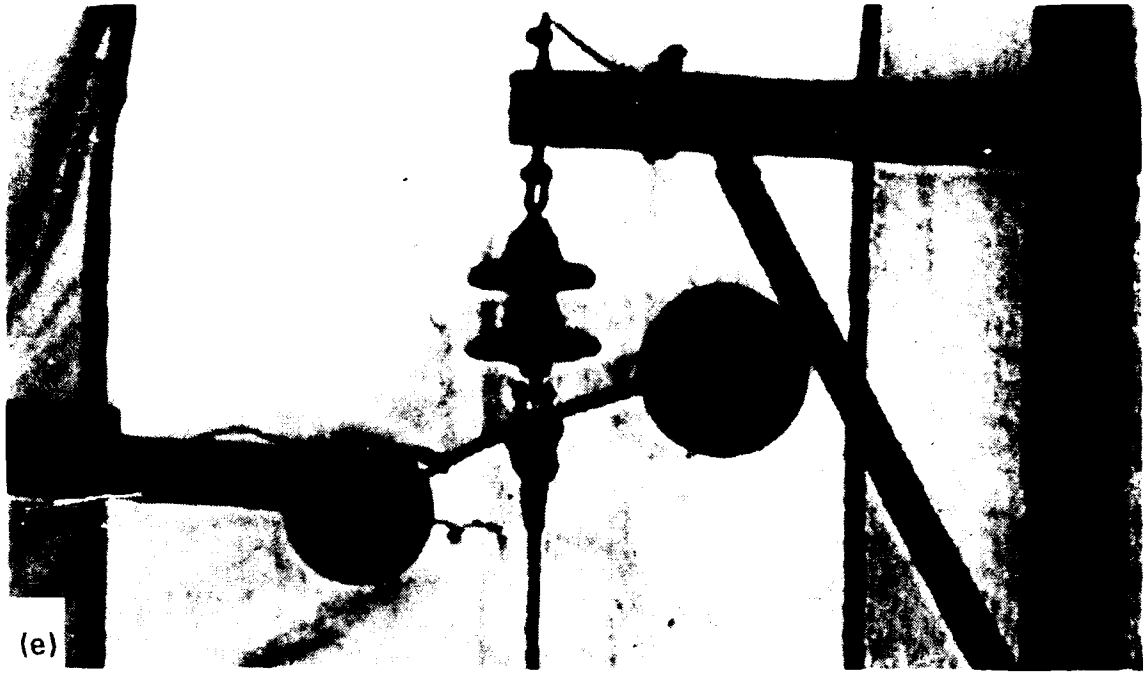

Fig. 4.16. (c) End of test sequence showing that line has not dropped.

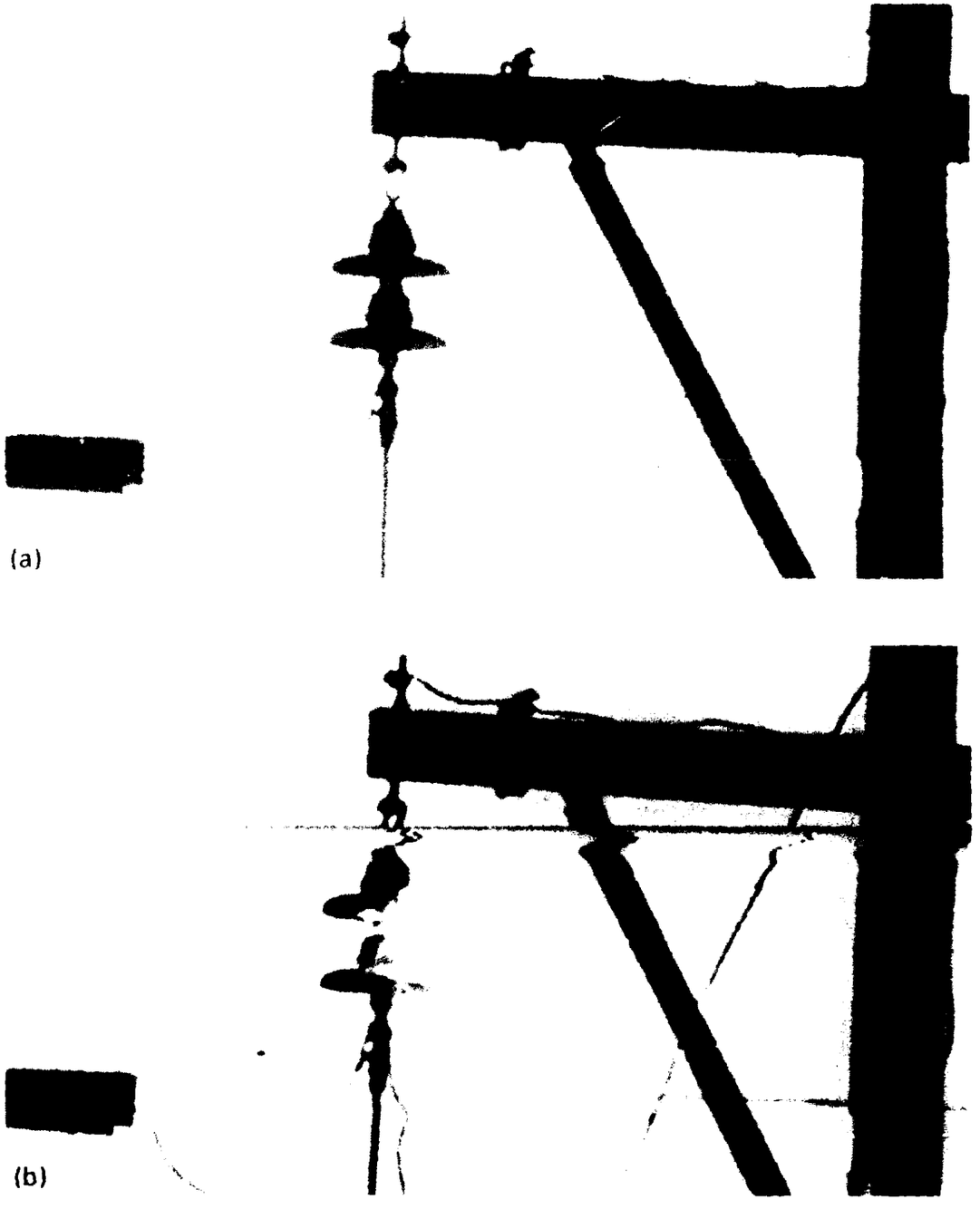

Fig. 4.17. Sequence of video frames showing flashover and fault-current arcing, incluing fracturing of the suspension disks accompanied by line dropping: (a) prior to test, (b) initial flashover.

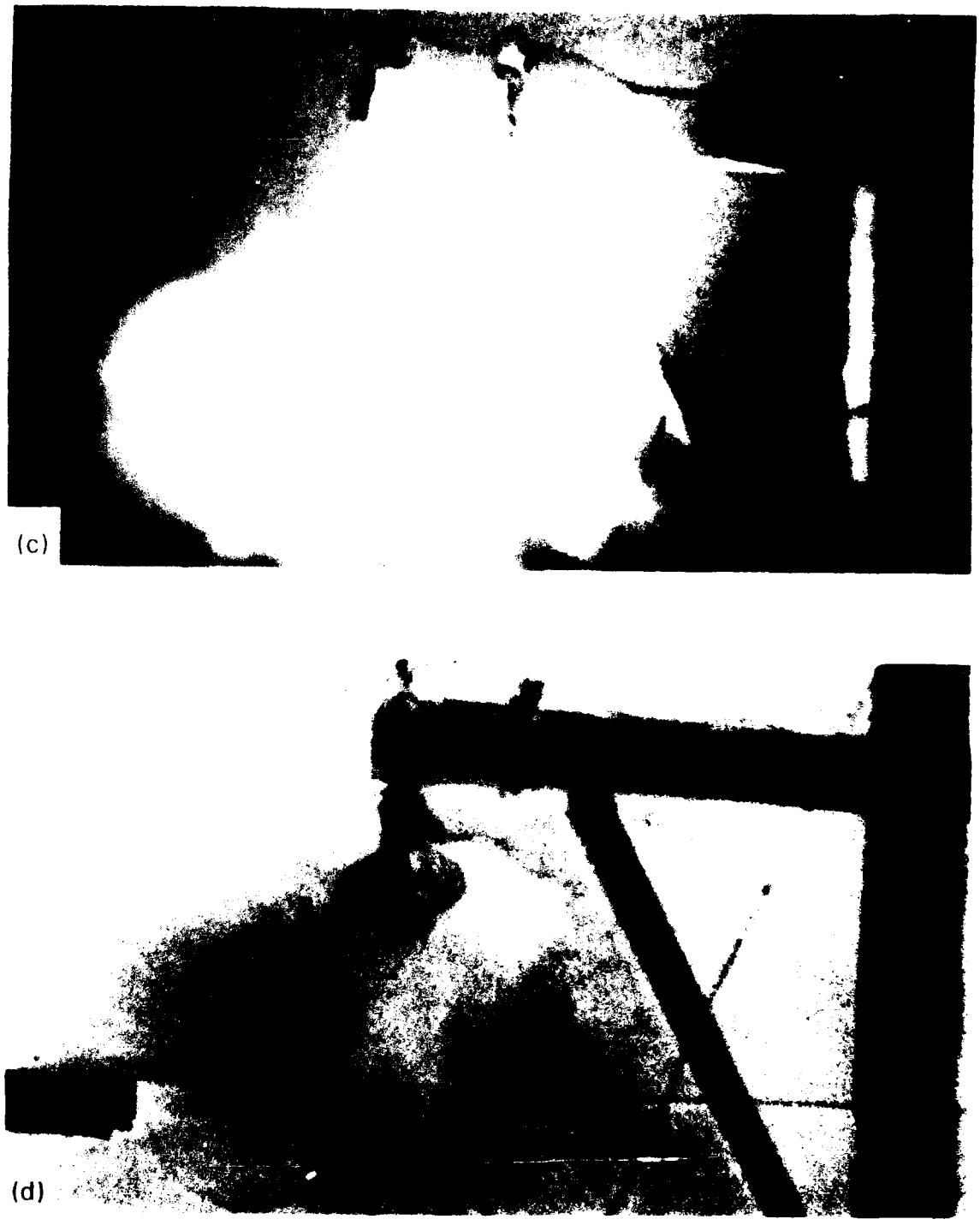

Fig. 4.17. (c) Maximum current and beginning of destruction of disk, (d) destruction of disk.

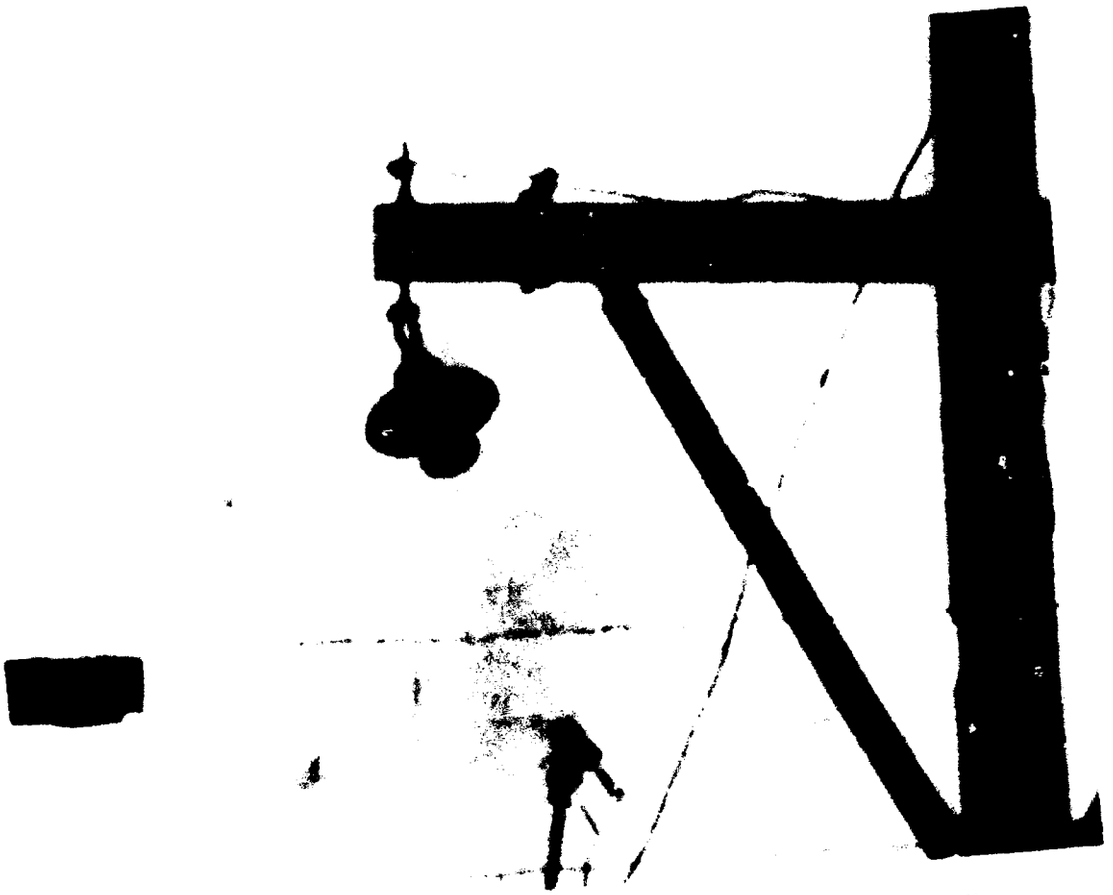

(e)

Fig. 4.17. (e) End of test sequence showing failed disk and dropped line.

4.5.2 Results of the Multistress Evaluation of the Suspension Insulators

Table 9 summarizes the results of the multistress evaluation of the suspension insulators.

Table 9. Results of multistress evaluation of suspension insulators

SPEC. NO.	NO. OF DISKS	APPLIED KV DC	AVAIL. FAULT I, 60-HZ CREST	NO. OF SHOTS		AVG FO (KV)		HWARE GRNDED?	NOTES
				−IMP. ON +60-HZ CREST	+IMP. ON −60-HZ CREST	+	−		
1.2	2	22.4–2..	991–1150	14	10	435	571	yes	Surface, 1
3.4	2	23.2–24	1044–1080	10	10	422	634	yes	Puncture, 1, 2
	2	21 pk 60 Hz	926–991	3	2	421	720	yes	Surface, 4
5.6	2	21.6–23.2	1009–1080	10	10	430	608	yes	Surface, 1, 5, 6
7.8	2	21.6	973–1027	4	---	---	673	no	FO on tail
9.10	2	---	---	---	4	---	424	yes	FO on tail, 7
9.10	2	---	---	---	3	---	492	no	Surface, 1
9.10	2	2 .6–25.6	2337–2585	10	10	473	676	yes	Surface, 1
11.12	2	23.4–24.3	2408–2550	10	10	461	6.0	yes	8
13.14	1	24–24.6	2372–2514	5	5	492	650	yes	2 shot, puncture, 9
15	1	---	---	---	---	---	502	---	7 shot, puncture, 9
16	1	---	---	---	---	---	210–562	---	5 shot, puncture, 9
17	1	---	---	---	---	---	464–567	---	3 shot, puncture, 9
18	1	---	---	---	---	---	497–572	---	1 shot, puncture, 9
19	1	---	---	---	---	---	326	---	16 shattered, 10
19.16	2	23	2400	---	1	---	605	yes	19 shattered, 10
18.19	2	23	240	---	1	---	443	yes	8
20.21	2	23.2–23.9	2439–2499	---	3	---	682	yes	10
21.15	2	23.7	2499	---	1	---	540	yes	

Table 9. (cont.)

Notes:

1. Upper surfaces of both disks heavily damaged on all shots carrying fault current.
2. Upper disk punctured on the sixth shot, the first +impulse following five −impulses.
3. Five shots, four cycles 60-Hz follow current. Line did not drop.
4. Flashover and fault current flowed on every shot unless otherwise noted.
5. Fault current flowed on two shots only. Three additional shots showed delayed FO at 0.75 to 1.5 μs with voltages at FO of 450–858 kV, 906 kV available.
6. Wood gap flashed over on top of crossarm.
7. Wood gap flashed over on bottom surface of wood crossarm.
8. Line did not drop.
9. Impulse only.
10. Line dropped.

5. CONCLUSIONS AND RECOMMENDATIONS

In general, the response of electric-power insulation systems to SFSD impulses is more detrimental to the insulation systems than might be expected from the lightning-impulse response of such systems. However, as discussed below, methods exist for protecting the system against the SFSD impulse in the ranges (both waveshape and voltage/current) studied during this research effort.

Indeed, the strength (BIL) of all insulation systems studied—viz., oil/paper/enamel, oil/paper, and porcelain/air, as characterized in distribution and power transformers, structural insulation, and bushings—increases under SFSD impulse. As indicated, however, the increase of BIL is not as great as would be expected from extrapolation of lightning-impulse data, and there is strong evidence that delayed failure will result from cumulative exposure to SFSD impulse. Such failures may result from a series of SFSD impulses below the BIL required for a failure under a single SFSD impulse.

Simultaneous external FO and internal puncture was observed during the course of these investigations for both structural insulation (suspension disks) and paper/oil systems (power-transformer bushings). Catastrophic failure occurred in one case for the power-transformer bushings under impulse only. In the case of suspension insulators, catastrophic failure was also demonstrated for the combined impact of SFSD impulse and 60-Hz power follow currents greater than 2.4 kA.

Because the nominal waveshapes used in this study were chosen to bound the range of rise times and durations of interest (1.2 by 50 μs, 100 by 500 ns, and 10 by 150 ns), the results are applicable to sources ranging from the standard lightning impulse to the fastest coupled EMP impulse. The peak magnitudes of the impulses used were chosen to reflect the peak values expected from the source waveform. In many cases, failure or FO occurred before the peak value was reached. Flashover or arrester action also limited applied peak voltages, and the resulting data was used to suggest protective methods and practices.

The statistical significance of the results of these experiments must be noted. Because of limited resources, the decision was made to use a small number of test specimens with a large number of impulses. The results therefore provide a correct response for the samples tested at the expense of a probability distribution of failure and FO performance, and attempts to develop such distributions from the summary data must be discouraged.

The following conclusions are drawn on the basis of the evaluations performed using conducted SFSD impulses.

1. Conducted steep-front impulses have been shown to flash over and damage or puncture unenergized, unprotected apparatus having BILs of 550 kV and less. The likelihood of damage increases as the BIL decreases. A BIL range susceptible to damage is 115–200 kV. The susceptibility of apparatus with BILs of 95 kV and below was not determined.

2. Under energized conditions, suspension insulators and transformers without direct-connected arresters have been damaged by exposure to a conducted wave simulating the EMP-coupled wave. The damage to suspension insulators has been catastrophic. Damage to distribution transformers

without direct-connected arresters reduces the expected service life of same, and may lead to complete failure of the units at an undeterminable time in the future.

3. Adhering to good protection practices by using conventional lightning arresters will reduce dramatically the incidence of insulation damage to apparatus such as transformers and their associated bushings when exposed to these steep-fronted transients. It is strongly recommended that all distribution transformers be protected with appropriately rated lightning arresters, either SiC type or MOV type.

   It is further recommended that these lightning arresters be tank-mounted and direct-connected to the transformer input bushing, which can be accomplished by retrofit as well as by new or replacement construction. The behavior of under-oil arresters when subjected to these SFSD impulses is not well known, but with minimum lead length they should provide similar protection. It is recommended that lightning arresters be located immediately adjacent to the higher-voltage-rated (30 kV and higher) distribution- and transmission-class transformer bushings, reducing the connecting-lead length to an absolute minimum.

4. The likelihood of damage to the structural porcelain insulation can be reduced by using additional insulators, thereby increasing the BIL and reducing FO probability at lower impulse levels.

   Consideration should be given to over-insulating critical distribution lines while maintaining present overvoltage protection levels.

5. The likelihood of catastrophic failure of suspension insulators increases at higher available fault currents. Dielectric failure induced by steep-front impulse to both porcelain/air and paper/oil systems may not be instantaneously followed by catastrophic failure. A delayed total failure is more likely.

6. As indicated by this project's attempts to model the transient behavior of transformers, using closed-form analytical models to predict insulation system behavior is not economically viable. The classical representation of experimentally derived data is the easiest and most economically practical way to understand insulation system response to the SFSD impulse.

All the work reported herein used conducted impulses on energized or unenergized discrete devices, without taking into account that other nearby devices could interact with and possibly ameliorate the effects of these impulses. Protective devices located within one or two pole spans could reduce the impact of the coupled wave. However, such devices that are located beyond the next ground points, typically 5 or 6 pole spans away, would be less likely to help.

Finally, for EMP studies, it is recommended that staged tests be performed illuminating a section of a distribution line and line substation, using an EMP generator. Such an exercise would provide additional insight into EMP/distribution system coupling factors, structural-insulation performance, protective-equipment performance, and circuit-breaker/circuit-recloser/control performance. The evaluation should be performed both with the system energized and with the system unenergized.

6. REFERENCES

1. L. M. Burrage et al., *Assess the Impact of the Steep Front, Short Duration Impulse on Electric Power System Insulation - Phase I Final Report,* ORNL/Sub/85-28611/1, Oak Ridge Natl. Lab., Martin Marietta Energy Systems, Inc., February 1987.

2. *IEEE Standard Techniques for High Voltage Testing,* ANSI/IEEE Std. 4-1978, Wiley Interscience, John Wiley & Sons, Inc., New York, 1978.

3. J. H. Park and H. N. Cones, "Spark-Gap Flashover Measurements for Steeply Rising Voltage Impulses," pp. 197-207, *J. of Res. of the Natl. Bureau of Standards,* C. Engineering and Instrumentation, Vol. 66C, No. 3, July-Sept. 1962.

4. *IEEE Guide for Transformer Impulse Tests,* IEEE Standard 93, ANSI C57.98, New York, 1968.

7. LIST OF OTHER PUBLICATIONS RESULTING FROM THIS WORK

1. B. W. McConnell and L. M. Burrage, "Assess the Impact of Steep-Front, Short-Duration Impulse on Power System Insulation—A Review of Progress to Date," Nuclear EMP Meeting, Univ. of New Mexico, Albuquerque, May 19-23, 1986, p. 81 of NEM 1986 RECORD.

2. L. M. Burrage, P. F. Hettwer, and B. W. McConnell, "Impact of Steep Front Short Duration Impulses on Power System Apparatus and Insulation: A Critical Review," IEEE International Symposium on Electrical Insulation, Paper D-5, Washington, D. C., June 8-11, 1986.

3. L. M. Burrage et al., *Assess the Impact of the Steep-Front Short Duration Impulse on Electric Power System Insulation, Phase I Final Report,* ORNL/Sub/85-28611/1, Oak Ridge Natl. Lab., Martin Marietta Energy Systems, Inc., February 1987.

4. E. F. Veverka and B. W. McConnell, "Steep Front Short Duration Low Voltage Impulse Performance of Distribution Transformers, IEEE/PES Winter Meeting, February 1-6, 1987, New Orleans, La., *IEEE Trans Power Delivery,* Vol. PRWD-2, No. 4, pp. 1152-1156, October 1987.

5. J. H. Shaw, "Instrumentation System Used to Determine the Effects of Steep Front Short Duration Impulses on Electric Power System Insulation," Paper 88SM636-3, IEEE Summer Meeting, Portland, Oreg., July 24-29, 1988.

6. L. M. Burrage, J. H. Shaw, and B. W. McConnell, "Distribution Transformer Performance When Subjected to Steep-Front Impulses," Paper 89TD400-3 PWRD, IEEE PES T&D Conference and Exposition, New Orleans, April 2-7,1989.

7. B. W. McConnell, P. R. Barnes, and L. M. Burrage, "Steep-Front Short Duration Impulse Tests on Energized Insulators," *Proceedings of the Sixth International Symposium on High Voltage Engineering,* New Orleans, August 28 - September 1, 1989.

8. L. M. Burrage and B. W. McConnell, "Impact of Steep-Front, Short-Duration Impulse on Lightning Arresters," to be submitted to the IEEE Power Engineering Society.

APPENDICES

A. TRANSFORMER MODELING OF STEEP-FRONTED SURGES

This appendix discusses modeling of the effects of steep-fronted surges on shell-form distribution transformers and core-form power transformers.

A.1 SHELL-FORM DISTRIBUTION TRANSFORMERS

The low-voltage impulse-distribution data taken on the shell-form distribution transformer, Section 2.1.3.1, and the core-form power transformer, Section 2.1.3.3, were used as input. Simulations were performed using a conventional lumped-element model of the transformer, Fig. A.1. This is basically a ladder network of capacitance between windings and from winding to ground with the inductances superimposed. All inductances are strongly coupled. The most influential losses are those related to eddy currents; these losses are represented by resistances in shunt with the inductances.

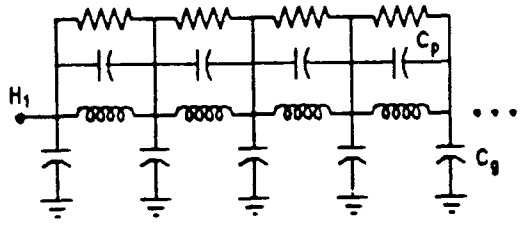

Fig. A.1. General form of the transformer model.

The model of the transformer, where the inductances are computed for the transformer's major sections (disk coil, layer winding, etc.), works well for the 1.2- by 50-μs surge. For faster surges, the model generally results in a simple capacitive division of the surge throughout the network, indicating that the model inductances are not involved. However, the measurements showed that there were high-frequency oscillations within the transformers for all three waves. The inductances required to cause these oscillations appear to be very small. Therefore, it was concluded that they are stray inductances of some sort. As of this writing, the source or sources of these stray inductances have not been identified.

It is now apparent that significantly smaller portions of the winding would have to be modeled in order to study and understand these effects. This implies that individual turns of the winding might have to be modeled, which at this time appears to be a monumental undertaking from both experimental and computational points of view.

A.1.1 Model Parameters for the Shell-Form Distribution Transformer

The inductances and capacitances of the shell-form distribution transformer were computed using the SHELLZ computer program [1]. This is a PC-based program that is designed to compute the model parameters for a large, shell-form power transformer, but the basic assumptions are also satisfied for the particular distribution transformer used in this study.

The fundamental assumption is that the smallest element is a full-layer winding, or, in the terminology of some, a pancake or disk winding. The layer winding must be approximately symmetrical in the window. Transformers satisfying this assumption have the basic geometry shown in Fig. A.2.

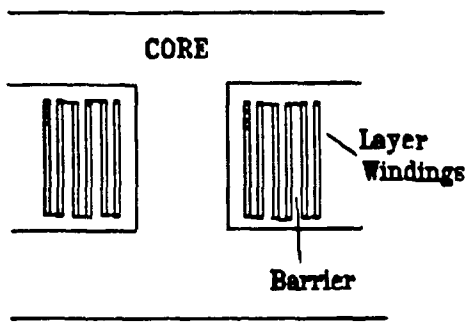

Fig. A.2. Transformer geometry to which SHELLZ program applies.

The short-circuit inductances between each pair of layer windings are computed and then converted to NODAL GAMMA MATRIX form (inverse of nodal inductance matrix).[2] This is a relatively straightforward linear algebra manipulation on the matrix. If we say that X_{SCij} is the short-circuit impedance between two windings, i and j, then we can construct the conventional utility power system "Z_{BUS}" matrix as follows:

DIAGONAL ELEMENTS: $$Z_{Bus_{ij}} = X_{SC_{i,i-1}} \quad \text{and} \quad i = 1\text{-}N\text{-}1 \ ,$$

where N = number of windings.

Winding 1 is the reference winding (one winding must be chosen as a reference).

OFF-DIAGONAL ELEMENTS: $$Z_{Bus_{ij}} = 0.5\left(Z_{Bus_{ij}} + Z_{Bus_{ij}} - X_{SC_{i-1,j-1}}\right) , \text{ and } i \neq j \ .$$

Z_{Bus} is then inverted and converted to nodal admittance form using a standard power-invariant transformation. If X_{SC} is in per unit form, the turns ratios must be incorporated into the GAMMA matrix that results from this transformation.

The capacitances between layers are computed using the simple parallel-plate formula and a relative permittivity of 3.5, an empirical value that well represents a composite paper-oil insulation system.

$$C = 0.225(3.5)A/d \ \ (pF) \ ,$$

where

A = plate area in square inches,
d = plate separation in inches.

Consecutive layer windings that are connected in series are assumed to have an equipotential surface halfway between the layers. Thus, the capacitance from a layer to the equipotential surface is twice the capacitance between layers. The capacitance is then split in half, and one half is placed at each end of the winding. Therefore, the capacitance across the winding in the model in Fig. A.1 is simply the layer-to-layer capacitance.

The capacitance from the edge of the layer winding to the core is also computed based on the simple parallel-plate formula. However, the fringing field is not negligible because of the narrowness of the edge of the coil relative to the ground plane offered by the core. If we were to energize a group of layer windings from one terminal with the other terminal open, we would find that the multiple edges approximate a continuous plane. Therefore, we have empirically determined that a good way to compute edge capacitances to ground is to assume that the winding edge extends halfway into the barrier on either side.

The dimensional data used to represent the y-connected, 75-kVA, 14.4/24.9-kV→120/240-V distribution transformer in the SHELLZ program is shown in Table A.1. Design values are: 225 kVA, 3 phase, 10.909 V/turn, 9-in. core-window width, 20 windings, 1000-Ω loss resistance.

Table A.1. Dimensional data for SHELLZ Transformer Model

COIL NO.	MEAN TURN LENGTH	BUILD RADIUS	DUCT	WIDTH	MOLD CLEARANCE	NO. OF TURNS
LV1	29.80	8	0.079	0.6799	0.5	11
1	33.19	7.75	0.172	0.056	0.625	75.5
2	33.799	7.75	0.039	0.056	0.625	75.5
3	34.408	7.75	0.039	0.056	0.625	75.5
4	35.017	7.75	0.039	0.056	0.625	75.5
5	35.626	7.75	0.039	0.056	0.625	75.5
6	36.236	7.75	0.039	0.056	0.625	7.75
7	36.844	7.75	0.039	0.056	0.625	7.75
8	37.454	7.75	0.039	0.056	0.625	75.5
9	38.06	7.75	0.039	0.056	0.625	75.5
10	38.67	7.75	0.039	0.056	0.625	75.5
11	39.28	7.75	0.039	0.056	0.625	75.5
12	39.89	7.75	0.039	0.056	0.625	75.5
13	40.5	7.75	0.039	0.056	0.625	75.5
14	41.1	7.75	0.039	0.056	0.625	75.5
15	41.72	7.75	0.039	0.056	0.625	75.5
16	42.33	7.75	0.039	0.056	0.625	75.5
17	42.936	7.75	0.039	0.056	0.625	75.5
18	43.54	3.75	0.039	0.056	2.625	36.5
LV2	46.76	8	0.172	0.6799	0.5	11

NOTE: Last duct 0.0322. All dimensions in inches.

The low-voltage windings were each represented as a one-layer winding, while the primary winding was divided into 18 layer windings (the actual number). The windings were connected as shown in Table A.2.

Table A.2. Winding connecus for SHELLZ Transformer Model

COIL	FROM	TO	TOP OF COIL (FROM OR TO)
LV1	xi	GROUND	F
1	N1-2	GROUND	T
2	N2-3	N1-2	F
3	N3-4	N2-3	T
4	N4-5	N3-4	F
5	N5-6	N4-5	T
6	N6-7	N5-6	F
7	N7-8	N6-7	T
8	N8-9	N7-8	F
9	N9-10	N8-9	T
10	N10-11	N9-10	F
11	N11-12	N10-11	T
12	N12-13	N11-12	F
13	N13-14	N12-13	T
14	N14-15	N13-14	F
15	N15-16	N14-15	T
16	N16-17	N15-16	F
17	N17-18	N16-17	T
18	H1	N17-18	F
LV2	LV2	GROUND X3	T

The high-voltage winding was variously modeled as 18 one-layer windings, 9 two-layer windings, and 6 three-layer windings. Essentially, this was accomplished by making a reduced equivalent of the GAMMA MATRIX after it was computed, with each winding explicitly represented. The model that used 9 two-layer windings was the best match to the 1.2- by 50-μs test results. The model that used 18 one-layer windings introduced a higher-frequency oscillation that was not seen in the measurements. This phenomenon had been experienced previously with other simulations and is apparently the result of inadequate damping of an unidentified mode of oscillation in the model.

Losses in the model are difficult to predict. The predominant damping of the 1.2- by 50-μs wave is caused by induced eddy currents. The approximate value of resistance to use in the model may be determined from the tested core loss. Also, the model frequently shows a minor mode of oscillation

in the 50-kHz range that has very little damping. In the actual transformer, this mode is often visible, but heavily damped. It is visible in the measured response of the transformer, Fig. A.3.

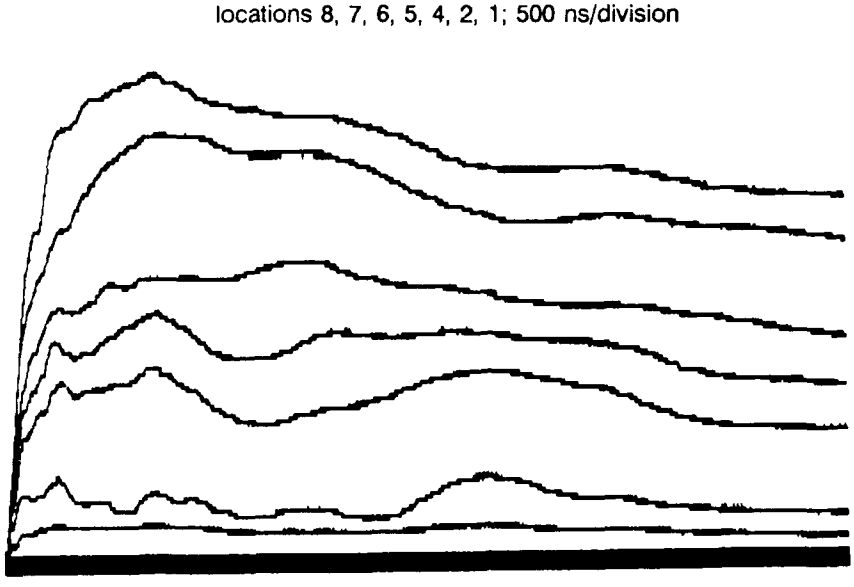

Fig. A.3. Measured response of shell-form distribution transformer for the 1.2- by 50-μs wave.

A.1.2 Modeling Response

The modeling response and the measurements at 1.2 by 50 μs agree well. It is not known what loss mechanism causes the damping, but two possible mechanisms are dielectric losses and conductor skin-effect losses.

- The transformer's measured response and the model's response are shown in Figs. A.4 and A.7, respectively, for the 100- by 500-ns wave. The measured response displays a pronounced ~1-MHz component resulting in a 1.1/unit magnitude voltage of ~300 ns. Neither of these factors appear in the model's computed response for 100- by 500-ns injection.

- Figure A.6 displays the output of the model for the 1.2- by 50-μs wave.

- Figures A.5 and A.8 display the measured and computed responses for the 10- by 150-ns wave. The measured response shows a significant ~50-MHz oscillation, among others, that is absent in the computed response.

- To the best of the authors' knowledge, this endeavor is the first in which instrumentation capable of measuring frequencies greater than 1 MHz has been applied to transformers of this type.

- It is apparent that the faster-front impulses are exciting previously unrecognized resonances in the transformer. These resonances can produce changes in the voltage stress on the insulation system, creating high stress in perhaps unexpected locations. This stress may be a partial cause of the anomalous failure problem.

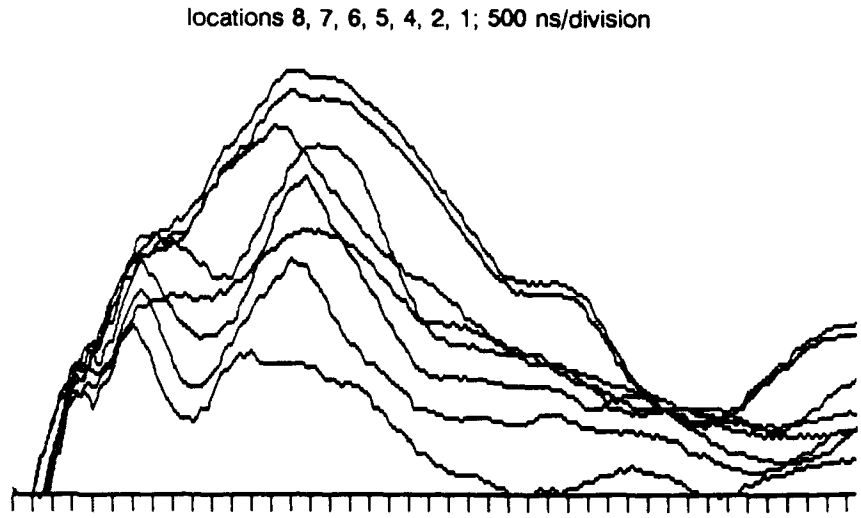

Fig. A.4. Measured response of the shell-form distribution transformer for the 100- by 500-ns wave.

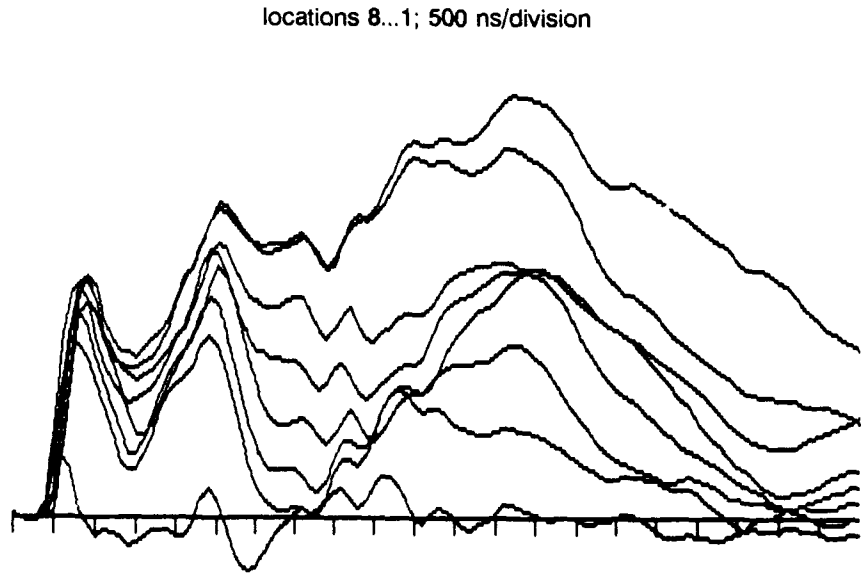

Fig. A.5. Measured response of the shell-form distribution transformer for the 10- by 150-ns wave.

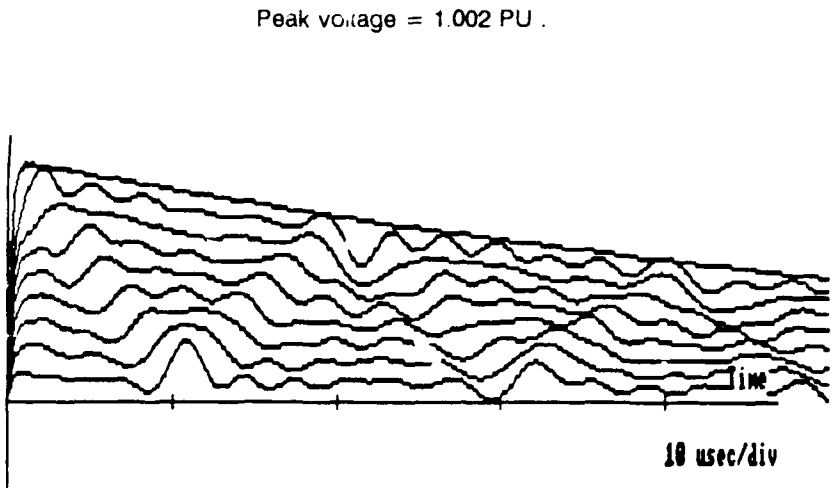

Fig. A.6. Computed response of the shell-form distribution transformer for the 1.2- by 50-μs wave.

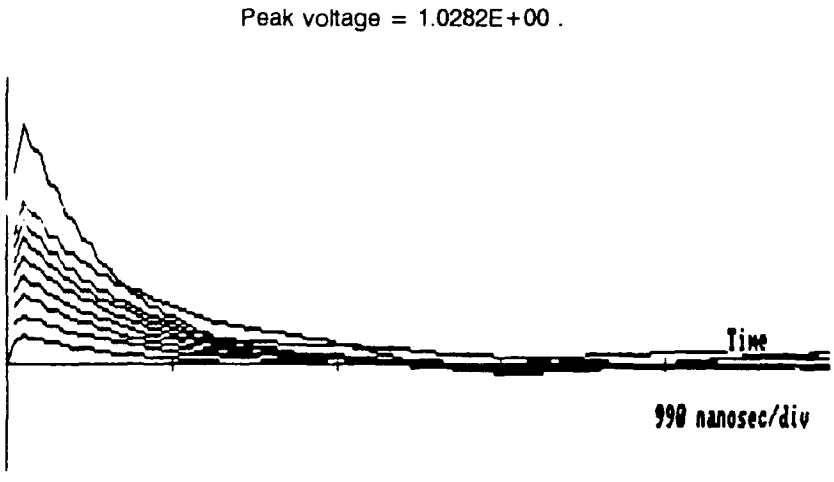

Fig. A.7. Computed response of the shell-form distribution transformer for the 100- by 500-ns wave.

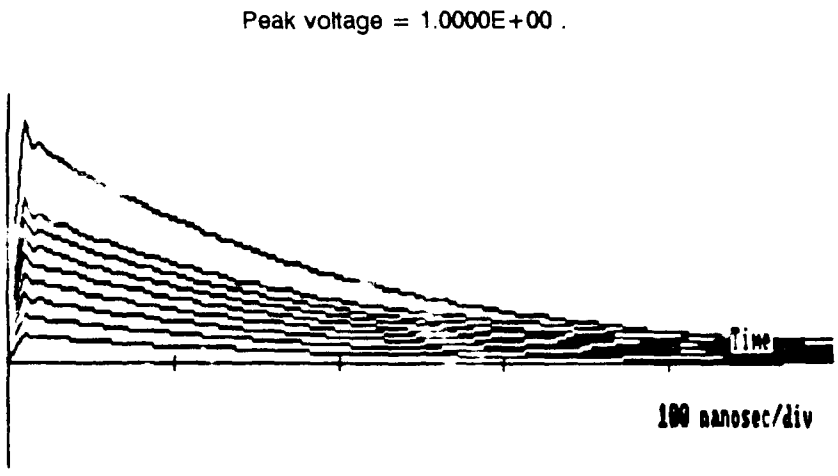

Fig. A.8. Computed response of the shell-form distribution transformer for the 10- by 150-ns wave.

- It is concluded that the model developed provides a good solution for the 1.2- by 50-μs impulses. The model does not provide an acceptable simulation for either of the faster waves, however, but additional understanding was obtained about modeling requirements and possible anomalous failure mechanisms.

A.2 CORE-FORM 16-MVA POWER TRANSFORMER

Each phase of the high-voltage winding of this transformer utilizes 160 disk coils. It is a center-start design, with the H1 terminal connected to the middle of the physical winding and with the two 80-coil halves being symmetrical and in parallel. There is a tap section in each half of the high-voltage winding. The tap section is approximately in the middle (fortieth coil) of each half.

A.2.1 Simulations Performed

Two types of simulations were performed on the 16-MVA core-form transformer. First, the three test waveforms were simulated on the model with each disk coil represented individually. When the simulations failed to show the same oscillatory behavior that the actual measurements did, a second investigation was carried out to try to determine what could be causing the oscillations. Somewhat similar comparisons were achieved by replacing the coupled disk-coil models with uncoupled small inductances across the coil-to-coil capacitances.

The individual and mutual inductances of each disk-coil were computed using finite element methods. The transformer was modeled with each disk-coil explicitly represented. It was assumed to be symmetrical, i.e., the same surges appeared in each half of the high-voltage winding. Thus, the number of coupled inductances was reduced from 160 to 80. The effect of identical surge currents' flowing in the other half was incorporated in the reduction of the (Z_{Bus}) matrix (see Section A.1.1). This was done by making the currents in the top half equal to the mirror image currents in the bottom half and combining equations.

The capacitances were computed as described for the shell-form distribution transformer. The capacitance to ground from the outside edge of the coil was arbitrarily assumed to be half the

capacitance from the inside edge of the disk coil to ground. This capacitance was about 10 pF per coil. The coil-to-coil capacitance was computed to be approximately 2200 pF. A snapshot of the inductance matrix computed for this transformer is given below on a per unit basis (one turn per coil).

This matrix must be modified according to the number of active turns in each disk coil. The diagonal elements are multiplied by the turns squared. The off-diagonals are multiplied by the number of turns in each of the two coils involved.

As can be seen, the inductance of each turn is about 100 μH. While searching for the inductances causing the oscillations on the SFSD waves, it was determined that an inductance of about 0.7 to 1.0 μH would be required. This implies that the "stray" inductance is certainly less than one turn, or that perhaps we are observing oscillatory behavior within a disk coil. If the latter is the case, the current in one turn is nearly matched by an opposite current in an adjacent turn, resulting in a low apparent inductance.

A.2.2 Results of Simulations

The results of the simulation of the core-form power transformer are disappointing. The major phenomena of the 1.2- by 50-μs impulse response follow the correct trend, but the oscillatory phenomenon clearly present in the first 5 to 10 μs in the measurements (Fig. A.9) is absent in the simulations (Fig. A.12). The model seems to have a dominant frequency response somewhere in the neighborhood of 15 kHz. It takes about 50 μs for the main surge to propagate through the model winding (see the computed step response, Fig. A.16).

Naturally, the model fails to predict the 2-MHz phenomenon observed on the faster impulses of 100 by 500 ns (Figs. A.10 and A.13) and 10 by 150 ns (Figs. A.11 and A.14). The inductance model is much too coarse; the inductances are so large that there is no appreciable current flow during the time period of interest. Thus, the model shows a simple capacitive-divider effect.

Figure A.15 shows the results of using the model with small uncoupled inductors instead of the large coupled ones: oscillatory behavior occurs that is somewhat like that seen in the measured 100- by 500-ns surge in Fig. A.10. This model requires refinement.

REFERENCES

1. SHELLZ, Ver. 1 [computer program], Cooper Power Systems, Franksville, Wis., 1987.

2. G. W. Stagg and A. H. El-Abiad, *Computer Methods in Power Systems Analysis*, McGraw-Hill, N.Y., 1968.

locations 1 through 15; 500 ns/division

Fig. A.9. Measured 1.2- by 50-μs response of the core-form power transformer.

locations 1...; locations 2 and 3 higher than 1; 500 ns/division

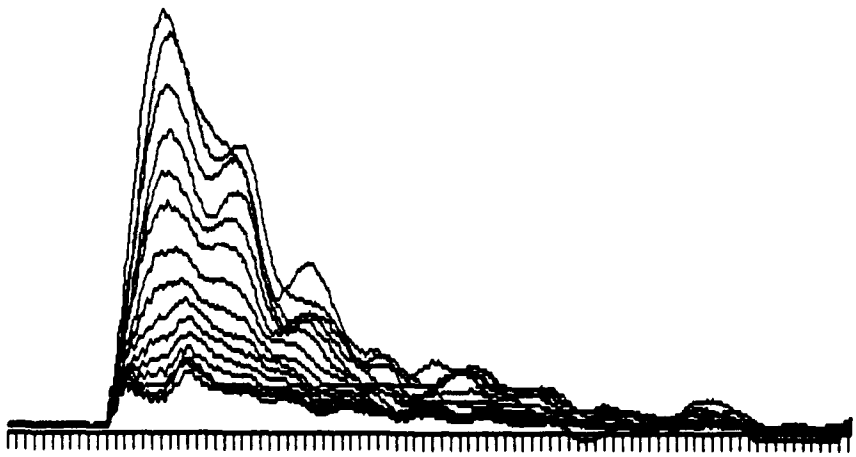

Fig. A.10. Measured 100- by 500-ns response of the core-form power transformer.

locations 1 through 15; locations 2 and 3 higher than 1; 500 ns/division

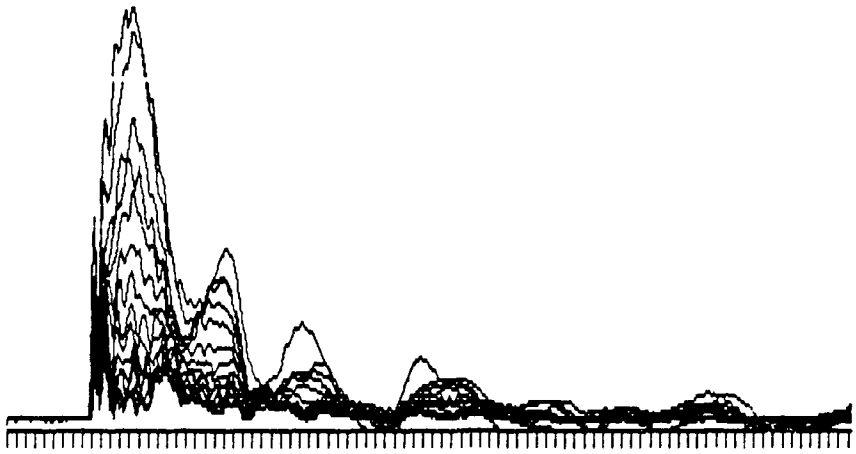

Fig. A.11. Measured 10- by 150-ns response of the core-form power transformer.

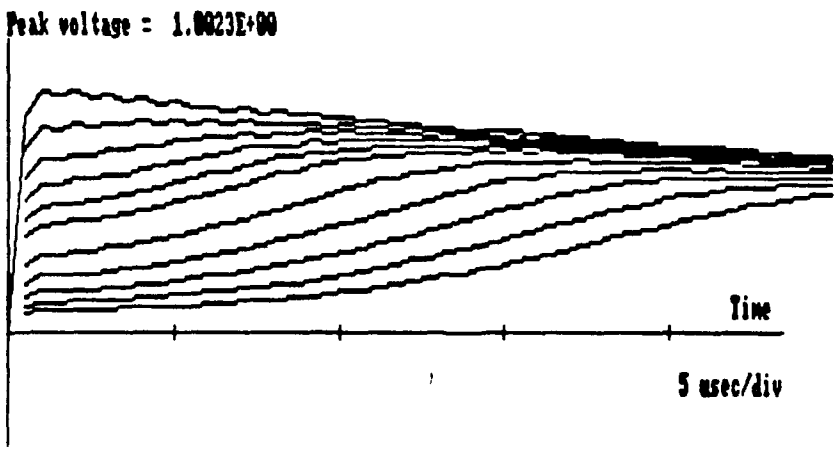

Fig. A.12. Computed 1.2- by 50-μs response of the core-form power transformer.

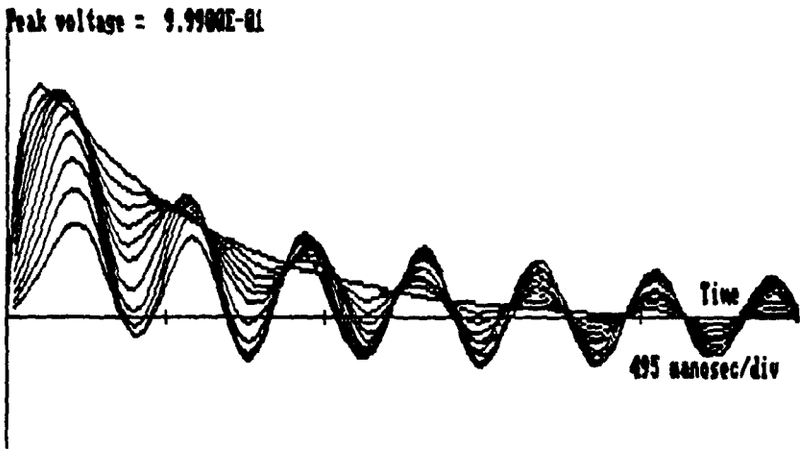

Fig. A.13. Computed 100- by 500-ns response of the core-form power transformer.

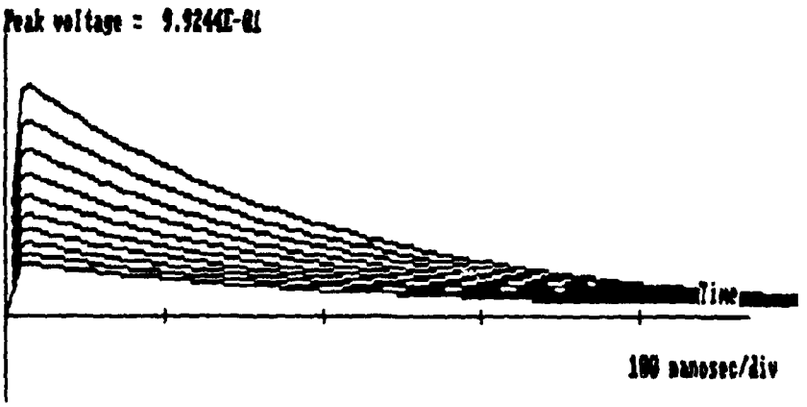

Fig. A.14. Computed 10- by 150-ns response of the core-form power transformer.

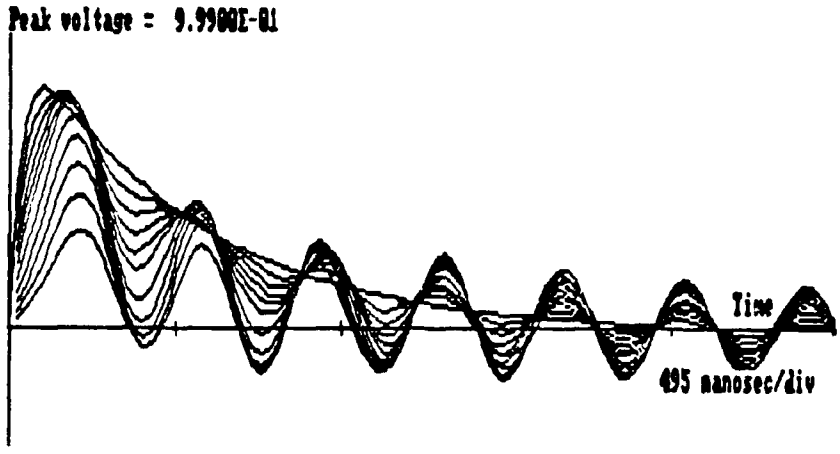

Fig. A.15. Computed 100- by 500-ns response with decoupled, 0.7 μH stray inductances in the core-form power transformer.

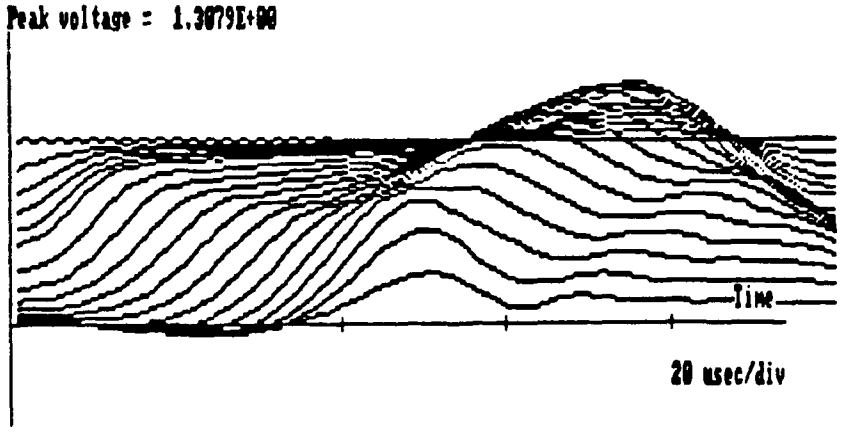

Fig. A.16. Computed step response of the core-form power transformer model.

B. DATA SUMMARIES, IMPULSE ONLY

DATA SUMMARY B.1

SHELL-FORM DISTRIBUTION TRANSFORMER, IMPULSE ONLY

SPECIMEN NO.	WAVESHAPE	NO. OF SHOTS	BIL KV	COMMENTS
1	1.2 x 50 μs	4	127	
2	1.2 x 50 μs	14	126	
3	1.2 x 50 μs	9	127	
4	1.2 x 50 μs	10	126	
5	1.2 x 50 μs	9	125	Lead on terminal block trained incorrectly.
5	1.2 x 50 μs	8	129	Lead training corrected.

DATA SUMMARY B.2.1

30-KV DISTRIBUTION CLASS, SIC

SPECIMEN NO.	WAVESHAPE	NO. OF SHOTS	MIN. KV	MAX. KV	AVE. KV	WITH-STAND	COMMENTS
9	1.2 x 50 μs	3	---	---	72	---	Negative polarity
10	1.2 x 50 μs	7	---	---	78	---	Negative polarity
11	1.2 x 50 μs	2	- -	---	65	---	Negative polarity
12	1.2 x 50 μs	8	67	76	71	75	
13	1.2 x 50 μs	9	81	85	83	82	
14	1.2 x 50 μs	17	75	90	81	81	
9	100 x 500 ns	5	183	202	193	---	
10	100 x 500 ns	5	187	197	193	---	
11	100 x 500 ns	5	153	190	175	---	
9	1.2 x 50 μs	3	---	---	70	---	After 100 x 500 ns
10	1.2 x 50 μs	6	82	83	82	---	After 100 x 500 ns
11	1.2 x 50 μs	3	---	---	69	---	After 100 x 500 ns
12	HEMP	5	461	517	490	---	
13	HEMP	5	430	486	465	---	
14	HEMP	5	456	507	497	---	
12	1.2 x 50 μs	6	---	---	72	69	After HEMP
13	1.2 x 50 μs	5	---	---	91	87	After HEMP
14	1.2 x 50 μs	8	---	---	84	83	After HEMP

DATA SUMMARY B.2.2

30-KV MOV DISTRIBUTION ARRESTER

SPECIMEN NO.	WAVESHAPE	NO. OF SHOTS	MIN. KV	MAX. KV	AVE. KV	COMMENTS
15	1.2 x 50 μs	12	77	82	80	Current = 30 A
16	1.2 x 50 μs	8	78	82	80	
17	1.2 x 50 μs	6	80	81	80	
15	HEMP	5	425	451	436	Current = 5800 A

DATA SUMMARY B.3.1

96-KV SIC STATION-CLASS ARRESTERS

SPECIMEN NO.	WAVESHAPE	NO. OF SHOTS	MIN. KV	MAX. KV	AVE. KV	WITHSTAND KV	COMMENTS
5	1.2 × 50 μs	17	213	221	216	208	
6	1.2 × 50 μs	7	179	182	181	179	
7	1.2 × 50 μs	12	187	196	192	187	
6	1.2 × 50 μs	4	---	---	180	---	Before 100 × 500 ns
5	100 × 500 ns	4	343	364	356	346	
6	100 × 500 ns	4	320	356	338	305	
7	100 × 500 ns	3	---	---	307	269	
6	1.2 × 50 μs	3	---	---	184	---	After 100 × 500 ns
5	HEMP	5	901	968	946	---	
6	HEMP	5	850	937	902	---	
7	HEMP	5	896	916	902	---	
6	1.2 × 50 μs	3	---	---	191	---	After HEMP

DATA SUMMARY B.3.2

96-KV MOV STATION-CLASS ARRESTER

SPECIMEN NO.	WAVESHAPE	NO. OF SHOTS	MIN. KV	MAX. KV	AVE. KV	COMMENTS
8	1.2 x 50 μs	5	153	186	170	Start of test program
	100 x 500 ns	5	195	214	202	
	1.2 x 50 μs	5	---	---	172	
	1.2 x 50 μs	6	157	175	167	Before low HEMP
	LOW HEMP	4	223	287	248	Equivalent CISO
	1.2 x 50 μs	3	157	175	166	After low HEMP
	HEMP	4	666	696	685	Equivalent FOW
	1.2 x 50 μs	4	156	172	162	After HEMP

DATA SUMMARY B.4.1

POST INSULATOR

SPECIMEN NO.	WAVESHAPE	NO. OF SHOTS	NO. OF FOs	MIN. FO KV	MAX. FO KV	AVE. FO KV	WITHSTAND KV	COMMENTS
41	1.2 × 50 μs	29	4	167	168	168	---	
42	1.2 × 50 μs	24	5	169	170	170	---	
43	1.2 × 50 μs	18	6	163	169	164	---	
44	1.2 × 50 μs	20	8	154	160	154	---	
45	1.2 × 50 μs	31	7	178	191	188	---	
41	LOW HEMP	3	1	---	294	294	248	CIFO
42	LOW HEMP	2	2	---	294	294	233	CIFO
43	LOW HEMP	2	1	---	287	287	241	CIFO
44	LOW HEMP	2	1	---	264	264	228	CIFO
45	LOW HEMP	2	1	---	274	274	259	CIFO
42	HEMP	5	5	727	772	748	---	
43	HEMP	5	5	732	753	745	---	
44	HEMP	5	5	707	758	729	---	
120	1.2 × 50 μs	10	1	---	---	236	---	
121	1.2 × 50 μs	5	1	---	---	240	---	
122	1.2 × 50 μs	2	1	---	---	236	---	
120	100 × 500 ns	5	4	312	322	318	---	
121	100 × 500 ns	5	5	319	336	326	---	
122	100 × 500 ns	5	5	298	315	309	---	
120	1.2 × 50 μs	2	1	---	---	230	---	After 100 × 500 ns
121	1.2 × 50 μs	4	1	---	---	240	---	After 100 × 500 ns
122	1.2 × 50 μs	6	2	230	230	230	---	After 100 × 500 ns

DATA SUMMARY B.4.2

PIN-TYPE INSULATORS

SPECIMEN NO.	WAVESHAPE	NO. OF SHOTS	NO. OF FO	MIN. FO KV	MAX. FO KV	AVE. FO KV	WITHSTAND	COMMENTS
21	1.2 x 50 μs	6	4	150	167	162	150	Before. FO at crest or on tail.
23	1.2 x 50 μs	6	5	139	151	145	151	Before. FO on tail.
29	1.2 x 50 μs	20	6	160	168	162	---	
22	1.2 x 50 μs	3	1	---	---	168	---	
35	1.2 x 50 μs	4	3	150	159	158	---	
100	1.2 x 50 μs	3	2	156	158	157	---	
101	1.2 x 50 μs	2	1	---	---	158	---	
102	1.2 x 50 μs	5	1	---	---	168	---	
23	LOW HEMP	5	2	317	330	323	310	
21	LOW HEMP	3	1	---	---	328	287	
19	LOW HEMP	3	1	---	---	323	297	
102	LOW HEMP	8	6	326	331	329	---	1800 A
100	LOW HEMP	6	6	321	328	325	---	
101	LOW HEMP	5	4	312	326	319	---	
29	LOW HEMP	5	2	244	293	269	---	
131	100 x 500 ns	5	5	305	356	328	---	
132	100 x 500 ns	5	5	295	338	309	---	
130	100 x 500 ns	5	2	329	335	332	---	Specimen failed partially on shots 3 and 4. Failed completely on shot 5.
29	1.2 x 50 μs	3	1	---	---	158	---	After 100 x 500 ns
101	1.2 x 50 μs	8	3	154	156	155	---	
100	1.2 x 50 μs	5	2	150	156	153	---	

DATA SUMMARY B.4.2 (CONT.)

102	1.2 × 50 μs	3	1	---	---	160	---	
18	1.2 × 50 μs	5	---	---	---	149	---	Before HEMP
19	1.2 × 50 μs	4	---	---	---	142	---	Before HEMP
20	1.2 × 50 μs	5	---	---	---	147	---	Before HEMP
18	HEMP	5	5	819	850	839	---	15 × 500 ns applied, 42 × 600 ns measured. Punctured on fifth shot.
19	HEMP	5	5	788	855	821	---	
20	HEMP	5	5	804	840	820	---	

DATA SUMMARY B.4.3

CAP-AND-PIN INSULATORS

SPECIMEN NO.	WAVESHAPE	NO. OF SHOTS	NO. OF FOs	MIN. FO KV	MAX. FO KV	AVE. FO KV	COMMENTS
36	1.2 × 50 μs	45	5	207	216	210	
37	1.2 × 50 μs	7	3	196	199	197	
38	1.2 × 50 μs	25	6	210	216	212	
39	1.2 × 50 μs	12	2	210	210	210	
40	1.2 × 50 μs	15	3	210	214	213	
110	1.2 × 50 μs	5	1	---	---	204	
111	1.2 × 50 μs	6	1	---	---	216	
112	1.2 × 50 μs	3	2	190	200	195	
110	100 × 500 ns	5	3	345	366	359	
111	100 × 500 ns	5	5	376	385	382	
112	100 × 500 ns	5	4	352	371	365	
110	1.2 × 50 μs	2	2	---	---	210	After. 1.2 × 50 μs
111	1.2 × 50 μs	5	1	---	---	196	Specimen failed on second shot.
112	1.2 × 50 μs	4	1	---	---	198	
37	HEMP	5	5	814	835	825	
38	HEMP	5	5	804	850	825	
39	HEMP	5	5	794	814	805	

DATA SUMMARY B.4.4

SUSPENSION-DISK INSULATORS

SPECIMEN NO.	WAVESHAPE	NO. OF SHOTS	NO. OF FO	MIN. FO KV	MAX. FO KV	AVE. FO KV	WITHSTAND KV	COMMENTS
24	1.2 × 50 μs	46	--	---	---	142	142	
25	1.2 × 50 μs	36	--	---	---	146	146	
26	1.2 × 50 μs	22	--	---	---	143	143	
27	1.2 × 50 μs	28	--	---	---	139	139	
28	1.2 × 50 μs	15	--	---	---	147	145	
29	1.2 × 50 μs	19	--	---	---	144	143	
30	1.2 × 50 μs	5	--	---	---	138	138	
31	1.2 × 50 μs	42	--	---	---	148	148	
32	1.2 × 50 μs	21	--	---	---	147	147	
33	1.2 × 50 μs	23	--	---	---	129	129	
34	1.2 × 50 μs	11	--	---	---	134	134	
35	1.2 × 50 μs	24	--	---	---	148	148	
31	LOW HEMP	2	1	292	292	292	266	
32	LOW HEMP	5	1	287	287	287	276	
33	LOW HEMP	2	2	289	305	297	---	
34	LOW HEMP	2	1	282	282	282	287	
35	LOW HEMP	3	1	315	315	315	300	
31	1.2 × 50 μs	5	2	149	149	149	138	After LOW HEMP
32	1.2 × 50 μs	6	--	130	138	134	128	After LOW HEMP
33	1.2 × 50 μs	4	2	147	147	147	144	After LOW HEMP
34	1.2 × 50 μs	4	2	138	149	143	128	After LOW HEMP
35	1.2 × 50 μs	5	2	149	151	150	144	After LOW HEMP
31	HEMP	5	5	722	758	737	---	Failed on fifth shot
32	HEMP	5	5	722	742	728	---	Failed on fourth shot
33	HEMP	5	5	748	794	775	---	Failed on fifth shot

DATA SUMMARY B.4.5, PART 1

SUSPENSION-INSULATOR STRINGS

SPECIMEN	SPECIMEN NO.	NO. OF SHOTS	NO. OF FO	MIN. KV	MAX. KV	AVE. KV	COMMENTS
PRD-1	8 disks	2	0	---	---	---	Withstand 1110 kV
	6 disks	1	0	---	---	---	Withstand 1140 kV
	4 disks	6	6	1080	1130	1110	FO after crest, 1 disk punctured

DATA SUMMARY B.4.5, PART 2

STRINGS OF TWO SUSPENSION DISKS

SPECIMEN NO.	WAVESHAPE	NO. OF SHOTS	NO. OF FOs	MIN. FO KV	MAX. FO KV	AVE. FO KV	POLARITY	COMMENTS
8-27-1a & b	30 x 350 ns	3	3	634	634	634	–	Puncture on second shot
	1.2 x 50 μs	--	--	---	---	323	–	
8-27-2a & b	1.2 x 50 μs	--	--	---	---	323	–	
	30 x 350 ns	5	5	604	671	625	–	30 x 350 ns applied
		5	5	628	665	642	+	
	1.2 x 50 μs	--	--	---	---	339	–	
	30 x 350 ns	5	5	604	628	617	–	
		5	5	641	678	653	+	
	1.2 x 50 μs	--	--	---	---	293	–	
8-27-4a & b	1.2 x 50 μs	--	--	---	---	323	–	
	50 x 515 ns	5	5	641	678	653	+	
		5	5	598	622	611	–	I at FO = 3200 to 4200 A
	1.2 x 50 μs	--	--	---	---	342	–	
	50 x 515 ns	5	5	622	671	652	+	
		5	5	616	665	640	–	
	1.2 x 50 μs	--	--	---	---	326	–	

DATA SUMMARY B.5

POWER TRANSFORMER COILS

SPECIMEN NO.	WAVESHAPE	NO. OF SHOTS	MIN. KV	MAX. KV	FAIL KV	CURRENT (A)
2.6	100 x 500 ns	--	---	105	---	528
2.2a	100 x 500 ns	--	---	112	---	480
2.2b	100 x 500 ns	--	---	107	---	656
1.6	1.2 x 50 μs	29	---	249	---	---
1.2a	1.2 x 50 μs	--	---	101	---	---
1.2b	1.2 x 50 μs	--	---	51	---	---
3.6	10 x 150 ns	9	230	340	338	---
3.2a	10 x 150 ns	4	109	146	146	---
3.2b	10 x 150 ns	5	109	146	146	---
3.2c	10 x 150 ns	1	155	---	155	---

DATA SUMMARY B.6

BUSHINGS

SPECIMEN	WAVESHAPE	NO. OF SHOTS	POLARITY	MIN. KV	MAX. KV	AVE. KV	COMMENTS
2.7	100 x 500 ns applied	8	-	534	551	543	Crest 700 kV, 5.2 kA, FO at 528 kV on tail at 400 ns.
	~120 x 600 ns	5	+	545	574	557	
		5	-	648	665	658	6 kA
		3	+	585	591	588	Check shot
		5	-	772	795	782	6.9 kA
		3	+	596	602	598	Check shot
		5	-	812	875	842	7.4 kA
		1	+	---	---	596	Check shot
		5	-	824	914	---	Specimen failed on fourth shot.
3.5	30 x 350 ns applied	5	-	608	625	617	5 kA
		5	+	608	625	618	
		5	-	761	790	775	6.2 kA
		3	+	619	625	623	Check shot
		5	-	943	977	957	
		5	+	569	596	589	Alternate polarities on each shot
		5	-	932	966	944	

C. DATA SUMMARIES, MULTISTRESS

DATA SUMMARY C.1

MULTISTRESS, TRANSFORMERS/ARRESTERS

SPECIMEN TYPE	SPECIMEN NO.	NO. OF SHOTS	MIN. KV	MAX. KV	AVE. KV	POLARITY		COMMENTS
						IMPULSE	60 HZ	
XFMR + Direct-Connected Arrester	2.9	9	367	416	395	–	+	No failure
		5	297	378	323	+	–	No failure
		6	410	562	495	–	+	No failure
		5	329	362	340	+	–	No failure
XMFR + Gapped Arrester	2.9	5	383	529	474	–	+	No failure
		5	329	394	359	+	–	No failure
		5	432	562	493	–	+	No failure
		5	286	432	356	+	–	No failure
XMFR + Crossarm-Mounted Arrester	2.9	5	373	491	432	–	+	No failure
		5	292	367	329	+	–	No failure
		5	394	448	428	–	+	No failure
		5	221	329	293	+	–	No failure
XMFR + Direct-Connected Arrester	3.9	5	302	373	333	+	–	No failure
		5	448	540	487	–	+	No failure
		5	313	367	337	+	–	No failure
		5	448	594	517	–	+	No failure
XMFR + Gapped Arrester	3.9	5	292	356	336	+	–	No failure
		5	464	502	482	–	+	No failure

DATA SUMMARY C.1 (cont.)

		5	356	405	378	+	–	No failure
		5	421	518	476	–	+	No failure
XMFR + Crossarm-Mounted Arrester	3.9	5	286	400	332	+	–	No failure
		5	459	513	483	–	+	No failure
		5	302	378	346	+	–	No failure
		5	464	535	484	–	+	No failure
XMFR + Crossarm-Mounted Arrester	4.0	5	389	518	464	–	+	No failure
		5	275	373	330	+	–	No failure
		5	508	562	539	–	+	No failure
		5	286	367	320	+	–	Failed

DATA SUMMARY C.2, PART 1

MULTISTRESS INSULATORS

SPECIMEN NO.	NO. OF SHOTS	MIN. FO	MAX. FO	AVE. FO	POLARITY		60 HZ KV	FAULT I (A)	CONFIG.	COMMENTS
					IMPULSE	60 HZ				
1 + 2	5	481	614	555	–	+	21.6	982–1100	Line	600–800 A
	5	423	460	460	+	–	23.2	1036–1150	---	
	5	534	635	579	–	+	22.4–24	1027–1044	---	
	5	402	444	427	+	–	22.4–24	1027–1080	---	Specimens survived.
3 + 4	5	582	682	634	–	+	24	1027–1044	Line	
	5	391	434	414	+	–	23.2–24	1044–1080	---	Failed–no visible evidence
5 + 6	5	460	698	607	–	+	21.6–24	1009–1044	Line	
	5	397	476	443	+	–	22.4	1044–1062	---	
	5	566	651	610	–	+	21.6–22.4	991–1044	---	
	5	381	455	414	+	–	21.6–23.2	1062–1080	---	Specimens survived.
7 + 8	5	413	577	471	–	+	21.6	973	Line	With wood gap
9 + 10	4	397	460	423	–	+	---	---	---	No wood
	3	471	503	492	–	+	---	---	---	With wood gap under crossarm
	5	614	743	688	–	+	21.6–23.2	2089–2337	---	
	5	455	523	488	+	–	24	2550	---	
	5	545	788	667	–	+	21.6–25.6	2337–2408	Dead end	
	5	407	492	457	+	–	24–24.8	2550–2585	---	Specimens survived.
11 + 12	5	608	746	542	–	+	23.7–24.6	2373–2408	---	
	5	429	508	469	+	–	23.4–24.3	2514–2585	---	

DATA SUMMARY C.2, PART 1 (cont.)

	5	566	709	641	–	+	24–24.3	2373–2408	Dead end	
	5	423	476	452	+	–	23.7	2514–2550	---	Specimens survived.
13 + 14	5	587	730	650	–	+	24.3–24.6	2373–2408	Dead end	Specimens survived.
	5	460	529	492	+	–	24	2514	---	
15 + 16	7	540	748	646	–	+	---	---	Dead end	118 x 500 ns
	8	369	697	533	+	–	---	---	---	No. 15 punctured on seventh shot.
15	1	324	---	---	---	+	---	---	---	
16	4	421	680	537	---	–	---	---	---	72 ns FO
16	3	210	280	253	---	---	---	---	---	No. 16 punctured.
17	7	464	567	493	---	---	---	---	---	109 ns
17	2	416	454	435	---	---	---	---	---	No. 17 punctured.

DATA SUMMARY C.2, PART 2

MULTISTRESS INSULATORS

SPECIMEN NO.	NO. OF SHOTS	MIN. FO	MAX. FO	AVE. FO	POLARITY		60 HZ KV	FAULT (I)	CONFIG.	COMMENTS
					IMPULSE	60 HZ				
17	1	713	---	---	–	+	23	2400	Dead end	Destroyed, line dropped
18	2	497	572	538	--	--	---	---	---	100 ns, specimen punctured
19	1	326	---	---	--	--	---	---	---	98 ns rise FO on tail
19 + 16	1	605	---	---	--	--	---	---	Dead end	No. 16 failed, shattered, line dropped.
19 + 18	1	443	---	---	--	--	---	---	Dead end	No. 18 failed, shattered, line dropped
21 + 20	3	659	697	682	--	--	23.2 –23.9	2439 –2499	Dead end	Failed. No. 20 lost half of skirt. Line did not drop.
3 + 4	2	675	691	683	–	+	---	---	Dead end	Insulator no. 3 failed at 60 Hz, 958 A.
	2	389	454	421	+	–	---	---	---	Failed insulator
	1	740	---	---	–	+	---	---	---	Failed insulator, 991 A available. Line did not drop.

ORNL/Sub/85-28611/2
Dist. Category 97

INTERNAL DISTRIBUTION

1. P. R. Barnes
2. G. E. Courville
3. S. J. Dale
4. M. A. Kuliasha
5-14. B. W. McConnell
15. D. T. Rizy
16. Central Research Library
17. Document Reference Section
18. Energy Information Library
19. Laboratory Records - RC
20. Laboratory Records Department
21. ORNL Patent Section

EXTERNAL DISTRIBUTION

34. V. D. Albertson, Dept. of Electrical Engineering, University Of Minnesota, 123 Church Street, S.W., Minneapolis, MN 55455.

35. G. Applegren, Main Coordination Center, 1N301 Swift Road, P.O. Box 278, Lombard, IL 60148.

36. G. H. Baker, HQ DNA/RAEE, 6801 Telegraph Road, Alexandria, VA 22310-3398.

37. C. E. Baum, Air Force Weapons Lab/NTAAB, Kirkland AFB, NM 87117-6008.

38. W. D. Beatty, Hq DNA/RAEE, 6801 Telegraph Road, Alexandria, VA 22310-3398.

39. D. M. Benjamin, Director - Operations, North American Electric Reliability Council, 101 College Road East, Princeton, NJ 08540-8060.

40. P. D. Blair, Office of Technology Assessment, U.S. Congress, Washington, DC 20510-8025.

41. D. W. Boehm, DCA, Code R - 430, DCEC, 1860 Wiehill Avenue, Reston, VA 22090-5500.

42. J. N. Bombardt, R & D Associates, 105 E. Vermijo St., Suite 450, Colorado Springs, CO 80903.

43. J. J. Bonk, ABB Power Systems Inc., 777 Penn Center Boulevard, Pittsburgh, PA 15235-5927.

44. E. H. Brehm, Dipl.-Ing., ASEA Brown Boveri AG, Postfach 351, Abt. GK/NP 25, 6800 Mannheim 1, Germany.

45. B. G. Buchanan, Department of Computer Science, University of Pittsburgh, 206 Mineral Industries Building, Pittsburgh, PA 15260.

46. J. Burke, Power Technologies Inc., P.O. Box 1058, 1482 Erie Boulevard, Schenectady, NY 12301-1958.

47. L. M. Burrage, Cooper Power Systems, 11131 Adams Road, P.O. Box 100, Franksville, WI 53126.

48. J. Busse, U.S. Department of Energy, RM 8F089, 1000 Independence Avenue, S.W., Washington, DC 20585.

49. H. S. Cabayan, Lawrence Livermore National Laboratory, P.O. Box 5504, L-81, Livermore, CA 94550.

50. C. L. Carter, Manager Transmission & Electrical Program, Tennessee Valley Authority, 3N 42A Missionary Ridge Place, Chattanooga, TN 37410.

51. A. M. Chodorow, Mission Research Corporation, 1720 Randolph Road S.E., Albuquerque, NM 87106-4245.

52. P. Chrzanowski, Deputy Division Leader, Evaluation & Planning Program, Lawrence Livermore National Laboratory, P.O. Box 808, L-81, Livermore, CA 94550.

53. R. F. Chu, Research Engineer, Philadelphia Electric Co., Research Division (S10-1), 2301 Market Street, Philadelphia, PA 19101.

54. R. E. Clayton, Power Technologies, P.O. Box 1058, 1482 Erie Boulevard, Schenectady, NY 12301-1958.

55. H. W. Colborn, 3809 Hickory Hill Rd., Murrysville, PA 15668.

56. G. H. Coplon, U.S. Department of Energy, Rm. 8F089, 1000 Independence Avenue, S.W., Washington, DC 20585.

57. J. J. Cuttica, Vice President, Gas Research Institute, 8600 W. Bryn Mawr Avenue, Chicago, IL 60631.

58. G. Dahlen, Royal Institute of Technology, Tds, P.O. Box 70043, S-10044 Stockholm, Sweden.

59. N. Esser, ASEA Brown Boveri Ag (ABB), ABT. KW/NA13, Kallstadter Str. 1, 6800 Mannheim, Germany.

60. W. E. Ferro, Electric Research and Management, Inc., P.O. Box 165, State College, PA 16804.

61. G. J. Fitzpatrick, NIST, Bldg. 220, Rm. B-344, Gaithersburg, MD 20899.

62. J. Futterman, Lawrence Livermore National Laboratory, P.O. Box 808, L-95, Livermore, CA 94550.

63. R. Gates, EMP Program Manager, FEMA, 500 C Street, S.W., Rm. 606, Washington, DC 20472.

64. M. R. Gent, President, North American Electric Reliability Council, 101 College Road East, Princeton, NJ 08540-8060.

65. C. R. Gordon, HQ DNA/RAEE, 6801 Telegraph Road, Alexandria, VA 22310-3398.

66. V. Guten, National Security Agency (R-52), Fort Mead, MD 20755.

67. I. Gyuk, Program Manager, U.S. Department of Energy, 1000 Independence Ave., S.W., Washington, DC 20585.

68. D. Hansen, Manager of ABB EMI Control Center, ASEA Brown Boveri, Corporate Research, Department CRBE.4, CH-5405 Baden, Switzerland.

69. F. R. Fridoloin Heidler, LABG, Einsteinstrasse 20, D-8012 Ottobrunn Munchen, Germany.

70. D. Wayne Hilson, Tennessee Valley Authority, 1100 Chestnut St., Tower 2, Chattanooga, TN 37402.

71. N. Hingorani, Electric Power Research Institute, P.O. Box 10412, Palo Alto, CA 94303.

72. A. Hirsch, Vice President, Environmental Sciences, and Director, Washington Operations, Midwest Research Institute, 5109 Leesburgh Pk., Ste. 414, Falls Church, VA 22041.

73. J. Hurwitch, Senior Program Manager, Energetics, Inc., 9210 Route 108, Columbia, MD 20145.

74. R. H. Hutchins, BDM Corporation, 1801 Randolph, S.W., Albuquerque, NM 87106.

75. J. L. Koepfinger, Director, Sys. Studies & Research, Duquesne Light Co., 301 Grant St. (19-5), Pittsburgh, PA 15279.

76. V. J. Kruse, ABB Power Systems Inc., Advanced Systems Technology, 777 Penn Center Blvd., Pittsburgh, PA 15235-5927.

77. R. Launstein, EMP Program Manager, Defense Nuclear Agency, 6801 Telegraph Rd., Alexandria, VA 22310.

78. K. S. H. Lee, Kaman Science Corporation, Dikewood Division, 2800 28th Street, Suite 3780, Santa Monica, CA 90405.

79. K. D. Leuthauser, Fraunhofer Institute fur Naturwissenschaftlich, Technische Trendanalysen, Postfach 1491 Appelsgarten 2, D-5350 Euskirchen, Germany.

80. Library, Institute for Energy Analysis, ORAU, Oak Ridge, TN 37830.

81. Library, Defense Technical Information Center, Cameron Station, Alexandria, VA 22314.

82. R. Liimatainen, 374 Rayburn House Office Bldg, Rm.B, Washington, DC 20515.

83. T. K. Liu, P.O. Box 20913, Oakland, CA 94620-0913.

84. J. Lloyd/CEHND-ED-SY, U.S. Army, Engineering Division Huntsville, P.O. Box 1600, Huntsville, AL 35807.

85 C. L. Longmire, Mission Research Corporation, P.O. Drawer 719, Santa Barbara, CA 93102.

86. A. Mesland, N.V. Tot Keuring Van Elektrotechnische, Materialen, 6800 ET Arnhem, P.O. Box 9035, The Netherlands.

87. D. B. Miller, Professor, Mississippi State University, P.O. Drawer EE, Mississippi State, MS 39762.

88. D. E. Morrison, 333 Oxford Road, East Lansing, MI 48823.

89. K. Muller, IABG, Insteinstrasse 20, Ottobrunn 8012, Germany.

90. M. Nahemow, Consultant, 1238 Bellrock St., Pittsburgh, PA 15217.

91. H. P. Neff, University of Tennessee, Dept. of Electrical Engineering, Knoxville, TN 37916.

92. D. L. Nickel, Advanced Systems Technology, ABB Power Systems Inc., 777 Penn Center Boulevard, Pittsburgh, PA 15235-5927.

93. S. Nilsson, Program Manager, Electric Power Research Institute, Electrical Systems Division, 3412 Hillview Avenue, P.O. Box 10412, Palo Alto, CA 94303.

94. R. Oates, Atomic Weapons Research Establishment, Building D57 Aldermaston, Reading Rg74pr, England.

95. R. Ott, Engineer, Electricite de France, 34-40 Rue Henri-Regnault, Cendex 48 92068, Paris La Defense, France.

96. D. Parker, Senior Engineer, Gm-14, Defense Communications Agency, South Court House Rd., 8th St., Arlington, VA 22204.

97. R. L. Parker, Staff Member, R & D Associates, P.O. Box 9377, Albuquerque, NM 87119.

98. B. M. Pasternack, American Electric Power Service Corp., 1 Riverside Plaza, P.O. Box 16631, Columbus, OH 43216-6631.

99. M. Rabinowitz, Electric Power Research Institute, 3412 Hillview Avenue, P.O. Box 10412, Palo Alto, CA 94303.

100. W. A. Radasky, Metatech, P.O. Box 1450, Goleta, CA 93116.

101. A. Ramrus, Technical Director, Maxwell Laboratories, Inc., 8888 Balboa Avenue, San Diego, CA 92123 .

102. J. J. Ray, Division of Syst. Planning, BPA, P.O. Box 3621, Portland, OR 97208.

103. T. W. Reddock, Electrotek Concepts, Inc., 10305 Dutchtown Rd., Suite 103, Knoxville, TN 37932.

104. J. R. Rempel, Physicist, Defense Intelligence Agency, Washington, DC 20340-6761.

105. F. Rosa, Division of System Intg., Nuclear Regulatory Commission, MS P1030, Washington, DC 20555.

106. J. A. Rosado, Vice President, Jaycor, 1608 Spring Hill Road, Vienna, VA 22182.

107. R. R. Schaefer, Metatech, 7 C Beach Road, Belvedere, CA 94920.

108. G. K. Schlegel, R & D Associates, P.O. Box 92500, Los Angeles, CA 90009.

109. K. B. Schlichtenmayer, BWB - AT - NT/PT, Bundesministerium der Verteidigung, RuFo ^{2} - NT/PT, Postfach 13 28, D-5300 Bonn 1, Germany.

110. W. J. Scott, Hq DNA/RAEE, 6801 Telegraph Road, Alexandria, VA 22310-3398.

111. S. Spohn, Defense Nuclear Agency, DB-6E2, Washington, DC 20301-6111.

112. U. D. Strahle, Dipl.-Phys., Regierungsdirektor, Federal Ministry Of Defense, Postfach 1328, 5300 Bonn 1, Germany.

113. E. R. Taylor, ABB Power Systems Inc., 777 Penn Center Boulevard, Pittsburgh, PA 15235-5927.

114. R. L. Taylor, Director - Power Supply, Florida Power & Light Co., 9250 W. Flagler, Miami, FL 33102.

115. F. M. Tesche, Consulting Scientist, 6921 Spanky Branch Dr., Dallas, TX 75248.

116. B. Torres, BDM Corporation, 1801 Randolph S.W., Albuquerque, NM 87106.

117. M. A. Uman, Professor, University of Florida, Department of Electrical Engineering, Gainesville, FL 32611.

118. E. F. Vance, Senior Staff Scientist, Sri International, Route 3 Box 268a, Fort Worth, TX 76140.

119. D. R. Volzka, Senior Project Engineer, Wisconsin Electric Power Company, 333 West Everett Street, Milwaukee, WI 53201.

120. J. Vora, Nuclear Regulatory Commission, MS 5650 Nl, Alexandria, VA 22310.

121. C. L. Wagner, 4933 Simmons Dr., Export, PA 15632.

122. R. C. Webb, Defense Nuclear Agency, RAEE, 6801 Telegraph Road, Alexandria, VA 22310.

123. C. M. Wiggins, BDM International, 1801 Randolph Rd., S.E., Albuquerque, NM 87106.

124. E. P. Wigner, Consultant, 8 Ober Road, Princeton, NJ 08540.

125. M. W. Wik, Forsvarets Materielverk, Stockholm, S-11588, Sweden.

126. M. Williams, Professor, Department of Economics, Northern Illinois University, DeKalb, IL 60115.

127. D. D. Wilson, Power Technologies, Inc., P.O. Box 1058, Schenectady, NY 12301.

128. A. Woodford, System Planning Division, Manitoba Hydro, P.O. Box 815, Winnipeg, Manitoba R-3c-2pa, Canada.

129. S. E. Wright, Electric Power Research Institute, 3412 Hillview Ave., P.O. Box 10412, Palo Alto, CA 94303.

130. M. Wurm, IABG, Einsteinstrasse 20, D-8012 Ottobrunn Munchen, Germany.

131. F. S. Young, Director, Electrical Systems Division, Electric Power Research Institute, P.O. Box 10412, Palo Alto, CA 94303 .

132. Office of Assistant Manager for Energy, Research and Development, DOE-ORO, P.O. Box 2001, Oak Ridge, TN 37831-8600.

133-142. OSTI, U.S. Department of Energy, P.O. Box 62, Oak Ridge, TN 37831.